Emilie Kvaløy

Unraveling the role of LSD1 in murine intestinal epithelial development

Master's thesis in Molecular Medicine
Supervisor: Menno Johannes Oudhoff and Rosalie Theda Margien Zwiggelaar
June 2019

Master's thesis

NTNU
Norwegian University of Science and Technology
Faculty of Medicine and Health Sciences
Department of Clinical and Molecular Medicine

NTNU
Kunnskap for en bedre verden

Emilie Kvaløy

Unraveling the role of LSD1 in murine intestinal epithelial development

June 2019

NTNU
Norwegian University of
Science and Technology
Faculty of Medicine and Health Sciences
Department of Clinical and Molecular Medicine

Master's thesis

2019

Emilie Kvaløy

Master's thesis

NTNU
Norwegian University of
Science and Technology

NTNU
Norwegian University of
Science and Technology

NTNU
Norwegian University of
Science and Technology

Unraveling the role of LSD1 in murine intestinal epithelial development

Molecular Medicine
Submission date: June 2019
Supervisor: Menno Johannes Oudhoff
Co-supervisor: Rosalie Theda Margien Zwiggelaar

Norwegian University of Science and Technology
Department of Clinical and Molecular Medicine

Acknowledgements

The time I have had at the Centre of Molecular Molecular Inflammation Research (NTNU, Trondheim), has been a year filled with ups and downs. But most importantly, it has been a period of my life where I have grown as an individual and as a scientist. For that, I would like to thank my supervisors: PhD candidate Rosalie Zwiggelaar and Principal Investigator Menno Oudhoff of the Oudhoff lab. I would not have overcome the challenges I met without their patience and professional guidance. They have been inspirations and paragons for me and my work and given me valuable insights into the life of a researcher.
I would further like to extend my gratitude to the members of the Oudhoff lab: Fellow master's student Sigrid Hoel, PhD candidate Håvard Lindholm, the postdoctoral scholars Mara Martin Alonso, Alberto Diez, Jenny Ostrop and Naveen Parmar, and researcher Roos Spanjers, who has taken time off their schedules to assist me in the laboratory. To all the members of the Oudhoff lab: I thank you from the bottom of my heart. It has truly been an inspiration and pleasure to work under the guidance of experts in the field of molecular biology.

Additional acknowledgements are given to the lovely lab engineers at the Centre of Molecular Molecular Inflammation Research and the Cellular and Molecular Imaging Core Facility, to the animal facilities and "Fylkesmann H.B. Guldahl og hustru Lucy Guldahls legat til bekjempelse av kreft og andre alvorlige sykdommer". Their contributions have been of great assistance to this project.

Last, but not least, I would like to thank my family, friends and boyfriend for the loving support given to me throughout my studies. Their encouragement has played a pivotal role in making my dream a reality: To become a part of the research society.

Thank you.

Abstract

Background: The intestinal epithelium is a vital organ that absorbs nutrients and water from luminal contents and provide protection against pathogens and chemicals through the stimulation of the immune system and secretion of antimicrobials and mucus. The development and cellular maturation of the intestinal epithelium is orchestrated by signaling factors, epigenetic regulators and transcription factors, but it is still incompletely defined. Lysine-specific demethylase 1 (LSD1) is a chromatin-modifying enzyme expressed in the intestine and acts on methyl groups connected to lysines 4 or 9 on histone H3-tails. LSD1 has been implicated in processes including embryogenesis and tissue-specific differentiation, but its function in intestinal epithelial development remains unknown.

Objectives: The Oudhoff lab group has explored the expression and function of LSD1 in the intestinal epithelium of adult mice. Unpublished data has shown that mice with an intestinal epithelial deletion of *Lsd1* (*Lsd1*$^{\Delta IEC}$) have abnormal quantities of stem cells and differentiated cell types when compared to *wildtype* (*Lsd1*$^{f/f}$) mice. In this study, the expression pattern of the LSD1 protein in *wildtype* mice and the effects of its deletion on differentiated cell types in the intestinal epithelium during development were studied. The study aimed to elucidate how and when LSD1 affects intestinal epithelial cell differentiation during development.

Methods: To study the role of LSD1 in intestinal epithelial development, we used *wildtype*- and *knockout* mice from five developmental timepoints: E16.5, P0.5, P7, P14 and P21. Morphological features were visualized by hematoxylin- and eosin-staining. Staining patterns and cellular composition of the intestinal epithelium was studied by immunohistochemistry and immunofluorescence.

Results: Through two different staining methods, we retrieved two possible expression patterns of LSD1 during intestinal epithelial development. Immunofluorescent staining showed expression of LSD1 in the whole epithelium at every developmental timepoint, whereas immunohistochemical detection suggested a restriction of LSD1 towards crypts and intervillous zones in late development. When comparing *Lsd1*$^{f/f}$ with *Lsd1*$^{\Delta IEC}$ mice, no alterations to the proliferative compartment or to the intestinal morphology was observed. Goblet cells were significantly reduced in the *Lsd1*$^{\Delta IEC}$ mice from the second postnatal week in the duodenum and jejunum, whereas tuft cells were significantly increased in all small intestinal segments from P21. Enteroendocrine cells were unaffected by the tissue-specific knockout of *Lsd1*. Furthermore, immunohistochemical staining of H3K4me2 did not reveal any difference in staining intensity.

Conclusion: In this study, we have presented two potential expression patterns of LSD1 in the developing intestinal epithelium. The role of LSD1 in the intestinal epithelial development has been elucidated, where it regulates goblet- and tuft cell differentiation in late intestinal epithelial development and is intrinsic to Paneth cell development. Global staining of the active transcription mark H3K4me2 did not reveal any differences between the *Lsd1*$^{\Delta IEC}$- and *Lsd1*$^{f/f}$

mice, suggesting that the observed phenotype is controlled by the regulation of H3K4-dimethylation at distinct sites or through other regulatory mechanisms. Further investigation is required to validate these findings and uncover the exact role of LSD1 in intestinal epithelial differentiation.

List of Abbreviations

AR	Androgen receptor
ATOH1	Atonal Homolog 1
BSA	Bovine Serum Albumin
CDX2	Caudal type homeobox 2
CoREST	REST [Repressor element-1 silencing transcription factor] corepressor 1
Cre	Cre recombinase
D	Duodenum
DAB	HRP substrate
DCLK1 / DCAMKL1	Doublecortin Like Kinase 1
dH_2O	Distilled water
DLL1	Delta-like ligand 1
DNMT1	DNA methyltransferase 1
E14.5	Embryonic day 14.5
EEC	Enteroendocrine cell
FFPE	Formalin-fixed paraffin-embedded
FOX	Forkhead box protein
FOXM1	Forkhead box protein M1
GC	Goblet cell
GI tract	Gastrointestinal tract
GFI1	Growth factor independent protein 1
H&E	Hematoxylin and Eosin
H3K4	Lysine 4 on histone H3
H3K9	Lysine 9 on histone H3
H3K27	Lysine 27 on histone H3
HAT	Histone acetyltransferase
HDAC	Histone Deacetylase
HES	Hairy and Enhancer of Split
HNF-3A	Hepatocyte nuclear factor 3-alpha
HNF-3B	Hepatocyte nuclear factor 3-beta

HNF-4G	Hepatocyte nuclear factor 4-gamma
HRP	Horse-radish peroxidase
I	Ileum
IF	Immunofluorescence
IHC	Immunohistochemistry
IHH	Indian hedgehog
ISC	Intestinal stem cell
J	Jejunum
Ki67	Marker of proliferation Ki67
KLF4	Kruppel-like factor 4
KO	Knockout
LSD1	Lysine-specific demethylase 1
Lsd1$^{\Delta IEC}$	Intestinal epithelial-specific knockout model
M cells	Microfold cells
Me1	Monomethyl
Me2	Dimethyl
MUC2	Mucin-2
MXD3	Max dimerization protein 3
NEUROG3	Neurogenin 3
NGS	Normal Goat Serum
NICD	Notch intracellular domain
OLFM4	Olfactomedin 4
P7	Postnatal day 7
PBS	Phosphate-buffered saline
PC	Paneth cell
PCR	Polymerase chain reaction
POU2F3	POU domain class 2 transcription factor 3
PRC2	Polycomb repressive complex 2
PTK6	Protein tyrosine kinase 6
PTM	Post-translational modification
SI	Small intestine
SMA	Smooth muscle actin
SOX9	SRY-box 9

SPDEF	SAM pointed domain ETS factor
TA cell	Transit-amplifying cell/progenitor
TAE	Tris-acetate-EDTA
TBS-T	Tris-buffered saline-Tween
TC	Tuft cell
UEA-1	Ulex Europaeus Agglutinin I
Vil	Villin
WT	Wildtype

Table of Contents

List of tables

List of figures

1.0 Introduction

The intestine is an organ essential for the survival, welfare and growth of animals (Meyer et al. 2016, Odenwald et al. 2017). It forms the lower gastrointestinal (GI) tract: An intricate organ system specialized for energy harvesting. The GI tract comprise of a single continuous muscular tube extending from the mouth to the anus (figure 1.1), facilitating digestive processes that rely on peristaltic movement and secretion of gastric- and digestive fluids (Murphy et al. 2017, Schuenke et al. 2017). Consumed products are efficiently fragmentized during the journey through the system, from which released nutrients and water become available for absorption by the intestinal epithelium. The intestinal epithelium is the single columnar cell layer acting as a selective permeability barrier for nutrients and provide protection against harmful pathogens and chemicals (Noah et al. 2011, Elliott et al. 2015, Odenwald et al. 2017) .

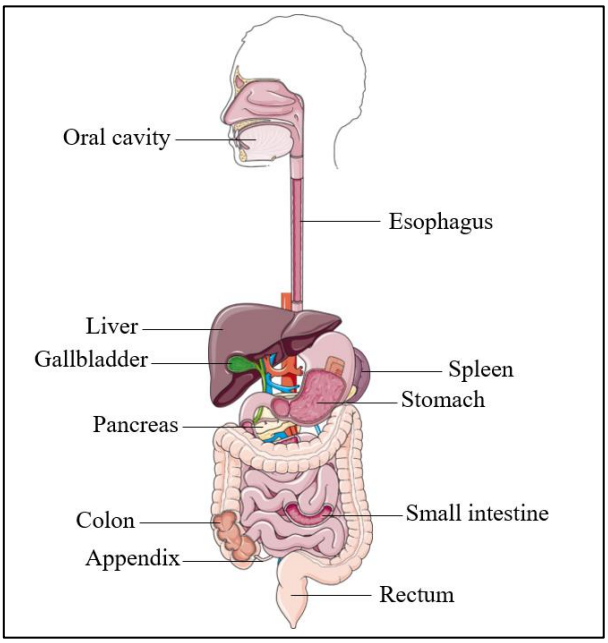

Figure 1.1: The gastrointestinal tract with accessory organs
The gastrointestinal tract is a continuous and hollow muscular tube comprised of the oral cavity, esophagus, stomach, small intestine and colon. Together with the salivary glands, liver, gallbladder, and pancreas, these organs make up the digestive system (Schuenke et al. 2017).

Image retrieved from Smart-Servier.

1.1 Diverging intestinal features and cellular heterogeneity bestow distinct anatomical and functional differences to the intestinal segments

The intestine consists of the small intestine (SI) and colon, which possess different roles in the digestive system. The primary role of the SI lie in transportation, digestion and absorption of nutrients, in contrast to reabsorption of liquids and processing of waste products by the colon

(Betts et al. 2013, Stubbs et al. 2015, Schuenke et al. 2017). The small intestinal epithelium has a massive number of structural units commonly referred to as crypt-villus, enlarging the absorptive surface area of the gut (Clevers 2013, Alberts et al. 2014, Schuenke et al. 2017). Villi are protrusions of the intestinal wall towards the gut lumen, where each villus-unit is comprised of an epithelial cell layer covering the loose connective tissue of the lamina propria. The lamina propria provides transportation of lymph and blood through central lacteals and capillaries, respectively (Clevers 2013, Bernier-Latmani et al. 2017). Smooth muscle extending from the underlying muscularis mucosae can be found along the central axis of the villi-cores, and peristalsis facilitate the movement of compounds at the luminal side of the intestine by rhythmic contraction and relaxation of the smooth muscle (Barker et al. 2008, Bernier-Latmani et al. 2017). Villi are not present in the murine colon, which has an enormous number of the other structural unit: Namely crypts (Ménard et al. 1994, De Santa Barbara et al. 2003). These invaginations punctuate the intestinal epithelium and surround the base of villi in the small intestine (Potten et al. 1987, Clevers 2013). At the bottom of each intestinal crypt resides a stem cell pool that give rise to all epithelial cells constituting the intestinal epithelial lining: The absorptive enterocytes, the mucus-producing goblet cells, the hormone-secreting enteroendocrine cells, cytokine-secreting tuft cells, the antimicrobial-producing Paneth cells, and the less characterized cup cells and microfold cells (Potten et al. 1987, Barker et al. 2008). The crypts of the colon and small intestine share similar features. Intestinal crypts harbor progenitors found in the transit-amplifying zone, while stem cells are positioned at the base of the intestinal crypts. In the small intestine, these stem cells are interspersed between Paneth cells (Barker et al. 2007, Sato et al. 2011). In contrast, colonic crypts lack Paneth cells (Barker et al. 2008, Kim et al. 2012). A schematic figure of the small intestinal epithelial structure is shown below, in figure 1.2.

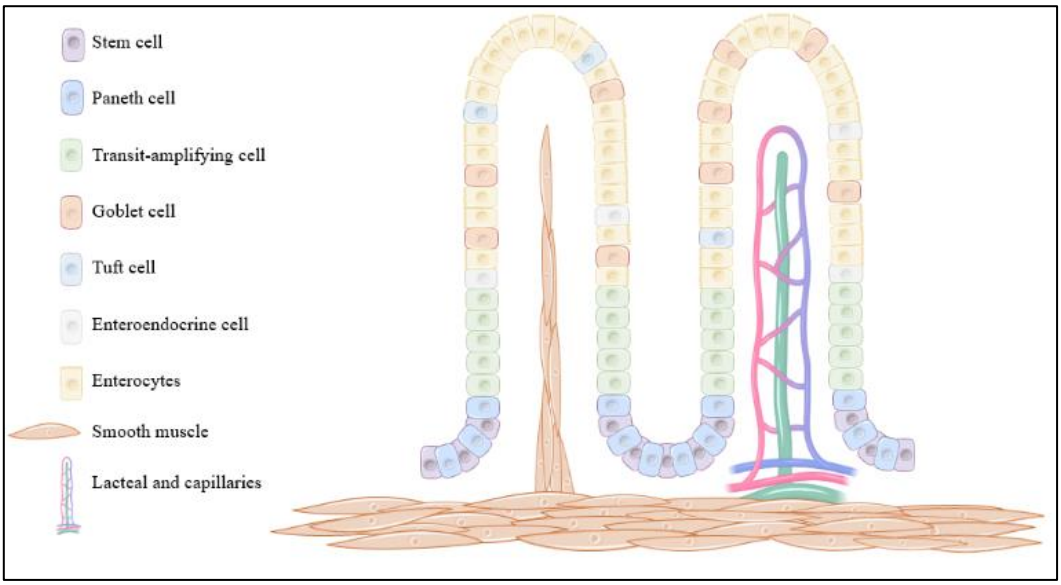

Figure 1.2: The structure of the small intestinal epithelium
The small intestine comprises of an epithelial cell lining covering connective tissues and muscle. Outgrowths and invaginations are present along the intestinal surface, with muscle, blood- and lymph vessels extending into the center of the protrusions known as villi. Most of the differentiated cell types are present in the villus epithelium, whereas the invaginating crypts harbor stem cells interspersed between Paneth cells at the base and a transit-amplifying zone separating the crypt from the villus unit

The figure was made in Powerpoint, with the lacteal and capillaries retrieved from BioRender, while muscle cells were retrieved from Smart-Servier.

The structural- and cellular divergence between the SI and colon are not exclusive to the two segments. Morphological variation and functional differences can be seen along the small intestinal epithelium, and provide a rationale for its segmentation into the duodenum, jejunum and ileum (Brennan et al. 1999, Clevers 2013). The duodenum begins at the pyloric sphincter, which connects the stomach to the proximal portion of the small intestine (Volk et al. 2017). Villi of the duodenum are longer and denser than in the downstream jejunal and ileal sections, and duodenal glands aid the digestive process by secreting digestive proteolytes, mucus and bicarbonate (Dworken et al. , Krause 2000, Betts et al. 2013). Except for the initial part of the duodenum, folds in the mucosal membrane can be found along the entire small intestine and contribute to increase the surface area available for nutrient uptake by specialized intestinal cells (Dworken et al. , Stubbs et al. 2015). Absorption of nutrients is mainly performed by jejunal enterocytes, owing to larger membrane pores and the differential expression profiles of transporter proteins (Takeuchi et al. 2004, Anderle et al. 2005, Thompson et al. 2017). Smaller pores in the membranes of ileal enterocytes allow for absorption of water and the

remainder nutrients, bile acids and vitamins from luminal contents. The residual material is ultimately discharged into the colon, where it is processed and stored before defecation (Dworken et al. , Betts et al. 2013, Volk et al. 2017).

1.2 The role of intestinal epithelial cells in digestive processes and mucosal immunity

As previously mentioned, at least 7 types of epithelial cells are known to constitute the small intestinal epithelium, in which only five are well-characterized (Barker et al. 2008). Enterocytes represent the most abundant cell type in both the small intestine and colon (Noah et al. 2011) and has the crucial task of nutrient-, salt- and water-absorption from luminal contents (Barker et al. 2008, Sato et al. 2013). The apical membrane of enterocytes have protrusions known as microvilli, which together with the morphology of the intestine increase the absorptive surface area of the intestine (Snoeck et al. 2005, Drozdowski et al. 2010). At the same side of the enterocytic membrane, negatively charged glycoproteins form a thick and filamentous brush border containing pancreatic- and intramembrane digestive enzymes. The brush border act as a diffusion barrier by restricting the contact between the membrane and luminal particles, chemicals, bacteria and viruses, in addition to providing a degradative environment that enhances digestion and nutrient absorption (Snoeck et al. 2005). Based on these functional properties, enterocytes are categorized to the absorptive lineage, diverging from the other epithelial cell types. Enteroendocrine cells, goblet cells, Paneth cells and tuft cells belong to the secretory lineage of epithelial cells (Noah et al. 2011). Their key roles range from sensory functions to protective mechanisms, involving the generation of a physical barrier, secretion of effector molecules and modulation of the immune system (Barker et al. 2008, Worthington 2015).

All components required for innate and adaptive immunity are found close to intestinal epithelial cells. Immune cells are present in the lamina propria and in immune structures emanating from the submucosa into the epithelium (Kalff et al. 1998, Yoo et al. 2017). One type of immune structure present exclusively in the small intestine during homeostasis are Peyer's patches. These small aggregates of lymphoid tissue harbor lymphocytes, which can be stimulated by antigens delivered by small intestinal M cells (Lelouard et al. 2012, Yoo et al. 2017). Antigen-sampling is also performed by enterocytes, where molecules can be processed and presented to T-lymphocytes or transcytosed into the cardiovascular system (Snoeck et al. 2005, Yoo et al. 2017).

The role of IECs in mucosal immunity is not restricted to the sampling of antigens. The microbial metabolite- and nutrient-sensors of the intestine, the enteroendocrine cells (EECs),

produce and secrete hormones in response to certain stimulants. The ultimate purpose of the secreted products is either to attain ideal conditions for nutrient absorption, regulate satiation or directly orchestrate intestinal immune responses (Moran-Ramos et al. 2012, Worthington 2015). The positioning of the EECs are closely related to immune cell location (Qhang et al. 2012), giving them a prime opportunity to influence the immune system directly. EECs have been shown to be key producers of cytokines and immunomodulatory serotonin, affecting antigen-presentation, cellular recruitment, phagocytosis and cytokine secretion by immune cells (Worthington 2015, Yoo et al. 2017). Similar functions are present in tuft cells; the chemosensors of the gut. Tuft cells relay information on luminal contents to immune cells or neurons by the secretion of cytokines (Noah et al. 2011, Haber et al. 2017), and are known inducers of type 2 immune reactions towards parasitic infections (Gerbe et al. 2016, Howitt et al. 2016, Yoo et al. 2017). Through these processes, the intestinal epithelial cells relay vital information to the immune system.

Further protection of the gut epithelium is enforced by Paneth- and goblet cells. When microbe-associated molecular patterns are recognized, secretory vesicles in Paneth cells degranulate and release antimicrobial peptides. The bactericidal products, such as lysozyme (Lyz) and angiogenin-4, restrict bacterial growth and protect the small intestinal crypts (Noor et al. 2016, Yoo et al. 2017). The protection given by Paneth cells is aided by a physical barrier provided by goblet cells (Hansson 2012). Mucus, a viscous fluid composed of water and glycan-covered Mucin 2 (MUC2)-proteins, protects the intestinal epithelial surface (Hansson 2012). Bacteria become trapped by the adhesiveness and high binding-affinity of the mucus to specific molecules present on these microbes and are eventually cleared away through the flow of mucus and peristalsis. Furthermore, the mucus separate the epithelium from potentially harmful pathogens and chemicals found at the luminal side of the intestine (Hansson 2012, Murphy et al. 2017). Through these mechanisms, the epithelial cell types each contribute to mucosal immunity and protection of the gut.

1.3 Proliferative capacity of intestinal stem cells maintain intestinal homeostasis

To maintain structural- and functional integrity under the stressful and potentially harmful conditions of the gut, the intestinal epithelium requires a constant production of epithelial cells. The intestinal epithelium is the fastest self-renewing epithelium in mammals (Sato et al. 2009) and has a turnover rate of less than a week (Barker et al. 2007). The only exception is the longer-cycling Paneth cells, which have a longevity of 3-8 weeks in murine intestines (Bjerknes et al. 1981, Ireland et al. 2005). The intestinal stem cell (ISC) pool located at the bottom of crypts

fuel the production of epithelial cells by generating one daughter stem cell and one transit-amplifying (TA) cell after a cycling time of app

roximately 24 hrs (Potten et al. 1987, Barker et al. 2007). Together, the proliferative ISCs and TA cells generate 300 cells/crypt every day in murine intestines (Potten et al. 1987, Marshman et al. 2002), providing a continuous replenishment of damaged or lost cells. A result of the continuous production of epithelial cells is the migration of the transit-amplifying- and differentiated cells along the crypt-villus axis, where secreted signaling factors and the death of pre-existing epithelial cells are additional mechanisms driving the migration process (De Santa Barbara et al. 2003, Williams et al. 2015). It is during the migration that the progenitor cells transition to a differentiated cell type (De Santa Barbara et al. 2003, Drozdowski et al. 2010). The TA cell commit to a differentiation program after three cell divisions, and reach a terminal differentiated state after a total of six generations (Marshman et al. 2002, Barker et al. 2008). The maturation of the cell to a specific differentiated state is complete when the cell reaches the crypt-villus junction (De Santa Barbara et al. 2003). The mature cell then continues on its journey to the villus apex (De Santa Barbara et al. 2003, Drozdowski et al. 2010), where it ultimately undergoes anoikis and is shed into the gut lumen (Alberts et al. 2014). However, there is one exception: Paneth cells. Paneth cells migrate in the opposite direction, towards the crypt bottom (De Santa Barbara et al. 2003, Barker et al. 2007, Sato et al. 2011, Sato et al. 2013). At the crypt base, Paneth cells secrete crucial factors involved in antimicrobial protection, crypt formation and stem cell maintenance, including WNT (Noah et al. 2011, Sato et al. 2011).

1.4 Distinct signaling pathways and effector proteins regulate proliferation and differentiation of intestinal epithelial cell lineages

Differentiation of intestinal epithelial cells has proven to be a complex process and has yet to be fully characterized. At the present time, factors involved in cell lineage specification range from epigenetic regulators to signaling pathways. Examples to the latter are the Wnt- and Notch signaling pathways: The drivers of development, proliferation and differentiation of the intestinal epithelium (De Santa Barbara et al. 2003, Elliott et al. 2015, Schaefer et al. 2019).

The canonical Wnt-pathway has been shown to control the proliferation of ISCs, through the alteration of the transcriptional program of target cells (Schaefer et al. 2019). Wnt-ligands act in an autocrine and paracrine manner, where they travel short distances to target cells and form complexes with their complementary membrane-bound receptor (Mah et al. 2016). The downstream signaling prevent targeted degradation of β-catenin by a destruction complex,

allowing β-catenin to translocate to the nucleus. Here, the effector protein is able associate with transcription factors to cause transcriptional activation of target genes (Mah et al. 2016, Schaefer et al. 2019). In the presence of Wnt-antagonists and deletion of Wnt-receptors, inactive Wnt-signaling lead to loss of crypts, reduced proliferative potential of ISCs and defects in Paneth cell development (Pinto et al. 2003, van Es et al. 2005). Thus Wnt-signaling is a critical regulator of intestinal architecture, stem cell maintenance and differentiation of the secretory cell lineage.

In contrast to the Wnt signaling pathway, Notch-signaling affect cellular differentiation programs through a process of intercellular lateral inhibition. Notch-signaling is activated by the interaction between membrane-bound Notch-receptors and their respective Delta ligands on receptor-expressing and ligand-expressing cells, respectively (De Santa Barbara et al. 2003, Elliott et al. 2015, Sancho et al. 2015). The activation of the Notch pathway results in the proteolytic cleavage of a Notch-receptor intracellular signaling fragment (NICD), which translocates to the nucleus to form a transcriptional activation complex. One of the genes activated codes for a transcription factor in the protein family Hairy and Enhancer of Split (HES family): HES-1. By repressing the gene encoding the transcription factor Atonal homolog-1 (ATOH1), HES-1 indirectly downregulates the expression of the Notch-ligand Delta (De Santa Barbara et al. 2003, Noah et al. 2011, Sancho et al. 2015). In the adjacent signal-transmitting cell, Notch-signaling levels are low, resulting in an enhanced production of Delta. The minor inhibitory signaling in the ligand-expressing cell amplifies the cellular differences and the ultimate differential program: Notch-high TA cells commit to the absorptive cell lineage while stimulating neighboring cells to differentiate into the opposite fate in the absence of Wnt-signaling (Noah et al. 2011, Yin et al. 2013, Sancho et al. 2015). If both Wnt- and Notch-signaling is activated, ISCs are retained in an undifferentiated and proliferative precursor state (Yin et al. 2013). Cell fates are thereby specified by the activity of the two signaling pathways during embryogenesis and in adulthood (Verzi et al. 2008, Noah et al. 2011, Demitrack et al. 2016).

Although Wnt- and Notch-signaling are involved in the differentiation of cell types, further maturation of epithelial cells relies on additional factors specifying each cell type. The expression and activity of the ATOH1-protein is one of the early cell lineage specification factors, regulated by the aforementioned signaling pathways. The protein undergoes strict transcriptional regulation by HES1, where the balance between the absorptive or secretory cell fate is regulated by HES1 and ATOH1, respectively (D'Angelo et al. 2010, Noah et al. 2011, Sancho et al. 2015). An additional layer of ATOH1-regulation is given by Wnt-signaling, where

activation of the pathway cause a degradation shift from β-catenin to ATOH1 (Tsuchiya et al. 2007, Noah et al. 2011, Peignon et al. 2011). Expression of both the Delta-like 1 (*Dll1*) ligand (Basak et al. 2014) and active ATOH1 specify the early secretory progenitor transcriptional program, where the ATOH1-dependent expression of the transcription factor Growth factor independent protein 1 (GFI1) guide the early secretory progenitors towards a Paneth- and goblet cell fate. This is mediated through the repression of the EEC-specifying *Neurogenin 3* gene (*Neurog3*) by GFI1, diverging the secretory progenitor from the enteroendocrine fate (Shroyer et al. 2005, Bjerknes et al. 2010).

Several other factors are involved in intestinal epithelial differentiation and maturation. The Hepatocyte nuclear factor 3-alpha and -beta (HNF-3A and HNF-3B, respectively) have been implicated to guide differentiation towards the goblet- and enteroendocrine cell types, with factors such as NEUROG3 and the Zinc-finger transcription factor Kruppel-like factor 4 (KLF4) determining the enteroendocrine- and goblet cell fate, respectively (Jenny et al. 2002, Katz et al. 2002, Ye et al. 2009). Furthermore, SAM pointed domain ETS factor (SPDEF) and the SRY-box 9 proteins (SOX9) have been proposed to be involved in the terminal maturation of goblet- and Paneth cells (Bastide et al. 2007, Gregorieff et al. 2009, Noah et al. 2010). These factors are not essential in the differentiation of Tuft cells, which instead require the POU domain class 2 transcription factor 3 gene (*Pou2f3*) for its specification (Gerbe et al. 2011, Gerbe et al. 2016). For the absorptive cell maturation, differentiation have been shown to be induced by the Indian hedgehog-signaling (IHH) pathway (De Santa Barbara et al. 2003, Kosinski et al. 2010), with alterations at the epigenetic, transcriptomic and proteomic level driven by the nuclear receptor HNF-4-gamma (HNF-4G) (Lindeboom et al. 2018). Further maturation of the absorptive cell lineage depends on the expression of the Forkhead box protein M1 (FOXM1), the Max dimerization protein 3 (MXD3) (Haber et al. 2017) and the presence of the Protein tyrosine kinase 6 (PTK6) (Haegebarth et al. 2006). Thus, differentiation and specialization of the epithelial cell types rely on an intricate intracellular and cell-cell signaling network requiring precise expression and activity to commit a cell to a distinct fate. A complete overview of all factors involved in the differentiation process are given in figure 1.3.

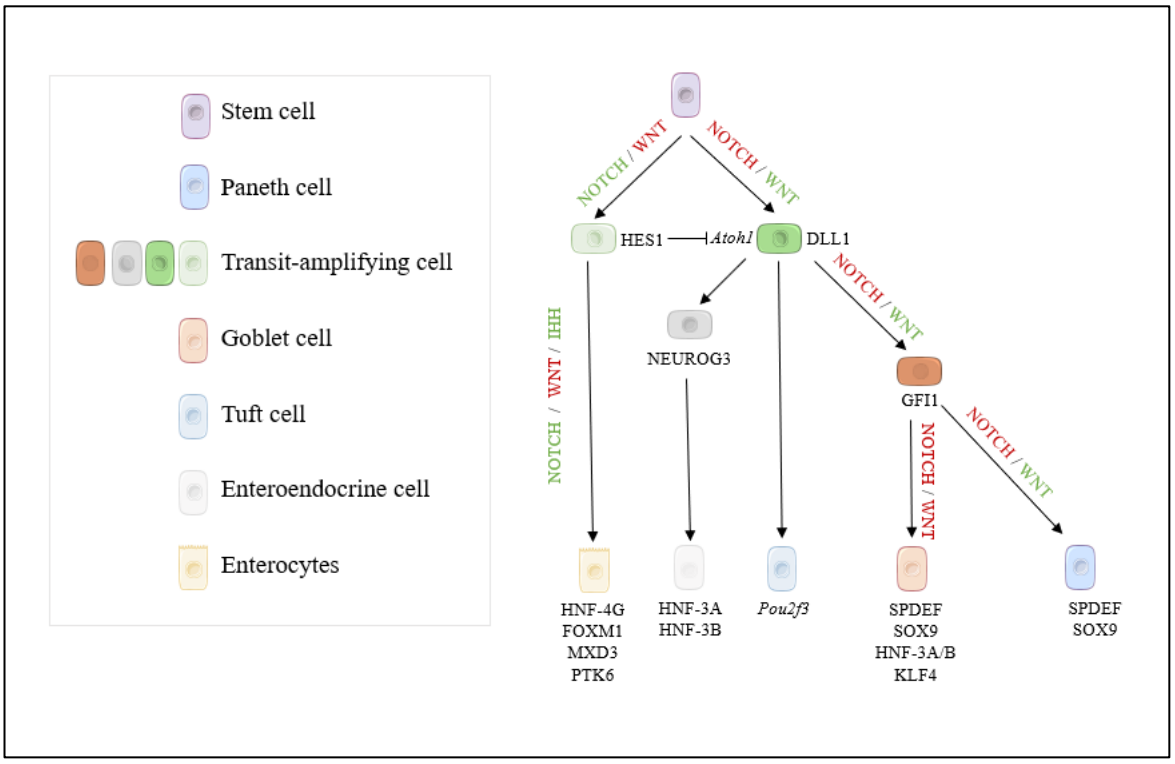

Figure 1.3: Intestinal epithelial differentiation
Maturation of epithelial cells constituting the intestinal epithelium require a complex interplay between signaling pathways and transcription factors. Active Notch- and Wnt-signaling maintain stem cells in a proliferative state. If Wnt-signaling becomes inactive, *Hes1*-transcription inhibits the production of the secretory cell lineage determinant ATOH1, ultimately resulting in the development of enterocytes in combination with active IHH-signaling. In the opposite case, *Atoh1*- and *Dll1*-transcription guide the progenitor cell towards the secretory lineage. Notch- and Wnt signaling further specifies goblet- and Paneth cell fate, through a common GFI1-expressing progenitor. SOX9 and SPDEF have been shown to induce Paneth- and goblet cell maturation, with the additional factors HNF-3A, HNF-3B and KLF4 maturing the goblet cell progenitor. Like goblet cells, enteroendocrine cells require the hepatocyte nuclear factors in addition to the EEC-specifying NEUROG3-protein for their differentiation. None of these factors are involved in the maturation of tuft cells, which rely on the gene *Pou2f3*.
Legends for cells and their colors are given to the left.

1.5 Proper murine intestinal development ensures epithelial structure and function

The commitment of a cell to a specific differentiation program is a process that originates in the embryo. By the end of the murine gestational period (19-21 days) (Murray et al. 2010), the embryonic intestine needs to be able to fulfill its roles and cope with the challenges presented by the unsterile external environment. The correct spatiotemporal development, organogenesis and differentiation is therefore a vital process to ensure proper morphology and function of the intestine (Ganz et al. 2018).

Intestinal morphogenesis begins at the transition from early-to-mid gestation. The first sign of an intestinal form appear as a primitive gut tube at 7.5-9.5 days post-fertilization, which is formed through the intubation and fusion of the endodermal layer along the anterior-posterior axis (Noah et al. 2011, Spence et al. 2011). By embryonic day 14.5 (E14.5), the intestinal epithelium has transitioned from an undifferentiated pseudostratified form to a stratified columnar cell lining (Grosse et al. 2011, Spence et al. 2011), which is followed by major epithelial reorganization. Elevations in the mesenchyme towards the gut lumen generate villi in a "wave"-like fashion from the duodenum to the colon (Sharbati 1982, Yang et al. 2001) and features of the lamina propria and the muscularis mucosae become distinguishable from the mesenchymal compartment (Sharbati 1982, Yang et al. 2001). At E16.5, villi-structures and intervillous regions are evident (Spence et al. 2011), with highly proliferative epithelial cells fueling the growth of the intestinal compartment and villi. At the same late-gestational phase, presence of differentiated cell types can be detected, including goblet cells, enteroendocrine cells and enterocytes. In contrast, Paneth- and tuft cells do not develop before the end of the first postnatal week (P7) (Bry et al. 1994, Jenny et al. 2002, Gerbe et al. 2011, Yanai et al. 2017). After birth, the tissue mass, length and girth of the intestine increase considerably (Bry et al. 1994, Dehmer et al. 2011, Aust et al. 2013). Crypts start to develop at P5, and the proliferative cells of the intestinal epithelium become restricted to the crypts (Bry et al. 1994). Crypts elongate from their emergence and into adulthood, and can reach depths up to 125 μm in the adult intestine (Gulbinowicz et al. 2004, Dehmer et al. 2011, Muncan et al. 2011, Yanai et al. 2017). Comparably, villi heights increase considerably during intestinal epithelial development, reaching lengths in the range of 200-600 μm in the full-grown murine intestine (Gulbinowicz et al. 2004, Dehmer et al. 2011, Wołczuk et al. 2011). Intestinal epithelial development continues through the suckling-to-weaning transition at P14-P28, resulting in a mature, full-grown intestine by P42-P56 (Dehmer et al. 2011, Muncan et al. 2011).

The development of the intestine is orchestrated by growth factors and transcriptional regulators working together or in parallel to ensure proper intestinal formation, patterning, morphology and cellular differentiation (Noah et al. 2011). The caudal-related homeobox transcription factor CDX2 is one of the early specification factors determining the intestinal fate and is a master regulator of intestinal epithelial development (Gao et al. 2009). The deletion of *Cdx2* in the gut epithelium result in impaired development of the colon, stunted villi, a reduction in the number of small intestinal enterocytes and the complete absence of enteroendocrine- and goblet cells (Gao et al. 2009, Verzi et al. 2010, Verzi et al. 2011). Similarly, the GATA-binding- and FOX-protein families of transcription factors are required

for proper intestinal development (Spence et al. 2011). A deficiency in these transcription factors result in abnormal gut morphogenesis and alterations in the level of secreted morphogens, such as WNT. Wnt-signaling is a driver of intestinal elongation and morphogenesis, increasing the girth and length of the primitive gut tube in the mid- and late-gestational period (Spence et al. 2011). A high-to-low gradient of WNT-proteins along the anterior-posterior axis lead to the segmentation of the intestine into the duodenal, jejunal, ileal and colonic compartments (Sherwood et al. 2011, Chin et al. 2017), and a similar expression pattern is found along the crypt-villus axis of the adult intestine (Mah et al. 2016). Furthermore, active Wnt-signaling direct the differentiation of epithelial cells and the postnatal formation of crypts (Pinto et al. 2003, van Es et al. 2005, Mah et al. 2016).

The development of intestinal structures and the differentiation of epithelial cell types are further controlled by the epigenetic regulation of gene accessibility and transcriptional activity (Spence et al. 2011, Elliott et al. 2015). Epigenetic factors regulate gene accessibility and transcriptional activity without altering the DNA-sequence itself, either by changing the chromatin structure or recruiting histone-modifying enzymes (Ganz et al. 2018). One well-known type of epigenetic mechanism is the methylation of DNA-residues. DNA-methylation is a vital process in mammalian development (Elliott et al. 2015), such as in the case of DNA-methyl transferase 1 (DNMT1): DNMT1-deficient mice die within a couple of weeks after birth. Furthermore, these mice have intestinal defects and cellular abnormalities, such as shorter intestinal lengths, mislocalization of Paneth cells and a reduction in goblet- and proliferative cells (Yu et al. 2015). The post-translational covalent modification (PTMs) of the nucleosome core proteins H2A, H2B, H3 or H4 is another type of epigenetic mechanism that can impact intestinal epithelial development (Bernstein et al. 2002, Ganz et al. 2018). PTMs mainly occur at the N- or C-terminal of histone tails, like acetylation, methylation, phosphorylation, and ubiquitination and act as positive or negative regulators of transcription depending on the type and location of the modification (Bernstein et al. 2002, Ganz et al. 2018). The acetylation of histone tails is associated with an increase in gene expression (Elliott et al. 2015, Kazakevych et al. 2017), and is frequently found on histones present at promoters and other regulatory regions (Kazakevych et al. 2017). Histone acetylation is regulated by histone acetyltransferases (HATs) and histone-deacetylases (HDACs), and is a mechanism used in the regulation of intestinal epithelial development (Spence et al. 2011, Bell et al. 2013). The p300 HAT, for instance, prevents premature development of villi and differentiation of epithelial cells. On the other hand, HDAC1 and -2 are required for proper crypt morphogenesis, maintenance of proliferative capacity and repression of the enterocytic cell fate (Tou et al. 2004, Spence et al.

2011, Zimberlin et al. 2015, Roostaee et al. 2016). The differentiation of the absorptive cell lineage is also controlled by the methylation status of histone tail residues (Benoit et al. 2012, Roostaee et al. 2016). The trimethylation of lysine 27 on histone 3 (H3K27) by the Polycomb repressive complex 2 (PRC2) result in a compact chromatin state, and are frequently found on genes involved in embryonic development and secretory cell differentiation (Benoit et al. 2012, Roostaee et al. 2016, Kazakevych et al. 2017). Together, these factors are crucial for the proper development of a well-functioning intestinal epithelium.

1.6 Lysine-specific demethylase 1 – A regulator of intestinal epithelial development and cell lineage specification?

Developmental biology has been a field of research for decades, and has given valuable insight into the fundamental mechanisms driving different developmental processes (Spence et al. 2011, Elliott et al. 2015). Lysine-specific demethylase 1 (LSD1) is an epigenetic modifier that has been a prime subject for research since its discovery in 2004, owing to its widespread expression across several organ systems and implication in embryo- and carcinogenesis (The Human Protein Atlas , Shi et al. 2004, Foster et al. 2010, Ding et al. 2013). LSD1 is present in tissues such as the reproductive organs, immune system and gastrointestinal tract, and has been proven to be essential for embryonic development, as *Lsd1*$^{-/-}$ mice display embryonic lethality at E6.5 (The Human Protein Atlas , Wang et al. 2007). Furthermore, LSD1 is involved in the maintenance of stem cell pluripotency, proliferation and cellular differentiation (Wang et al. 2007, Adamo et al. 2011, Haines et al. 2018, Tosic et al. 2018).

LSD1 functions as a transcriptional regulator by a flavin-dependent oxidative process, where covalently bound monomethyl- (me1) and dimethyl-groups (me2) on lysine residues 4 and 9 at histone 3-tails are removed (i.e. H3K4 and H3K9, respectively) (Shi et al. 2004, Greer et al. 2014). The process of demethylation is shown in fig. 1.4. However, demethylation is not performed by LSD1 alone. LSD1 associates with different complexes to regulate transcription, including the Corepressor of the Repressor Element-1 Silencing Transcription factor (CoREST) repressive complex and the androgen receptor (AR) activation complex. The binding partners of LSD1 determine the specificity and activity of the demethylase, and the specificity is further affected by PTMs in the vicinity of the substrate (Bernstein et al. 2002, Shi et al. 2004, Forneris et al. 2006, Krishnan et al. 2011).

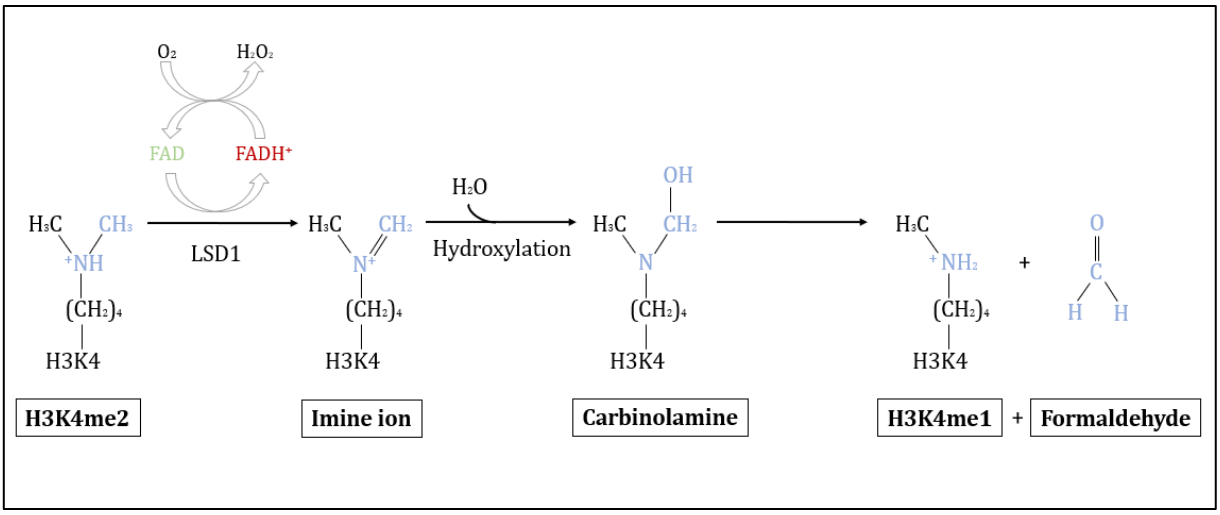

Figure 1.4: The catalytic process of demethylation by LSD1
LSD1, along with the cofactor flavin adenine dinucleotide (FAD), oxidize the substrate methyl group (blue) to a corresponding imine ion. The subsequent hydrolyzation remove the methyl-group in the form of formaldehyde, through an unstable intermediate carbinolamine (Shi et al. 2004, Clood et al. 2008). Here, the substrate H3K4me2 becomes demethylated to H3K4me1.

The epigenetic regulation by the LSD1-complex is frequently associated with either transcriptional repression or -activation, where the demethylation of H3K4me2 and H3K9me2 correlate with the former and latter cases (Bernstein et al. 2002, Shi et al. 2004, Forneris et al. 2006, Krishnan et al. 2011). In human embryos, stem cells are maintained in a pluripotent form by the demethylation of H3K4me2 and the resultant transcriptional repression of differentiation genes (Adamo et al. 2011). LSD1 have the opposite function in embryonic stem cells of mice, where it is required for proper differentiation of embryonic cells. Mouse embryonic stem cells deficient of LSD1 show an increase of H3K4me2, has premature expression of developmental genes and defects in early embryonic differentiation (Wang et al. 2008, Foster et al. 2010). Furthermore, LSD1 has been shown to regulate the mono- and dimethylation patterns during differentiation of B-lymphocytes to plasmablasts in adult mice, functioning as a repressor by affecting the accessibility of chromatin (Haines et al. 2018).

Although LSD1 has been studied for more than a decade, little is known about its role in intestinal epithelial development and cell lineage specification (Ganz et al. 2018). However, the Oudhoff group has started to discover its function in these processes. Unpublished results by the Oudhoff lab group has uncovered major alterations to the intestinal epithelial cell types in a tissue-specific *Lsd1*-knockout model. The deletion of *Lsd1* in the intestinal epithelium resulted in abnormal quantities of stem cells and differentiated cell types. *Lsd1*$^{\Delta IEC}$ mice

completely lacked Paneth cells, whereas an increase in stem cell numbers were observed (fig. 1.5). However, the effects during development had not been investigated.

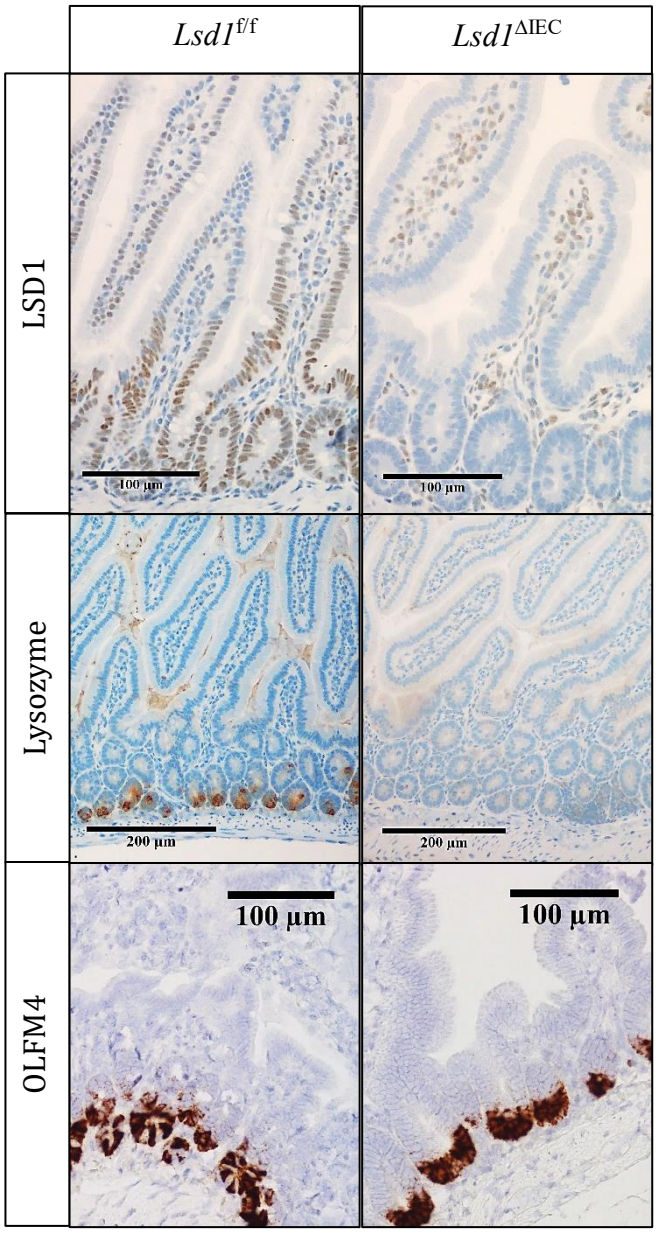

Figure 1.5: LSD1-, Paneth cell- and stem cell staining in adult Lsd1$^{f/f}$- and Lsd1$^{\Delta IEC}$-mice

Upper panel show representative IHC-stainings of LSD1 in the duodenum of wildtype (Lsd1$^{f/f}$) and knockout (Lsd1$^{\Delta IEC}$) mice. Scalebar: 100 µm.

Middle panel display IHC-staining of the Paneth cell marker Lysozyme in *Lsd1*$^{f/f}$ vs. *Lsd1*$^{\Delta IEC}$ duodeni. Scalebar: 200 µm.

Last panel: In situ hybridization of the stem cell marker Olfactomedin 4 (OLFM4) in the crypts of *wildtype* and *knockout* duodeni.

Scalebar: 100 µm.

(Unpublished data by Rosalie Zwiggelaar)

2.0 Aims of the Study

Even though biochemical mechanisms, tissue distribution and phenotypic traits governed by LSD1 have been studied for more than a decade, current knowledge on its expression and effects on the cellular composition of the intestinal epithelium is limited. Investigation on the role of LSD1 in the intestinal epithelium was initiated prior to this project, where the Oudhoff lab group had uncovered major alterations in intestinal epithelial cell types of adult *Lsd1*$^{\Delta IEC}$ mice. The intestines of these mice lacked Paneth cells and a resultant increase of stem cells at the base of crypts were observed. As the study revolved around the mature intestine, its effects during intestinal development remained unexplored. In regard to these findings, the aims of the project were as follows:

- Do *wildtype* mice display a uniform LSD1-expression pattern during development?
- From which developmental timepoint does alterations in intestinal epithelial cell types originate?
- Through which mechanisms does LSD1 inhibit Paneth cell differentiation?

3.0 Materials and Methods

3.1 Buffers, kits, materials and reagents

Table 3.1: Materials and reagents

Method	*Name*	*Manufacturer*	*Catalogue Number*
Genotyping	6x Orange DNA Loading Dye	ThermoFisher Scientific	R0631
	GelRed® Nucleic Acid Stain, 10000x	Biotium	41003
	GeneRuler 100 bp DNA Ladder	ThermoFisher Scientific	SM0241
	GeneRuler 1 kb Plus DNA Ladder	ThermoFisher Scientific	SM1331
	KAPA Mouse Genotyping Kit	Roche	KK7301
	KAPA2G Fast HotStart Genotyping Mix with dye	Roche	KK5621
General reagents	Ethanol ≥70% (v/v), TechniSolv®	VWR	83801.290
	Etanol, GPR Rectapur®	VWR	20824.296
	Ethanol absolute ≥99.8%, AnalaR Normapur®	VWR	20821.310
	Hematoxylin cryst. (C.I. 75290)	Merck	1043020100
	Hydrogen peroxide 30% (Perhydrol®) for analysis, Emsure®	Merck	1072091000
	Neo-Clear® (xylene substitute) for microscopy	Merck	1098435000
	Superfrost® Plus	Menzel-Gläser	631-9483
H&E-staining	Eosin Y (yellowish), Certistain®	Merck	1159350100
	Neo-Mount® Anhydrous Mounting Medium for microscopy	Merck	1090160500

Immunhistochemistry	Anti-DCAMKL1 antibody	abcam	ab31704
	Blimp-1 (5E7)	Santa Cruz	sc-130917
	Dako REAL™ EnVision™ Detection System, Peroxidase/DAB+, Rabbit/Mouse	Dako	K5007
	Di-Methyl-Histone H3 (Lys4) (C64G9) Rabbit mAb	Cell Signaling Technology	9725S
	EnVision+ System- HRP Labelled Polymer Anti-Rabbit	Dako	K4003
	Glycergel®, Aqueous Mounting Medium	Dako	C056330-2
	Lsd1 (C69G12) Rabbit mAb	Cell Signaling Technology	2184
	Mucin 2 (H-300)	Santa Cruz	sc-15334
	Polyclonal Rabbit Anti-Human Lysozyme EC 3.2.1.17	Dako	A0099
	SP-1 Chromogranin A (Porcine) Antibody	immunostar	20086
	Tween® 20 (Polysorbate), Technical	VWR	28829.296
Immunofluorescence	Anti-Actin, α-Smooth Muscle - Cy3™ mouse monoclonal antibody	Sigma-Aldrich	C6198-2mL
	Bovine Serum Albumin	Sigma-Aldrich	A7906-500G
	Elite Mini PAP Pen	DBS	K042
	Fluoromount-G™	invitrogen	00-4958-02
	Goat Anti-Rabbit IgG (H+L) Alexa Fluor 488	invitrogen	A-11034
	Hoechst 33342 Solution (20 mM)	ThermoFisher Scientific	62249
	Ki-67 Antibody (SP6)	ThermoFisher Scientific	MA5-14520
	Lsd1 (C69G12) Rabbit mAb	Cell Signaling Technology	2184
	Normal Goat Serum Blocking Solution	Vector laboratories	S-1000
	Olfm4 (D6Y5A) XP® Rabbit mAb (Mouse Specific)	Cell Signaling Technology	39141S
	Triton® X-100	Merck	1086031000
	Ulex UEA I Rhodamine	Vector Laboratories	RL1062

Tissue preparation	Biopsy processing/embedding cassettes, Slimsette®, M510	VWR	720-1599
	Bonn Micro Forceps	FST	11083-07
	Formaldehyd 4% stabilised, Technical, buffered (pH 7.0 ± 0.2)	VWR	9713.1000
	McPherson-Vannas Micro Dissecting Spring Scissors	Roboz Surgical Store	RS-5600
	Metal base moulds, 15x15x6 mm	VWR	LEIH3803081
	Microsurgical Kits, Integra™ Miltex	Integra® Miltex®	95042-540
	VWR® Q Path® biopsy pads	Q Path	720-2254E

Table 3.2: Self-made batches

Method	*Solutions*	*Constituents*	*Quantities*
Immunohistochemistry	Primary antibody diluent (IHC)	Bovine serum albumin	0,5%
		Tris-buffered saline stock	99,25%
		Tween	0,25%
	DAB solution	Dako REAL™ Substrate Buffer	20 µL
		Dako REAL™ DAB+ Chromogen	1000 µL
	Ethanol (80%)	Ethanol	96%
		Distilled water	16%
	Hydrogen peroxide (3%)	Hydrogen peroxide	30%
		Distilled water	70%
	Wash buffer (TBST)	Tween (20x)	0,5 mL
		Tris-Buffered Saline (10x)	100 mL
		Distilled water	900 mL
Immunofluorescence	Blocking buffer	NGS	2%
		BSA	1%
		Triton X-100	0,2%
		Tween	0,05%
		PBS	96,3%
	Primary antibody diluent (IF)	NGS	1%
		BSA	0,5%
		Triton X-100	0,2%
		PBS	Variable
		Primary antibody	Variable
	Secondary antibody diluent	Normal goat serum	1%
		Bovine serum albumin	0,5%
		Triton X-100	0,2%
		Tween	0,025%
		PBS	98,275%
	Wash buffer (1)	Tween	0,2%
		PBS/TBS	99,8%
	Wash buffer (2)	Tween	0,15%
		PBS/TBS	99,85%

Table 3.3: Genotyping primers

Primers	*Sequence*
Lsd1-Flox, Forward	5'-TTG AGT TGG TTG TGA GTC AC-3'
Lsd1-Flox, Reverse	5'-AGC GCT AAC TTT AGA GCT GG-3'
Cre, Forward	5'-GCG GTC TGG CAG TAA AAA CTA TC-3'
Cre, Reverse	5'-GTG AAA CAG CAT TGC TGT CAC TT-3'

Table 3.4: Immunodetection parameters

Antibody	*Dilution*	*Diluent*	*Buffer*	*pH*	*DAB exposure*
Blimp-1		IHC antibody diluent	Citrate buffer	6	-
Chromogranin A	1:2000	IHC antibody diluent	Citrate buffer	6	40 sec.
DCAMKL1	1:500	IHC antibody diluent	Citrate buffer	6	1 min.
H3K4me2	1:1500	IHC antibody diluent	Citrate buffer	6	1 min.
Hoechst 33342	1:150	Secondary antibody diluent	-		-
Ki-67	1:250	IHC antibody diluent	Citrate buffer	6	-
Lsd1 (IHC)	1:100	Primary antibody diluent (IHC)	Citrate buffer	6	5+5 min.
Lsd1 (IF)	1:200	Primary antibody diluent (IF)	Citrate buffer	6	-
Lysozyme	1:750	IHC antibody diluent	Citrate buffer	6	1 min.
Mucin 2	1:400	IHC antibody diluent	Citrate buffer	6	2 min 10 sec.
Olfactomedin 4	1:500	IHC antibody diluent	Citrate buffer	6	-
Smooth muscle actin	1:300	Secondary antibody diluent	-		-
UEA-1	1:500	Secondary antibody diluent	-		-

3.2 Mice models

3.2.1 Terms and approval of animal experiments

All animal experiments were approved by the Norwegian Food Safety Authorities, and performed under the regulations on the use of animals in experiments (Landbruks- og matdepartementet 2015).

3.2.2 Developmental studies

Lsd1-floxed mice (Lsd1$^{f/f}$), kindly gifted to us by Dr. Stuart Orkin, were bred with B6.Cg-Tg(Vil1-cre)997Gum/J mice harboring the *Villin-Cre* transgene (#004586, The Jackson Laboratory) to generate offspring with an intestinal epithelium deficient of *Lsd1* (*Lsd1*$^{\Delta IEC}$). The tissue-specific knockout-model is attained through the expression of the CRE recombinase, directed under the promoter of the epithelial-specific *Vil1*-gene. The presence and activity of the recombinase induces deletion of the lox-P-flanked *Lsd1*-gene, to generate *Lsd1*-knockout in villi and crypts of the intestinal epithelium (The Jackson Laboratory).

3.3 Genotyping

Genotyping is a method commonly used to study the presence or absence of a specific DNA-sequence or gene, identifying genotype-phenotype correlations. The method provides valuable information in both clinical and research laboratories worldwide (Helling et al. 1974, Tümmler 2014, Rowan et al. 2017).

3.3.1 Background

To perform genotyping on eukaryotic organisms, genetic material needs to be extracted from the cellular and nuclear lipid envelope and purified from other cellular components. Lipid membranes can be disrupted by heat-induced increase in membrane fluidity, breakage of disulfide bonds by redox reagents, or detergents. The heat-induced DNA-extraction method carry an advantage compared to others, as high temperatures inactivate nucleases (Elkins 2013). After extraction, the genetic material can be subjected to sequence-specific, exponential amplification by the polymerase-chain reaction (PCR). The amplification of a specific DNA sequence (i.e. amplicon) by PCR stem from cycling processes of DNA-denaturation, primer-annealing and amplicon-elongation.

PCR reagents are carefully selected to attain appropriate conditions for these reaction steps, with a standard reagent mixture containing a DNA polymerase-specific buffer, DNA

polymerase, target-specific primers, deoxynucleotides, DNA template and PCR-grade water (Lorenz 2012). The different reaction steps in PCRs fluctuate in temperature, facilitating each step separately. At high temperatures such as 95°C, heat-induced denaturation of double-stranded DNA to single stranded templates occur. Cooler temperatures around the 50-65°C range allow for the target-specific forward- and reverse primers to anneal to their respective single-stranded templates. Thermally stable DNA polymerase act at temperatures of 70-80°C, elongating the complementary template sequence; the amplicon. The same three-step procedure cycle 20-40 times to generate an exponential increase of target-specific DNA products (Lorenz 2012, Tümmler 2014). The PCR products can be run through an agarose gel (Lee et al. 2012, Lorenz 2012, Rowan et al. 2017), which is a gelated buffer-dissolved powder forming a size-discriminatory porous network affecting the migratory length of DNA molecules. For visualization purposes, DNA-intercalating agents such as ethidium bromide or other substitutes are supplemented the agarose gel prior to gelification. The PCR products are loaded onto the agarose gel submerged in an appropriate buffer and subjected to voltage, resulting in the migration of the negatively charged DNA fragments towards the positively charged anode. The distance migrated is dependent on the size and conformation of the PCR product, type of agarose and its concentration, choice of electrophoresis buffer and voltage applied (Lee et al. 2012). The resultant "fingerprint" of the migrated DNA fragments can be visualized by UV-exposure, where samples are compared to reference sequences for the determination of the genotype (Lee et al. 2012, Tümmler 2014, Rowan et al. 2017).

3.3.2 Experimental procedure

DNA isolation of mice tissues was performed with the KAPA Mouse Genotyping Kit (KK7301, KAPA Biosystems). A mastermix constituting 88 µL PCR-grade water, 10 µL 10X KAPA Express Extract Buffer and 2 µL KAPA Express Extract Enzyme per sample was made, and 100 µL aliquoted to each tissue clip. The sample tissues were lysed at 75°C for 12 minutes, and inactivation of the enzyme performed at 95°C for 5 minutes. DNA extracts were aliquoted into 0.2 mL thin-walled PCR tubes with filter tips and subjected to amplification by PCR. To 1 µL DNA sample, 1.25 µL of both forward- and reverse primer, 12.5 uL 2X KAPA2G Fast (HotStart) Genotyping Mix with dye, and 9 µL PCR-grade water were added. The PCR was set to run for 35 cycles at 95°C (3 min) for denaturation, 95°C (15 s), 60°C (15 s) and 72°C (45 s) for annealing of primers and amplification, 72°C (3 min) for additional elongation and 4°C as cooling temperature. Product size and purity determination was performed after a 45 min. constant voltage (120 V) gel electrophoresis on a 2% agarose gel supplemented 0,01% GelRed

in 1x TAE buffer, with a 1 kb or 100 bp DNA ladder and controls for wildtype and mutant genotypes. Visualization was performed with Gel Logic 212 Pro-system and imaged through the software Carestream MI SE.

3.4 Tissue preparation

After the euthanization of an animal, tissues of interest need be preserved in order to be maintained in a lifelike condition. After the circulation of blood has ceased, cells can remain alive by feeding on their internal energy supplies and anaerobic respiration. However, without the supply of nutrients, oxygen, and removal of toxic waste products, the cells eventually die. Organic matter from deceased animals can provide good growth conditions for fungal spores and bacteria, which may initiate anaerobic decomposition through the process of putrefaction. To avoid any structural- or cellular changes caused by post-mortem alterations, tissues need to be fixed in an appropriate fixing agent to effectively kill cells while maintaining cellular and structural integrity, inhibit enzymatic processes and prevent autolysis (Cook et al. 2015, Kim et al. 2016).

3.4.1 Background

A commonly used fixative is 4% formaldehyde (e. g. 10% formalin) (Cook et al. 2015). Formalin used in histopathological fixation is commercially sold in aqueous solutions consisting of formaldehyde dissolved in water supplemented methanol. The fixation process is initiated by the alcohol fixative, which mediates dehydration and hardening of the tissue. The fixation process is followed by a cross-linking phase mediated by the two forms of formaldehyde found in formalin; the non-hydrated formaldehyde and the hydrated methylene glycol. The two compounds rapidly penetrate the tissues and form stabilizing methylene bridges between proteins; the basis of fixation (Kiernan 2000, Thavarajah et al. 2012, Feldman et al. 2014). Depending on tissue size, reversible cross-linkages are completed 24-48 hrs after immersion, in which prolonged immersion give rise to stable, non-reversible covalent bonds. It is the nature of the initial reversible cross-linkages that provide the foundation of antigen retrieval in a variety of molecular techniques (Thavarajah et al. 2012).

To enhance tissue rigidity prior to sectioning and to maintain its structural integrity and architecture during long-term storage, formalin-fixed tissue samples are embedded in paraffin (Feldman et al. 2014). Formalin-fixed paraffin-embedded (FFPE) samples stored under normal conditions, dry at room temperature, retain antigenicity of biomarkers and maintain stable nucleic acids for extended periods of time, and provide satisfactory results for most antigens

used in immunostainings (Xie et al. 2011, Kim et al. 2016). FFPE samples are commonly sectioned at 3-7 um on a microtome, in which 4 um is the recommended thickness for immunohistochemical stainings (Yaziji et al. 2006, Luongo de Matos et al. 2010, Kim et al. 2016). Thus, sectioning of tissues provides 2-dimensional representations of the intricate 3-dimensional morphology and architecture of animal anatomy.

3.4.2 Experimental protocol

Intestines from embryos (E16.5), neonates (P0.5) and postnatal mice (P7, P14 and P21) were harvested as intact intestinal rolls or separate duodenal, jejunal, ileal and colonic swiss rolls, dependent on the fragility of the tissues and the method with the best preservation of intestinal structures. For the harvest of embryonic tissues, microsurgical tools were utilized, opposed to regular-sized dissection-equipment.

E16.5, P0.5 and P7 mice were euthanized by decapitation. Postnatal (P14, P21) and adult mice were euthanized by exposure to high levels of CO_2. Dissection forceps and scissors were used to cut into the abdomen of the mice to expose the inner organs. The intestine was identified, traced to the rectum distally and to the stomach proximally before detachment. The intestine was transferred to a flat, covered surface for further handling. The cecum was cut from the distal small intestine and proximal colon and discarded. The murine intestines were then flushed gently with cold phosphate-buffered saline (PBS) by an oral gavage-connected 20-50 mL syringe. Flushing was omitted on embryonic and neonatal tissues due to their fragile natures. Excess fat tissue or mesenteric connective tissue was removed using a pair of forceps. Tissues not processed were transferred to a PBS-filled reservoir, awaiting further handling. For swiss rolls, the small intestine was further divided into three sections of equal length constituting the proximal duodenum, mid jejunum and distal ileum. The intestinal segments were cut longitudinally, spread out with the luminal side up, and wrapped around a thin, wooden application stick, beginning with the proximal end. With the luminal side facing upwards, the intestine was rolled around to form a swiss roll and fixated in formaldehyde before transferring the tissues to embedding cassettes. Intact intestinal segments were rolled proximal end first onto a PBS-coated paper on a flat surface, gently wrapped, put into properly labeled embedding cassettes and fixated in formaldehyde. The tissues remained in formalin for 24-96 hrs, with subsequent processing by a Leica ASP300S tissue processor and embedding in molten paraffin. The paraffin blocks were sectioned at 4 μm by a microtome and collected on positively charged Superfrost™ slides. The sample sections were dried and stored at room temperature before use.

3.5 Immunohistochemical detection of epithelial cells and expression patterns

When a section of animal tissue is viewed under a microscope, it will lack contrast and appear colorless. To make the composition of the tissue or cellular components visible, staining is required (Cook et al. 2015). Immunohistochemistry is a method based on immunostaining - an exploitation of antibodies that specifically bind to antigens of interest, to visualize cellular, bacterial or viral components in tissues, ranging from nucleic acids to proteins (Luongo de Matos et al. 2010). The method cover identification confirmation, differential and exclusive roles in pathology (Luongo de Matos et al. 2010, de Nanassy et al. 2017), and provide a reproducible and reliable assay when performed on adequately fixed and processed paraffin-embedded tissues under standardized conditions (Lin et al. 2014).

3.5.1 Background

As the hydrophobicity of paraffin wax repels aqueous solutions used in staining techniques, the FFPE sections require dewaxing and rehydration prior to endogenous substance blocking and epitope retrieval. Hydrogen peroxide can be used to prevent interference from peroxidase activity on immunohistochemical results, as boiling does not affect peroxidase in the same manner as other endogenous enzymes. Enzyme-mediated or heat-induced epitope retrieval is essential to unmask target antigens for antibody-binding, by breaking cross-linkages caused by fixation (Chen et al. 2010). A following blocking buffer incubation step prevent nonspecific antibody binding and background staining. Primary and secondary antibodies are diluted in a buffer that promote antibody stability, uniform diffusion into the tissue sample and prevent nonspecific binding. Wash buffers used in-between application of antibodies are formulated to remove unbound or nonspecifically bound antibodies, with a minimization of signal interference (O'Hurley et al. 2014, Kim et al. 2016). For signal detection, a direct or indirect method with enzymes conjugated to the primary or secondary antibodies, respectively, are frequently used. In the presence of an appropriate substrate, the enzyme converts the substrate to a colored, insoluble precipitate at the target antigen's location (figure 3.1). The chromogenic DAB substrate used in this experiment produce a brown precipitate at the reaction site of the HRP-conjugated antibodies (O'Hurley et al. 2014, Kim et al. 2016). To provide contrast to the principal stain, counterstaining enable an easier visualization of morphological details of the surrounding tissue and analysis of stained targets. The resultant staining can be viewed by brightfield imaging or microscopy (O'Hurley et al. 2014), and compared to positive and negative controls to verify the staining results.

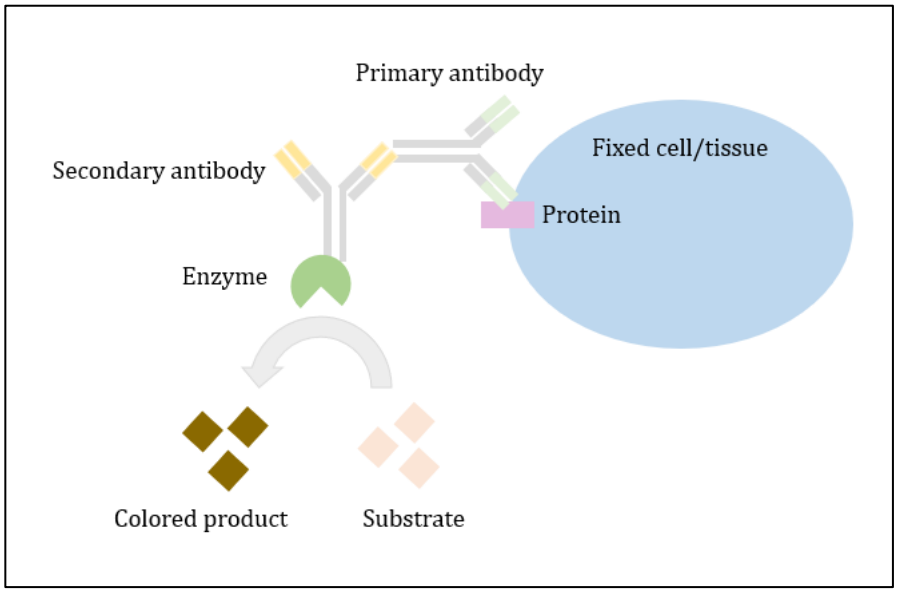

Figure 3.1: The principle of immunohistochemical stainings
The figure provides a schematic overview of the staining process. When a target protein on a fixed cell/tissue is recognized, the primary antibody binds to it. A secondary antibody targeting the primary antibody amplifies the signal, whereas its conjugated enzyme converts its substrate to a colored product at the reaction site.

3.5.2 Experimental procedure

To melt the paraffin, the sample-covered slides were arranged in a metal rack and placed in a heating cabinet at 60°C for 30 minutes. The slides were then deparaffinized in serial solutions; 2x10 min. in Neo-Clear®, 2x in absolute alcohol, and once through 96% ethanol, 80% ethanol and 70% ethanol for ~30 seconds each and rinsed for 5 min. in distilled water (dH_2O). Endogenous peroxidase activity was blocked by transferring the specimens to a solution of 3% hydrogen peroxide for 10 min., and rinsed in distilled water (dH_2O) for 5 min. The slides were further arranged in staining containers with the appropriate epitope retrieval buffer: Tris-EDTA (pH 9) or citrate buffer (pH 6). The container was placed in a microwave and heated until boiling, followed by incubation for 15 min. at 90-160W based on container size, and cooled at room temperature for 20-30 min. The slides were washed 2x5 min. in TBS-Tween (TBS-T) wash buffer before the removal of excess liquid and application of 100-200 µL of the appropriately diluted primary antibody. Incubation with the primary antibody was performed in a humidified chamber at 4°C overnight. The following day, slides were drained off, washed

2x5 min in TBS-T and incubated with the proper secondary antibody in a humidified incubation chamber for 30 min. at room temperature. The slides were further washed in TBS-T 2x5 min., drained and applied 100 µL of newly made DAB-solution. The DAB-solution was applied for visualization of targeted cells under the light microscope Nikon Optiphot-2 at 10x, until wanted staining intensity was reached. The stained slides were washed and stored in distilled water before counterstaining by the following procedure: Hematoxylin (5-10 sec.), running, lukewarm tap-water (3-5 min.) and cold dH_2O. Mounting was performed with Glycergel® and coverslips. Imaging of slides were done at 20x magnification by a Nikon Eclipse Ci, connected to a Nikon DS-Fi1 microscope camera and Nikon Digital Sight DS-U2 Microscope Camera Controller. Quantifications of positive cells were executed manually under a light microscope at 10x and 20x magnifications, for 10-30 crypts or crypt-villi units per tissue type, dependent on the cell type. Immunohistochemical staining results on Paneth-, goblet-, tuft- and enteroendocrine cells in adult *Lsd1*$^{f/f}$ and *Lsd1*$^{\Delta IEC}$ mice used in this project were performed by PhD candidate Rosalie Zwiggelaar and researcher Roos Spanjers, respectively, prior to the start-up of this project (unpublished data).

3.6 Hematoxylin and Eosin staining for morphological features

Hematoxylin- and eosin-staining (H&E-staining) have been used for decades in research and pathology (Greenson 2003, Fischer et al. 2008, Feldman et al. 2014). The eosin-counterstain, an acid- and anionic dye, unspecifically stain acidophilic proteins which contain positively charged amino acids. The dye appear as varying shades of pink in the eosinophilic cytoplasm of cells, which contrasts the purple- or dark blue color of the basic hematoxylin stain in the nuclei (Fischer et al. 2008, Cook et al. 2015). The staining pattern of hematoxylin and eosin depend on the formulation used. producing diverge staining colors and patterns (Feldman et al. 2014). Eosin formulations share a common feature in staining pattern, with three distinct shades of color separating erythrocytes, collagen and smooth muscle, where the former exhibit the highest staining intensity(Fischer et al. 2008). The method provide information on tissue morphology, intracellular components and intranuclear details (Fischer et al. 2008), delivering a detailed view of the tissue of interest.

3.6.1 Background

The H&E-staining is a rapidly performed method consisting of four main steps: Deparaffinization and rehydration, hematoxylin-immersion, counterstaining and dehydration,

clearing and mounting. The method thus shares most of the staining principles as IHC written in section 3.5.1.

3.6.2 Experimental procedure

Tissues were harvested, fixated and embedded as previously described in section 3.4.2, whereas deparaffinization and rehydration were performed as the first section of paragraph 3.5.2. The slides were not submerged in hydrogen peroxide. For visualization of nuclei, the specimens were submerged in Meyer's hematoxylin for 5 min. and rinsed under running, lukewarm tap water for 3-5 min and placed in cold dH_2O. Further immersion in eosin for 5 min. visualized cytoplasm and granules, before the slides were rinsed in approximately 5 seconds in dH_2O before rapid dehydration in 1x serial solutions of 80% alcohol, 96 % alcohol, and a final step in Neo-Clear for 5 min. The slides were mounted with Neo-Mount® and covered with appropriately sized coverslips. Imaging was performed with the Invitrogen Evos FL Auto 2.0 Imaging System at 10x magnification and with the Nikon Eclipse Ci at 20x magnification.
3 wild-type and 3 knock-out murine intestinal replicates were used in the measurement of intestinal structures. 15-30 measurements of crypt widths, crypt depths and villi heights were performed in ImageJ (Laboratory for Optical and Computational Instrumentation et al. 2018).

3.7 Immunofluorescent visualization of Lsd1-expression pattern, stem cells and proliferation

Immunofluorescence (IF) is a histochemical staining technique based on the targeted specificity and sensitivity of antigen-binding antibodies with subsequent visualization using a fluorophore. It provides information on the presence and location of one or more target biomolecules providing both static and dynamic information of tissue components (Mao et al. 2009, Katikireddy et al. 2011).

3.7.1 Background

The principle behind immunofluorescence lie in the chemical and photophysical properties of fluorochromes (i. e. fluorophores); probes conjugated to -thiol or amine-groups of amino acids constituting the antibody (Lavis et al. 2008, Mao et al. 2009). The fluorescence derives from the emission of light, generated by UV-exposure. The exposure of the fluorochrome to high-energetic light induce the absorption of photons with suitable energies and excitation of electrons. Decay of the excited state cause emission of photons with longer wavelengths, visible as fluorescence (Lavis et al. 2008, Mao et al. 2009). Rhodamine and fluorescein isothiocyanate

are commonly used fluorochromes with distinct absorption and emission spectra (Mao et al. 2009, Katikireddy et al. 2011). The latter dye is visible in a green color under a fluorescent microscope, absorbing wavelengths at 490 nm and emitting photons at 520 nm wavelengths. The fluorescent color of rhodamine appear orange-red, with wavelength absorption and emission in the 500-600 nm spectrum (Mao et al. 2009). The availability of differently chromophore-conjugated antibodies thus renders simultaneous staining of multiple tissue- and/or cell components feasible.

Fluorescent staining can, as other immunodetection methods, be performed directly or indirectly, dependent on the conjugation of the fluorescent probe to either the primary antibody or the secondary antibody, respectively (figure 3.2). In the indirect technique, multiple fluorescent-labelled secondary antibodies bind to each non-probed primary antibody, amplifying the staining signal and yielding a sensitive assay advantageous for most laboratory practices (Coons et al. 1941, Coons et al. 1955, Katikireddy et al. 2011, Makki 2016).

The same principles for steps in the immunofluorescence protocol can be found in the section for immunohistochemistry, 3.5.1. Diverging factors result from optimization of the method, crucial for FFPE samples that were traditionally thought unsuitable for immunofluorescent techniques due to high autofluorescence (i. e. natural background staining) (Mohan et al. 2008, Katikireddy et al. 2011, Kajimura et al. 2016). Recent studies have refuted the idea, proving optimization as key to minimize autofluorescence and enhance target-specific antibody signal (Robertson et al. 2008, Kajimura et al. 2016).

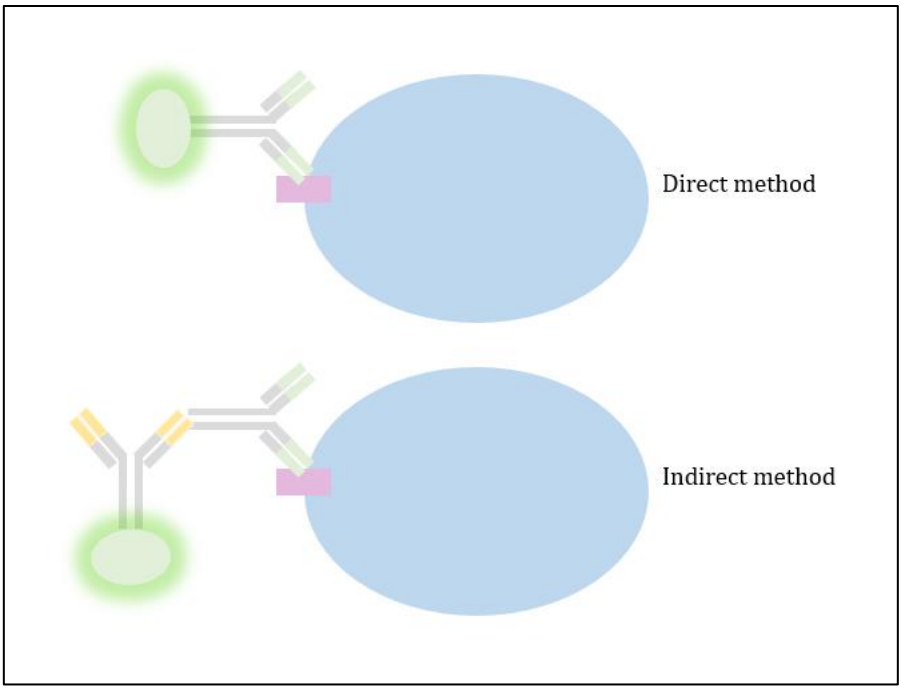

Figure 3.2: The direct and indirect immunostaining methods
In the direct method, a fluorophore is coupled to the primary antibody (upper figure). In the indirect method, the secondary antibody targeting the primary antibody is conjugated to the fluorophore instead.

3.7.2 Experimental protocol

The procedure was performed as described in the first section of paragraph 3.5.2, with the omission of the hydrogen peroxidase blocking step. After heat-induced antigen-retrieval, the slides were encircled by a hydrophobic pen and incubated with a blocking buffer designated to immunofluorescence in a humidified chamber at room temperature for 1h. The blocking buffer was then drained off and the appropriately diluted primary antibody applied. After incubation in a humidified chamber overnight at 4°C, the specimens were washed 3x10 min. in 0,2% Tween in TBS (Lsd1) or PBS (Olfm4, Ki67), and applied a dilution of the fluorescence-tagged secondary antibody, nuclear Hoechst-fluorescent counterstain and Ulex Europaeus Agglutinin I (UEA-1) (RL1062, VL) or SMA (C6198-2mL, S-A) antibody. Incubation lasted for 1h for the Olfm4 (39141S, CST) and Ki67 (2184, CST) or 2h for the Lsd1 (#2184, CST) staining at room temperature in a dark, humidified incubation chamber. The slides were proceedingly washed 2x in 0,15% Tween in TBS or PBS for 10 min. each, mounted with Fluoromount-G™ and stored dark at 4°C. The specimens were imaged with the Invitrogen Evos FL Auto 2.0 Imaging System at 10x for measurements and with the confocal microscopes Zeiss LSM 510 Meta Live or Zeiss LSM 880 at 20x magnification.

3.8 Microscopy techniques

Despite the visualization of tissue components by staining techniques, the distinction between individual cells constituting animal tissues is not possible with the naked eye. Visualization of the stained tissues is therefore dependent on microscopy and corresponding imaging tools (Cooper 2000).

3.8.1 Background

Optical microscopes, commonly referred to as light microscopes, rely on a system of lenses and illumination to magnify images of small-sized objects (Cooper 2000, Goodwin 2014). The light from an illuminator is focused onto the specimen by a condenser lens, passed through the tissue and collected by an objective lens. The objective lens redirects the light towards a tube lens, projecting the image to the oculars or a detector (Goodwin 2014, Thorn 2016). The amount of light collected by the objective lens determine the microscope's sensitivity, whereas magnification and resolution can be adjusted by a change in the objective lens used. It is the resolution which determines the ability of the microscope to reveal fine details. Image details are restricted by the resolution limit in which two objects closer than 0.2 mikrons appear indistinguishable and the image becomes unclear (Cooper 2000, Thorn 2016). Resolution is highly affected by the illumination system, in which the wavelength of light and the maximum light-collection angle by the objective lens are determinants for the microscope's resolution. As the light detected in fluorescence specimens originate from the specimen itself, illumination does not affect the resolution in fluorescence microscopy (Goodwin 2014).

Fluorescent microscopy provides a sensitive method to study inter- and intracellular distribution of stained molecules (Cooper 2000). Confocal microscopy is a method utilizing a focused laser beam to illuminate a single point in the sample, resulting in the emission of light that is passed through a pinhole and detected by a detector. The technique builds up images point-by-point through parallel scanning lines directed by scanning mirrors and ensures the exclusion of out-of-focus light. The resultant image can be displayed as a single-planed 2D image or reconstructed into 3D constructs by imaging different depths of the specimen (Z-stacks) (Cooper 2000, Thorn 2016). Maximum projection combine the brightest pixels in each layer of a Z-stack into a 2D image and has the ability to uncover otherwise hidden or hard-to-see fluorescent features presented by a single plane (Cromey et al. 2018).

3.8.2 Confocal imaging procedure

Imaging of fluorescent slides were performed with maximum projection of Z-stacks of each replicate.

3.9 Quantifications and measurements

Quantification and measurements were performed on 5-30 units per replicate, as indicated in table 3.5. Crypts and villi selected for analysis were intact along the longitudinal axes, where dented crypts and bent villi were excluded. Villi heights were measured from the base of intervillus zones to the apeces of villi in embryonic and neonatal intestines, and from the crypt-villus junction to villi apeces at P7-P21. A centred line from crypt bottoms to the cypt-villus junction was used to measure crypt depth, whereas crypt widths were measured along the widest transverse axis. Measurements of proliferation height followed the same principle as crypt depth, but dictated by the continuous line of Ki67-positive cells. Stem cell expression of Olfm4 was measured by marking the selected Olfm4-poitive area, measuring its intensity and correcting it by subtraction of intensity measurements in Olfm4-negative areas of equal sizes. For cell type quantifications, only clear and distinctive positive cells were counted.

Table 3.5: Number of crypts and/or villi quantified or measured per tissue type in a replicate

Type	*Unit*	*Number of quantifications*
Villus height	Villus	15-30
Crypt depth	Crypt	20-30
Crypt width	Crypt	20-30
Proliferation height	Crypt-villus	15-30
Stem cell expression	Crypt	5-25
Paneth cells	Crypt	10
Goblet cells	Crypt-Villus	10
Tuft cells	Crypt-Villus	15-20
Enteroendocrine cells	Crypt-Villus	10-30

3.10 Statistical analysis

Statistical analysis was performed in the program Graphpad Prism 8. Unpaired t-test was used to evaluate differences between the means of wild-type and *Lsd1*$^{\Delta IEC}$ mice. Significance was defined as $P<0.05$.

4.0 Results

4.1 The LSD1 expression pattern in neonatal and postnatal small intestine

To investigate the role of LSD1 in intestinal epithelial development, an intestinal epithelial-specific knockout model (*Lsd1*$^{\Delta IEC}$) was generated by crossing *Villin-Cre* mice with *Lsd1*$^{fl/fl}$ mice. The genotype of offspring was analyzed by amplification and detection of the *Lsd1*-floxxed sequence and the *Cre*-gene, and successful deletion of the *Lsd1*-gene validated by immunohistochemical- and immunofluorescent staining (Fig. 4.1A and 4.1C, respectively). The expression pattern of LSD1 was visualized by immunohistochemical detection at five developmental timepoints in the *Lsd1*$^{f/f}$ (WT) and *Lsd1*$^{\Delta IEC}$-mice (KO): E16.5, P0.5, P7, P14 and P21 (fig. 4.1A). A surprising observation was the dynamic change in the LSD1-expression at each developmental timepoint in *Lsd1*$^{f/f}$ mice. Based on these data, a schematic figure was made (fig. 4.1B): At early stages of development (E16.5 and P0.5), LSD1 is expressed in the whole epithelium but in varying degrees: LSD1-staining is stronger in the villi than the intervillous zones. As the morphology of the intestine change, so does the expression pattern. Upon the emergence of crypts, the invaginating epithelial cell lining lacked LSD1 (P5-P7). During the postnatal period of P7-P21, LSD1-positive cells appear in the proliferative compartment with a simultaneous increase in LSD1-negative cells at the apex of villi, suggesting a restriction of LSD1 to the intervillous zones. Ultimately, LSD1-expression display a gradient along the crypt-villus axis in adulthood, with high expression in crypts and low or none expression at the villi tips (fig 1.5 and 4.1B). To validate these findings, an immunofluorescent staining was performed (fig. 4.1C-D). Interestingly, *Lsd1*$^{f/f}$ mice did not display the same expression pattern in IF as in IHC, with contradicting results at late-developmental stages (fig. 4.1A and 4.1D). The immunofluorescent staining lacked the same gradual emergence of LSD1-positive cells in the crypt compartment as the immunohistochemical result. In the IF results, the whole epithelium was stained positive for LSD1 at every developmental timepoint.

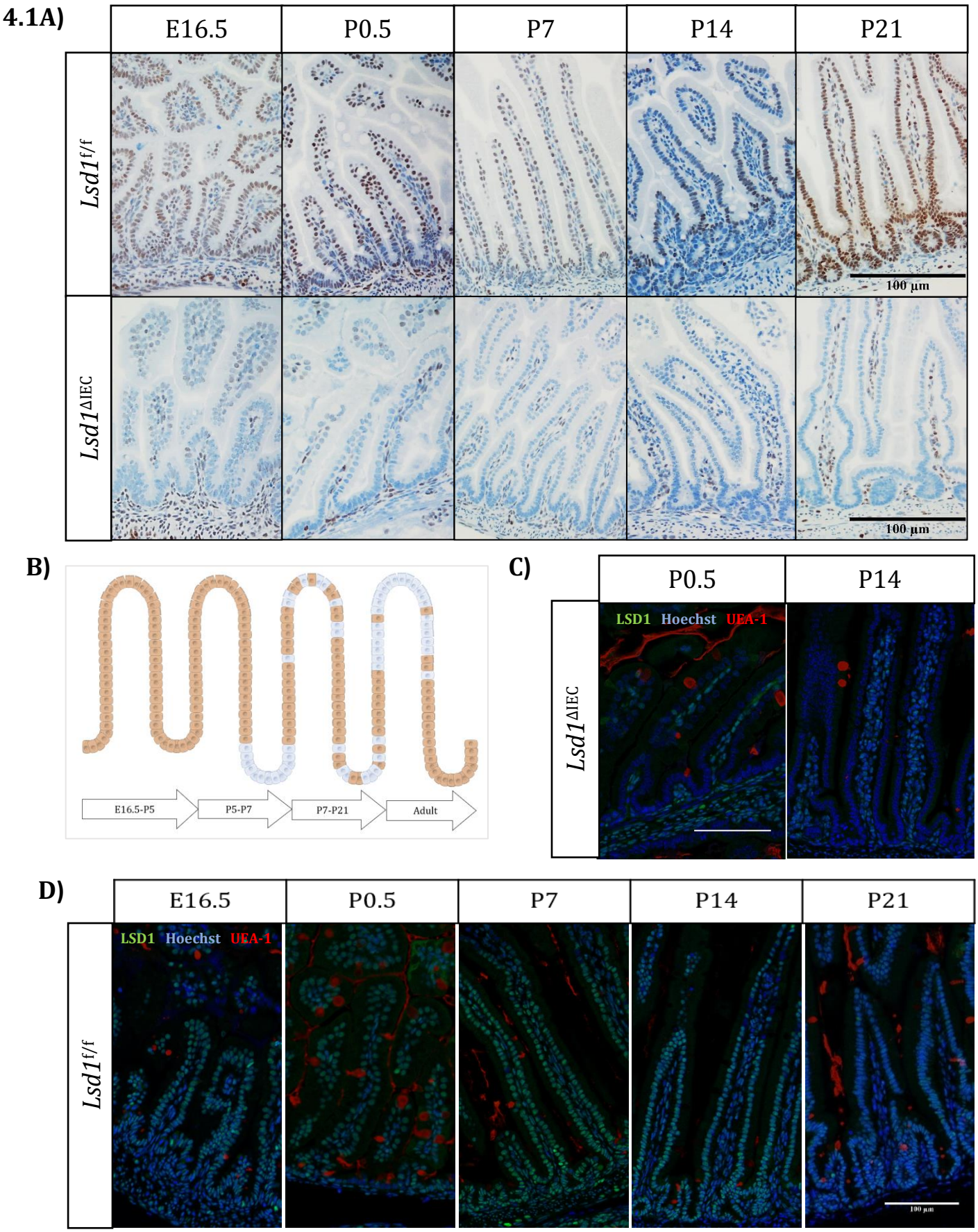

Figure 4.1: LSD1 expression pattern in the intestinal epithelium

Representative LSD1-expression as shown by **A)** IHC (brown) and **C-D)** IF (Green) in the duodenum at E16.5-P21 of *Lsd1*$^{f/f}$ and *Lsd1*$^{\Delta IEC}$ mice. Scalebar: 100 µm.

B) A hypothesized model for LSD1-expression during development, based on IHC-results of 4.1A.

4.2 Knockout of Lsd1 does not alter morphological features of embryonic, neo- and postnatal intestines

Histological analysis of the *Lsd1*$^{f/f}$- and *Lsd1*$^{\Delta IEC}$-mice was performed to uncover potential differences in morphological features of the small intestine between the two groups (fig. 4.2A). Villi heights, crypt depths and crypt widths were measured in the duodenum of three replicates for each applicable developmental timepoint and genotype (fig. 4.2B-D and table 4.1). Duodenal villi increased in lengths from E16.5 to P7, stabilizing at lengths of 180-200 μm at P7-P21 (Fig. 4.2B). Villi of embryonic mice ranged 110-170 μm in length and grew to an average of 177.6 μm and 168.0 μm in neonatal WT and KO small intestines, respectively. The highest lengths were attained by P7, at means of 196.6 μm (WT) and 197.3 μm (KO). Villi lengths became slightly reduced at P14 and P21 compared to P7, ranging within the 150-230 μm and 170-210 μm spectrum, respectively. Villi lengths at P21 were slightly elevated compared to villi heights at P14, with WT and KO mice exhibiting means of 187.2 μm and 188. μm, respectively. No significant changes were observed between the *Lsd1*$^{f/f}$- and *Lsd1*$^{\Delta IEC}$-small intestines for any of the developmental timepoints.

Measurements of crypt depths and crypt widths were limited to three developmental timepoints: P7, P14 and P21 (fig. 4.2C and D, respectively). In-between the short period of crypt emergence to the end of the first postnatal week, crypts had rapidly increased in length and reached a mean depth of 18.65 μm in the duodeni of *Lsd1*$^{f/f}$- and 18.32 μm in *Lsd1*$^{\Delta IEC}$-mice (fig 4.2 and table 4.1). However, only a modest increase could be detected at P14, with mean depths of 20.80 μm (WT) and 19.86 μm (KO). A substantial increase in crypt depth occurred from the second to third postnatal weeks, increasing by approximately 50% and reaching an average of approximately 31 μm in both groups. No major developmental changes were observed for crypt widths. Crypt widths averaged 16-17.5 μm at P7, 13-14.5 μm at P14 and 15.5-16.5 μm at P21, with no significant changes between the *Lsd1*$^{f/f}$- and *Lsd1*$^{\Delta IEC}$ mice in any of the crypt parameters (table 4.1).

4.2A)

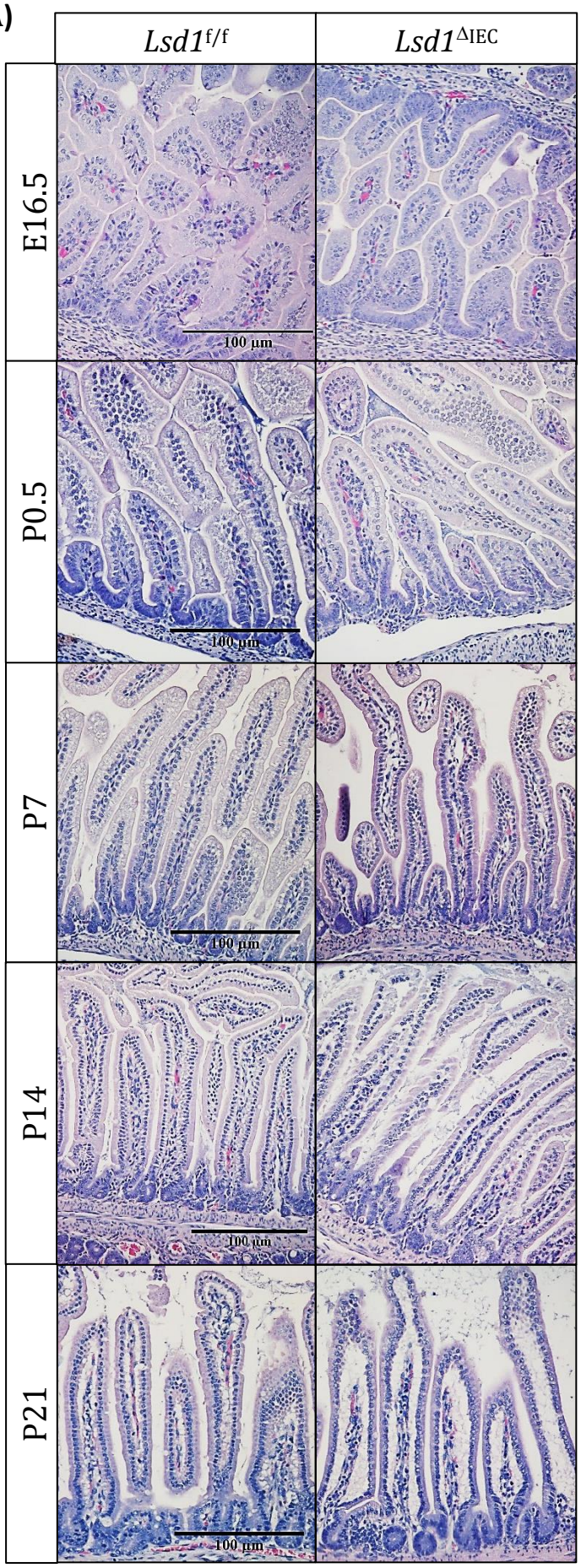

B)

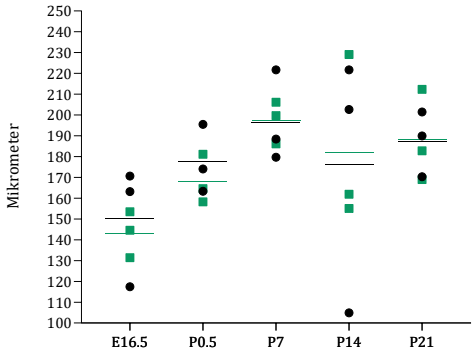

C)

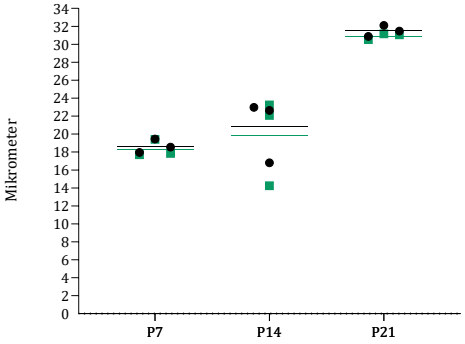

D)

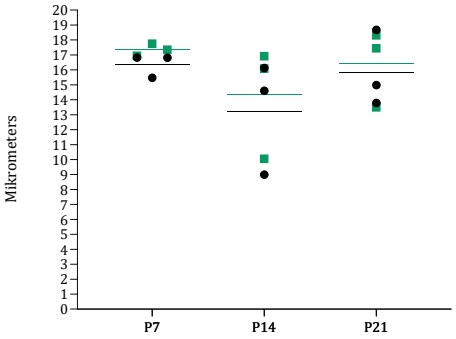

Figure 4.2: Measurements of structural units in the small intestine at different developmental timepoints

A) Example images of duodenal H&E staining in E16.5-P21 of *Lsd1*$^{f/f}$ and *Lsd1*$^{\Delta IEC}$ mice. Scalebar: 100 µm.

B-D) Measurements of villi height (B), crypt depth (C) and crypt width (D) in the duodeni of *Lsd1*$^{f/f}$ (black) and *Lsd1*$^{\Delta IEC}$ (green) mice, with corresponding means (lines).

Table 4.1: Means, standard deviations of the mean and statistical values of villi heights, crypt depths and crypt widths in duodeni of *wildtype*- (WT) and *knockout* (KO) mice at E16.5-P21

Variable	***Genotype***	***Developmental timepoint and measurements***				
		E16.5	***P0.5***	***P7***	***P14***	***P21***
Villus Height	WT	150.4 ± 23.5	177.6 ± 13.4	196.6 ± 18.1	176.4 ± 51.1	187.2 ± 12.8
	KO	143.2 ± 9.1	168.0 ± 9.6	197.3 ± 8.3	182.0 ± 33.4	188.0 ± 18.1
Significance		N.S.	N.S.	N.S.	N.S.	N.S.
Crypt Depth	WT	-	-	18.65 ± 0.6	20.80 ± 2.8	31.49 ± 0.5
	KO	-	-	18.32 ± 0.8	19.86 ± 4.0	30.91 ± 0.3
Significance		-	-	N.S.	N.S.	N.S.
Crypt Width	WT	-	-	16.38 ± 0.6	13.25 ± 3.1	15.83 ± 2.1
	KO	-	-	17.35 ± 0.3	14.35 ± 3.1	16.41 ± 2.1
Significance		-	-	N.S.	N.S.	N.S.

Data presented as mean ± standard error of the mean. Statistical comparisons between *wildtype* and *knockout* mice within the same age group indicated by not significant (N.S.) or significant (*, **, ***).

4.3 Comparisons of WT and KO mice revealed no differences in the proliferative compartment

Since previous results by the Oudhoff group suggested an increase in stem cells in the absence of Paneth cells in the *Lsd1*$^{\Delta IEC}$-mice (fig. 1.5), it was hypothesized that the increase in stem cell numbers would lead to an increase in the number of proliferative cells. To assess if this held true during development, immunofluorescent staining of the stem cell marker OLFM4 and the proliferative marker Ki67 was performed in each developmental timepoint of *Lsd1*$^{f/f}$- and *Lsd1*$^{\Delta IEC}$ mice (fig. 4.3A and C, respectively). Distinguishable OLFM4-expression was first detected in a couple of intervillous zones in neonatals, whereas expression was either too faint or non-existent in embryonic duodeni (fig. 4.3A). By the end of the first postnatal week, OLFM4-expression had become restricted to the base of crypts and was present in all epithelial depressions. The same staining pattern was observed in P14- and P21 mice. The original intention behind the staining was to quantify stem cell numbers. However, the diffuse appearance of the OLFM4-expressing stem cells made it challenging to perform a quantitative analysis. However, neither an increase or decrease in stem cell numbers or Olfm4-expression were apparent between *Lsd1*$^{f/f}$- and *Lsd1*$^{\Delta IEC}$ mice by visual interpretation. However, to determine if OLFM4-expression was indeed not affected by the loss of LSD1, a preliminary evaluation of intensity differences in the *Lsd1*$^{f/f}$- and *Lsd1*$^{\Delta IEC}$-mice were applied to the duodeni of three replicates for each parameter (fig. 4.3B). As embryonic mice did not display presence of Olfm4, E16.5 was excluded from the analysis. The resultant measurements showed no significant changes in WT vs. KO at any phase during development (table 4.2).

Although stem cell quantities were unaffected by the intestinal epithelial deletion of *Lsd1*, the effect on the proliferative capacity remained to be determined. Differences between the *Lsd1*$^{f/f}$- and *Lsd1*$^{\Delta IEC}$-mice were investigated by the measurement of proliferation heights in 3-4 replicates of WT and KO mice at E16.5-P21 (fig. 4.3D). As shown in figure 4.3C Ki67-staining was present in the intervillous zones of embryonic and neonatal tissues, decreasing from a mean of 41.2 um and 42.2 um in embryonic intestines to 21.0 um and 22.6 um in neonatal WT and KO mice, respectively. At P7-P21, proliferative cells had become restricted to crypts. An increase in mean proliferation height occurred from P7 to P21, from 16.9 um to 29.0 um in WT- and 18.5 um to 28.9 um in KO mice. None of the parameters showed significant differences between the *Lsd1*$^{f/f}$- and *Lsd1*$^{\Delta IEC}$ measurements, indicating none alterations to stem cell-quantities or the proliferative capacity in the absence of LSD1.

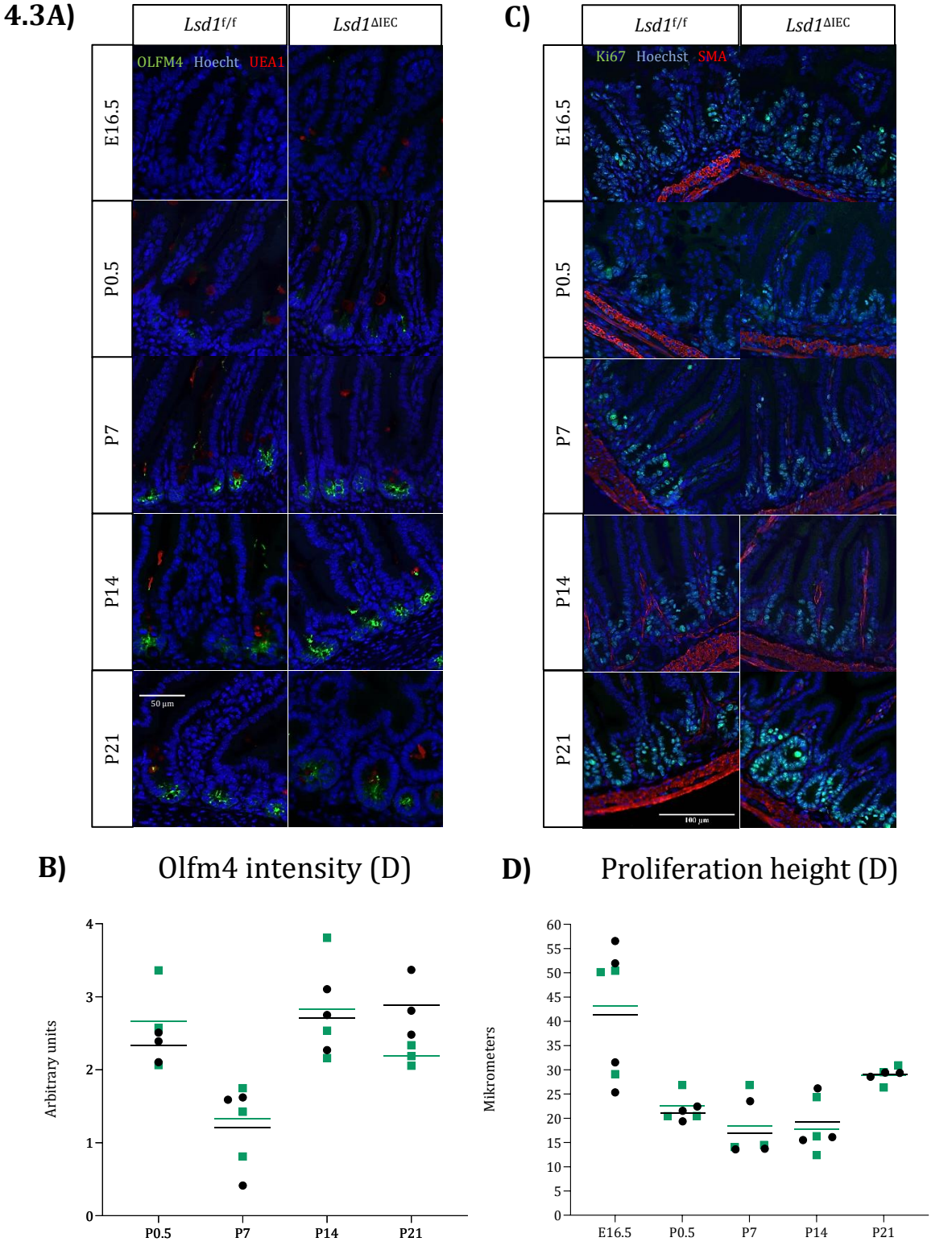

Figure 4.3: No apparent differences in proliferation, stem cell quantities or OLFM4-expression present in the Lsd1$^{f/f}$- and Lsd1$^{\Delta IEC}$-mice

A, C) Representative images of OLFM4- (A) and Ki67 (C) expression in E16.5-P21 mice (D). Scalebars: 50 µm (OLFM4) and 100 µm (Ki67)

B) Preliminary OLFM4-intensities for WT (black) and KO (green) mice detectable at the given timepoints with the corresponding means (lines).

D) Measurements of proliferation height in the five age groups for WT (black) and KO (green) mice. Lines indicate the corresponding mean values.

Table 4.2: Means, standard deviations of the mean and statistical values of proliferation height (µm) and Olfm4-expression (arbitrary units) in duodeni of *wildtype*- and *knockout* mice at E16.5-P21

Variable	***Genotype***	***Developmental timepoint and measurements***				
		E16.5	***P0.5***	***P7***	***P14***	***P21***
Ki67-height	WT	41.2 ± 13.1	21.0 ± 1.3	16.9 ± 4.6	26.1 ± 4.9	29.0 ± 0.4
	KO	43.2 ± 10.0	22.6 ± 3.0	18.5 ± 5.9	17.7 ± 5.0	28.9 ± 1.9
Significance		N.S.	N.S.	N.S.	N.S.	N.S.
Olfm4-intensity		-	2.33 ± 0.17	1.21 ± 0.56	2.71 ± 0.34	2.89 ± 0.37
		-	2.67 ± 0.53	1.33 ± 0.39	2.83 ± 0.70	2.19 ± 0.12
Significance		-	N.S.	N.S.	N.S.	N.S.

Data presented as mean ± standard error of the mean. Statistical comparisons between *wildtype*- and *knockout* mice within the same age group indicated by not significant (N.S.) or significant (*, **, ***).

4.4 LSD1 regulate Paneth cell differentiation

Although no changes to the morphology or proliferative cells in the small intestine were observed, further exploration of the role of LSD1 in intestinal epithelial development was addressed by immunohistochemical detection of lyzosyme-positive Paneth cells (fig. 4.4A). Mean values of positive cells per crypt with standard deviations of the mean were plotted against the timepoints in a graph, representing a developmental timeline of Paneth cells in the duodeni, jejuni and ilea of *Lsd1*$^{f/f}$- and *Lsd1*$^{\Delta IEC}$ mice (fig. 4.4B-D). A scant number of Paneth cells in crypt-regions of the three small intestinal segments was observed at P7 for both the WT and KO mice (fig. 4.4B-D and table 4.3), which increased between the first and third postnatal weeks in *Lsd1*$^{f/f}$ small intestines. However, only a modest change was seen in the intestines of *Lsd1*$^{\Delta IEC}$ mice, averaging 0-0.33 cells/crypt from ileum to duodenum at P21; substantially less than the 1-2 cells present in crypts in *Lsd1*$^{f/f}$ mice at the same developmental timepoint. Furthermore, clear differences were seen in the number of Lyz-positive and -negative crypts. ≥50% of the *Lsd1*$^{\Delta IEC}$-replicates lacked Paneth cells completely at P7-P21, in contrast to one in five *Lsd1*$^{f/f}$ mice at P7 and P14. At P21, all crypts in *Lsd1*$^{f/f}$ mice harbored Paneth cells.

As Paneth cells were present in the knockout model, it did not match the hypothesis postulated by the Oudhoff group, in which Paneth cell differentiation were thought to be inhibited by the deletion of *Lsd1*in the intestinal epithelium. Investigation into the LSD1-staining and the overlapping pattern in the lysozyme-stainings provided an explanation. Incomplete knockout of *Lsd1* led to LSD1-positive patches in the intestines of *Lsd1*$^{\Delta IEC}$ mice, which coincided with Paneth cell appearance (fig.4.4E). Thus, strengthening the hypothesis that LSD1 is indispensable for Paneth cell differentiation.

Although no Paneth cells were quantified prior to P7, an interesting discovery was made in the small intestine of neonatal mice. Even though distinct Paneth cells were first detected after the first postnatal week, closer inspection of P0.5 mice revealed <10 lysozyme-positive cells scattered in their small intestines. The morphology and location of these cells did not match the granular appearance of crypt-residing Paneth cells (fig. 4.4A and 4.5). It was proposed that these cells could be immature Paneth cell progenitors, which was investigated by staining and comparing the mutual exclusive differentiation marker lysozyme (IHC) with the proliferative and stem cell markers Ki67 and Olfm4 (IF). Surprisingly, staining of different replicates provided diverging results. The majority displayed an overlap with the proliferative marker, but not with the stem cell marker (fig 4.5, example 1), whereas others exhibited no overlap between the different stainings at all (fig. 4.5, example 2). Thus, the staining did not present any conclusive results on the status of these cells.

4.4A)

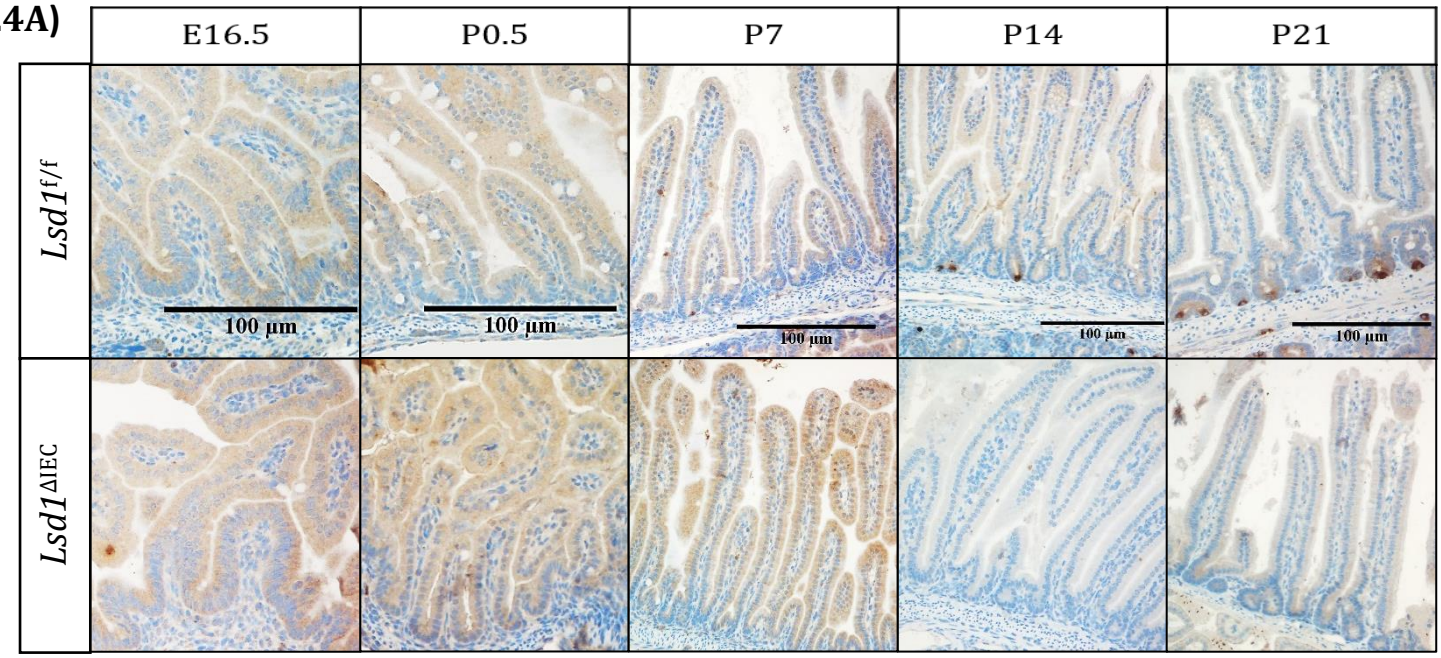

B)

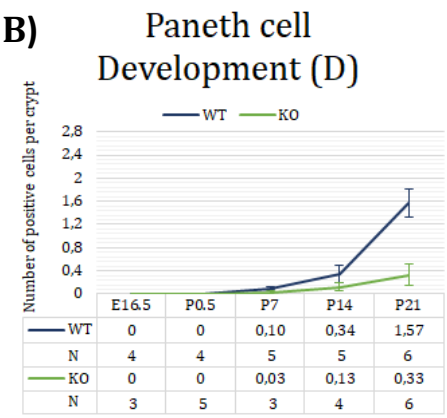

	E16.5	P0.5	P7	P14	P21
WT	0	0	0,10	0,34	1,57
N	4	4	5	5	6
KO	0	0	0,03	0,13	0,33
N	3	5	3	4	6

C)

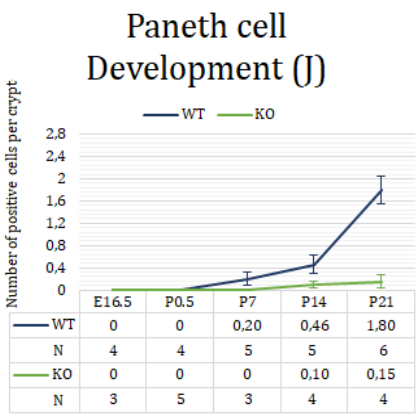

	E16.5	P0.5	P7	P14	P21
WT	0	0	0,20	0,46	1,80
N	4	4	5	5	6
KO	0	0	0	0,10	0,15
N	3	5	3	4	4

D)

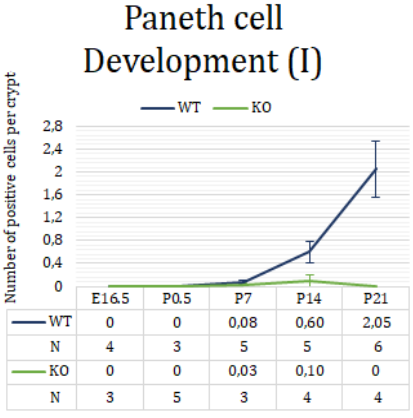

	E16.5	P0.5	P7	P14	P21
WT	0	0	0,08	0,60	2,05
N	4	3	5	5	6
KO	0	0	0,03	0,10	0
N	3	5	3	4	4

E)

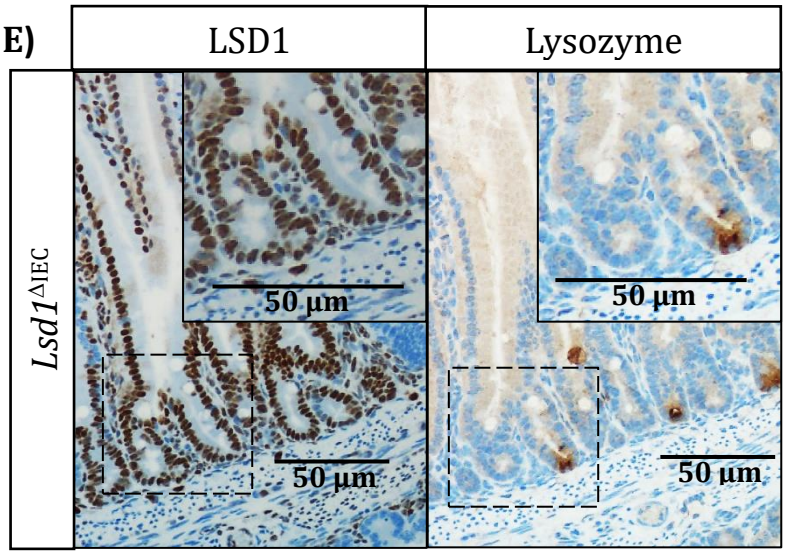

Figure 4.4: In the absence of Lsd1, the differentiation of Paneth cells is prevented

A) Representative images from the detection of Paneth cells by lyzosyme-staining (IHC) in duodeni of *Lsd1*$^{f/f}$ and *Lsd1*$^{\Delta IEC}$ mice. Scalebar: 100 µm.

B-D) Paneth cells quantifications at the different developmental timepoints in B) Duodenum, C) Jejunum and D) Ileum.

E) LSD1-positive patches appear in *Lsd1*$^{\Delta IEC}$ mice (left), coinciding with Lysozyme-expression (right). The representaticve images derive from a P14 *Lsd1*$^{\Delta IEC}$-replicate. Scale bar: 50 µm.

4.5)

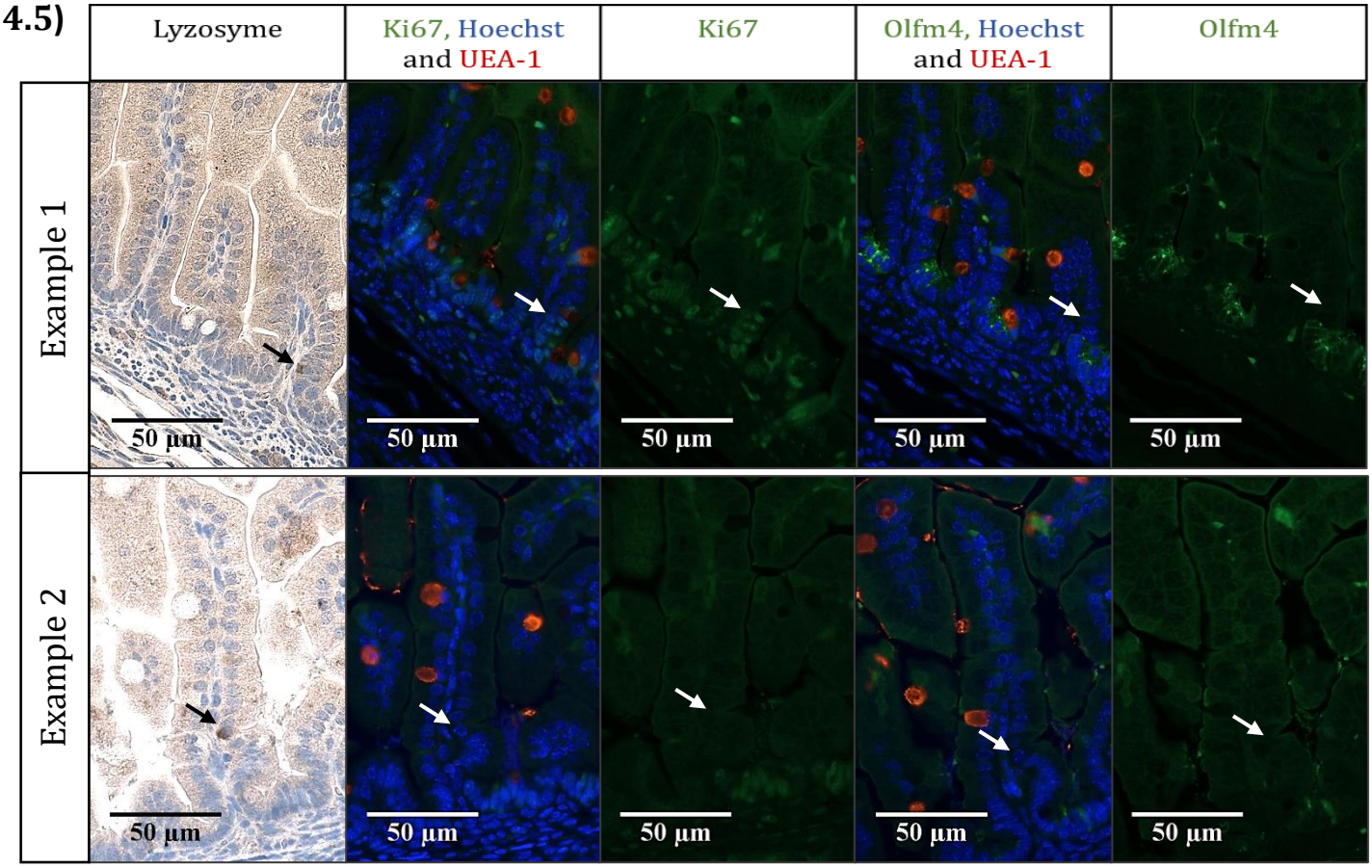

Figure 4.5: Serial sections of P0.5 intestines undergone Lysozyme-IHC, Ki67- and OLFM4 IF
Example 1 shows an overlap of the Lysozyme-positive cell with Ki67, but not of OLFM4, as indicated by the arrows. Example 2 displays no positive overlap of the different stainings. Scale bars: 50 µm.

Table 4.3: Means, standard deviations of the mean and statistical values of Paneth cell quantification in duodeni (D), jejuni (J) and ilea (I) of *Lsd1*$^{f/f}$- and *Lsd1*$^{\Delta IEC}$-mice at E16.5-P21

Variable	***Genotype***	***Segment***	***Developmental timepoint and quantifications***				
			E16.5	***P0.5***	***P7***	***P14***	***P21***
Paneth cell #	WT	D	0	0	0.10 ± 0.03	0.34 ± 0.15	1.57 ± 0.24
	KO	D	0	0	0.03 ± 0.03	0.13 ± 0.75	0.33 ± 0.19
Significance			-	-	N.S.	N.S.	**
Paneth cell #	WT	J	0	0	0.20 ± 0.11	0.46 ± 0.16	1.80 ± 0.24
	KO	J	0	0	0	0.10 ± 0.06	0.15 ± 0.12
Significance			-	-	N.S.	N.S.	***
Paneth cell #	WT	I	0	0	0.08 ± 0.04	0.60 ± 0.18	2.05 ± 0.49
	KO	I	0	0	0.03 ± 0.03	0.10 ± 0.10	0
Significance			-	-	N.S.	N.S.	*

Data presented as mean ± standard error of the mean. Statistical significance between *wildtype* and *knockout* mice within the same age group indicated by not significant (N.S.) or significant (*, **, ***).

4.5 *Lsd1*$^{\Delta IEC}$-mice display changes in the composition of epithelial cells of the secretory lineage compared to *Lsd1*$^{f/f}$-mice

Similar to Paneth cells, the effect of epithelial deletion of *Lsd1* on other differentiated epithelial cell types of the small intestine was investigated by immunohistochemical detection of goblet cells by the marker Mucin-2 (fig. 4.5A), Doublecortin like kinase 1 (DCAMKL1) to visualize tuft cells (fig. 4.6A) and Chromogranin A-staining for enteroendocrine cells (fig.4.7A). Mean values of positive cells per crypt-villus unit with standard deviations of the mean from *Lsd1*$^{f/f}$- and *Lsd1*$^{\Delta IEC}$-mice at different developmental timepoints were plotted in graphs displaying their development in duodeni, jejuni and ilea (fig. 4.6B-D, 4.7B-D, 4.8B-D), with an overview of the same values and the significance provided in Table 4.4. The results displayed divergent effects on the intestinal epithelial cell types. For goblet cells, major differences were not detected before the second postnatal weeks, with significantly fewer goblet cells observed at P14 to adulthood for proximal and mid small intestine of *Lsd1*$^{\Delta IEC}$ mice, except for the mid SI of P21 mice (fig. 4.6B-C, respectively, and table 4.4). In contrast to the lowered goblet cell numbers in *Lsd1*$^{\Delta IEC}$-mice, tuft cell numbers were significantly elevated in the small intestine of the knockout model at P21 and in adults (table 4.4). Tuft cells were not present in the small intestine of embryos or the mid- and distal small intestinal segments of neonatal mice, but developed in the proximal potion by P0.5 and by the first or second postnatal weeks in the other small intestinal segments (fig. 4.7B-D). A steady increase in tuft cell numbers were observed after their emergence in the duodeni, jejuni and ilea of both *Lsd1*$^{f/f}$- and *Lsd1*$^{\Delta IEC}$-mice, with a burst in small intestinal tuft cell quantities between P21 and the adult form. The same pattern was present for goblet cells in the whole small intestine and for enteroendocrine cell numbers in the duodenum; a slight increase occurred after the first or second postnatal weeks, with major leaps in quantities between the last two developmental stages. Enteroendocrine cells, like goblet cells, were present in the small intestine as early as E16.5 in both *Lsd1*$^{f/f}$- and *Lsd1*$^{\Delta IEC}$-mice (fig. 4.8B-D). No significant alterations were found in enteroendocrine numbers in most of the developmental timepoints and intestinal segments (table 4.6). A significant decrease was observed in the P14 duodeni and P0.5 jejuni of *Lsd1*$^{\Delta IEC}$-mice, but were not sustained at later phases. Collectively, these results indicate a role of LSD1 in goblet- and tuft cell maturation at a late developmental stage, while enteroendocrine cells remain unaffected by the *Lsd1*-deletion in the intestinal epithelium.

4.6A)

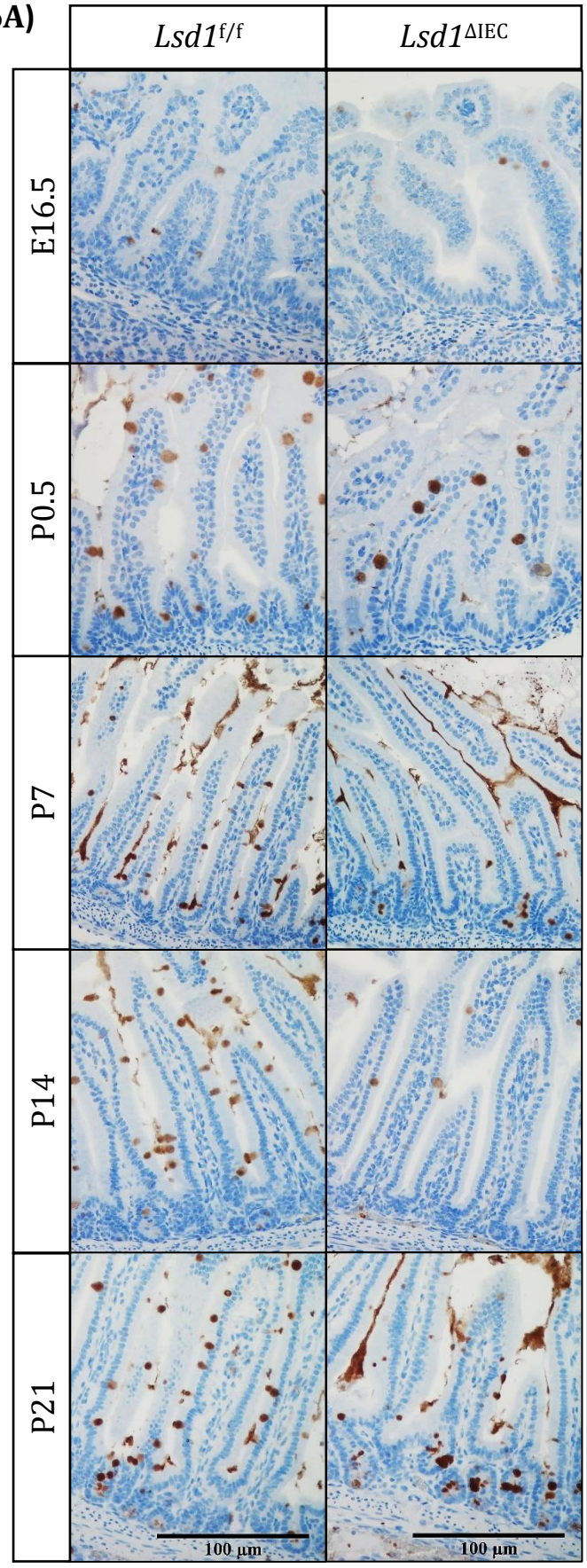

B)

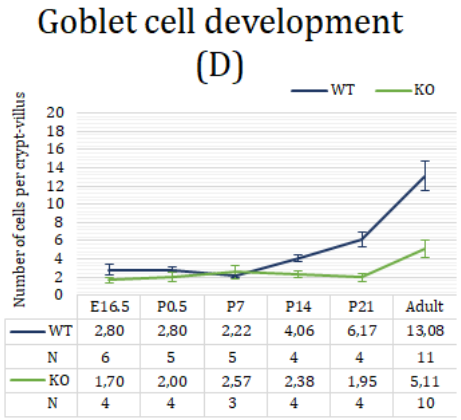

	E16.5	P0.5	P7	P14	P21	Adult
WT	2,80	2,80	2,22	4,06	6,17	13,08
N	6	5	5	4	4	11
KO	1,70	2,00	2,57	2,38	1,95	5,11
N	4	4	3	4	4	10

C)

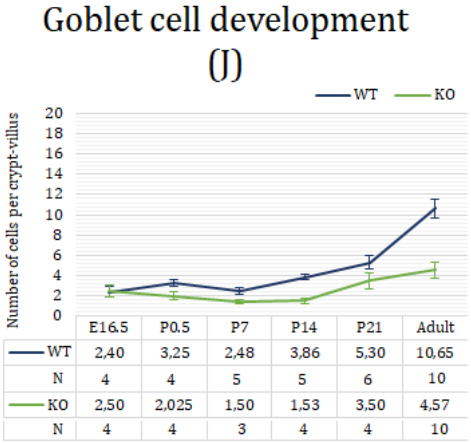

	E16.5	P0.5	P7	P14	P21	Adult
WT	2,40	3,25	2,48	3,86	5,30	10,65
N	4	4	5	5	6	10
KO	2,50	2,025	1,50	1,53	3,50	4,57
N	4	4	3	4	4	10

D)

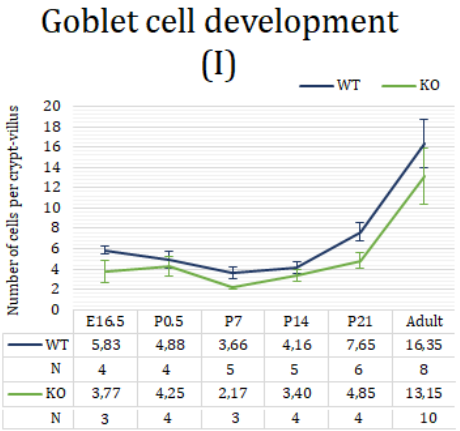

	E16.5	P0.5	P7	P14	P21	Adult
WT	5,83	4,88	3,66	4,16	7,65	16,35
N	4	4	5	5	6	8
KO	3,77	4,25	2,17	3,40	4,85	13,15
N	3	4	3	4	4	10

Figure 4.6: Lsd1$^{\Delta IEC}$ mice display decreased goblet cell numbers from P14.
A) Example images from the IHC of goblet cells by MUC2-staining in duodeni at E16.5-P21 of *Lsd1*$^{f/f}$ and *Lsd1*$^{\Delta IEC}$ mice.
Scalebar: 100 µm.
B-D) Quantifications of goblet cells in **B)** Duodenum, **C)** Jejunum and **D)** Ileum of *Lsd1*$^{f/f}$ (blue) and *Lsd1*$^{\Delta IEC}$ mice (green) at different developmental timepoints.

4.7A)

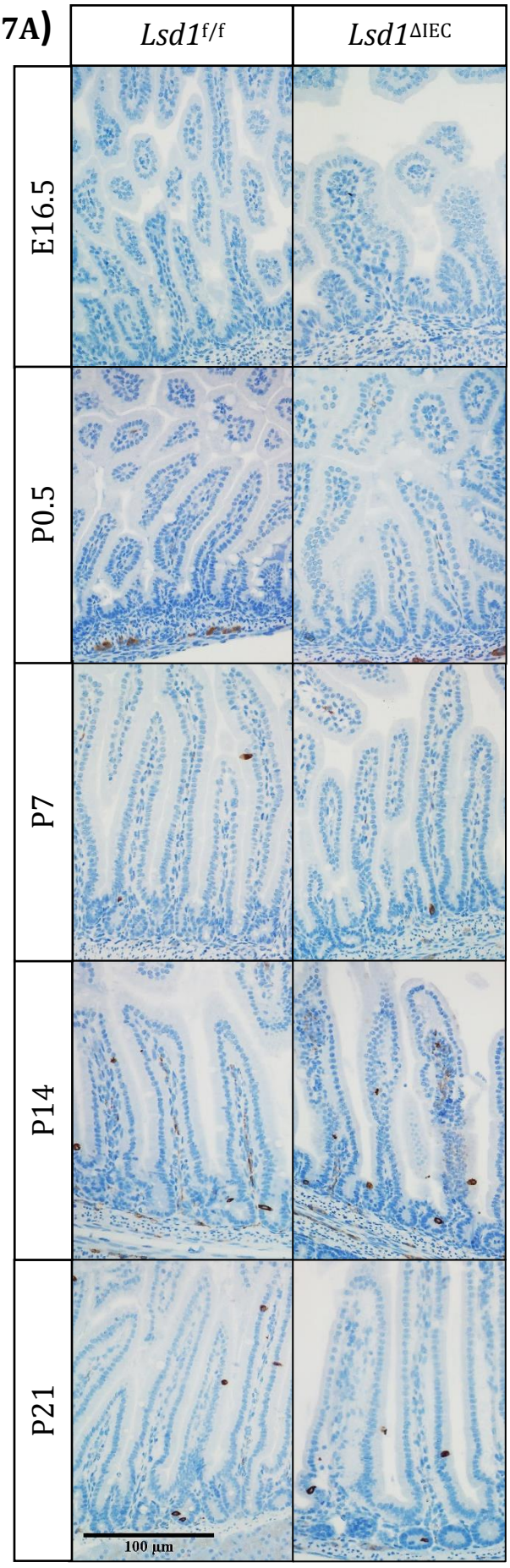

B)

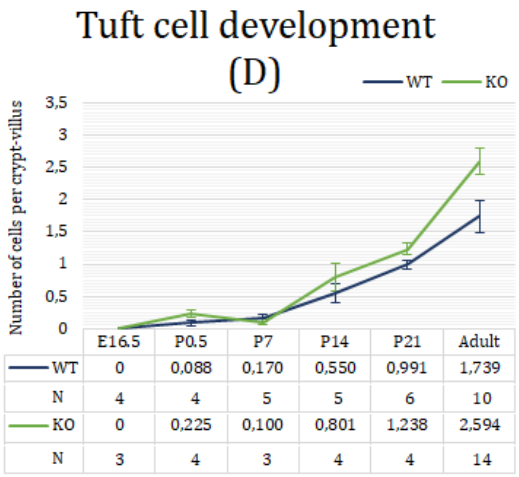

	E16.5	P0.5	P7	P14	P21	Adult
WT	0	0,088	0,170	0,550	0,991	1,739
N	4	4	5	5	6	10
KO	0	0,225	0,100	0,801	1,238	2,594
N	3	4	3	4	4	14

C)

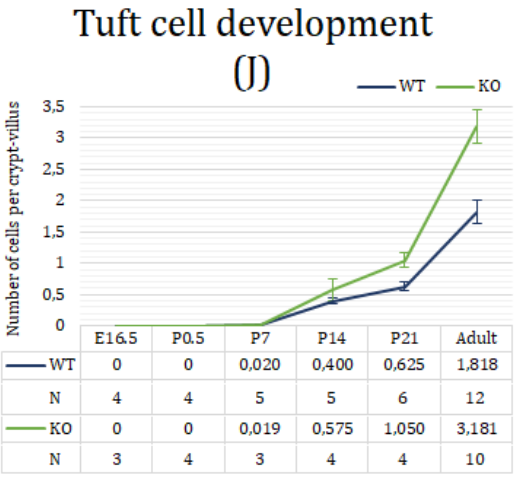

	E16.5	P0.5	P7	P14	P21	Adult
WT	0	0	0,020	0,400	0,625	1,818
N	4	4	5	5	6	12
KO	0	0	0,019	0,575	1,050	3,181
N	3	4	3	4	4	10

D)

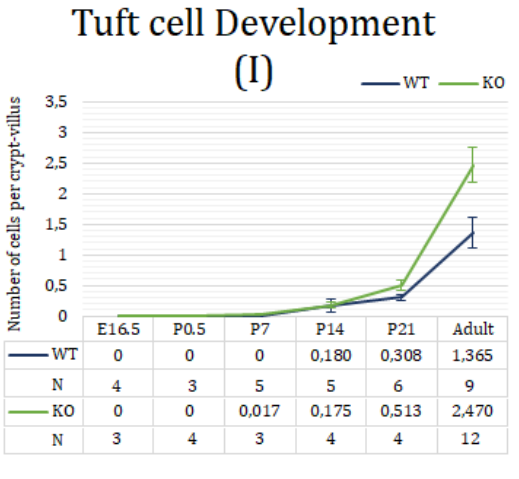

	E16.5	P0.5	P7	P14	P21	Adult
WT	0	0	0	0,180	0,308	1,365
N	4	3	5	5	6	9
KO	0	0	0,017	0,175	0,513	2,470
N	3	4	3	4	4	12

Figure 4.7: Lsd1$^{\Delta IEC}$ mice display an increased number of tuft cells from P21

A) Immunohistochemical detection of tuft cells by DCLK1-staining at E16.5-P21 in duodeni of *Lsd1*$^{f/f}$ and *Lsd1*$^{\Delta IEC}$ mice.
Scalebar: 100 µm.

B-D) Quantification of tuft cells in B) Duodenum, C) Jejunum and D) Ileum from E16.5 to adulthood in *wildtype* and *knockout* mice

4.8A)

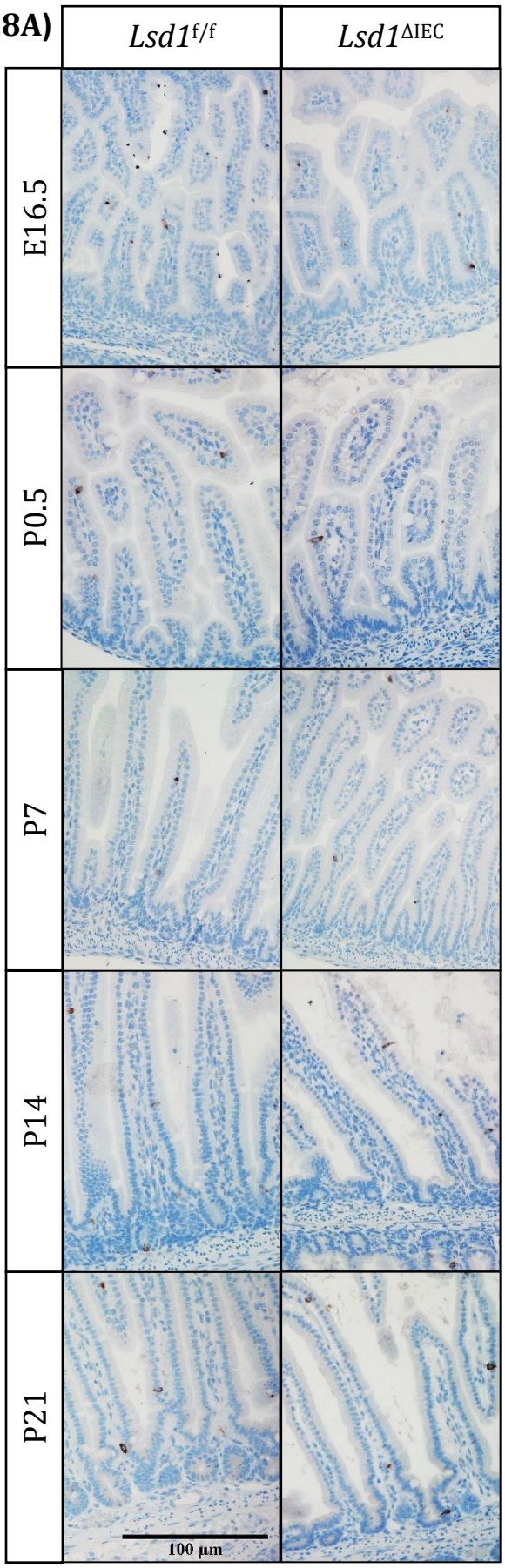

B)

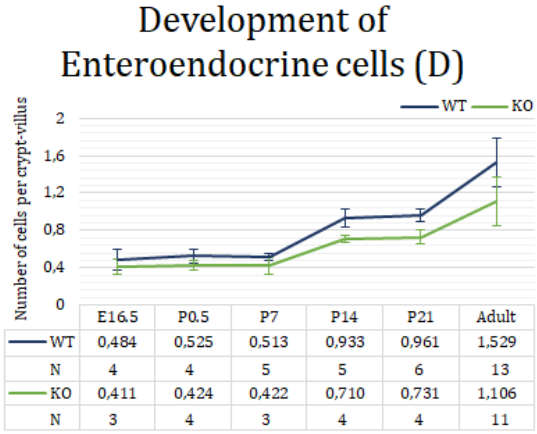

	E16.5	P0.5	P7	P14	P21	Adult
WT	0,484	0,525	0,513	0,933	0,961	1,529
N	4	4	5	5	6	13
KO	0,411	0,424	0,422	0,710	0,731	1,106
N	3	4	3	4	4	11

C)

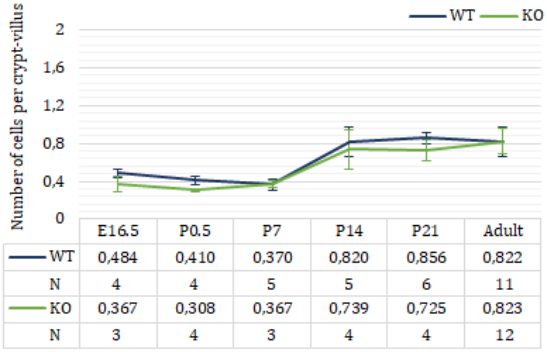

	E16.5	P0.5	P7	P14	P21	Adult
WT	0,484	0,410	0,370	0,820	0,856	0,822
N	4	4	5	5	6	11
KO	0,367	0,308	0,367	0,739	0,725	0,823
N	3	4	3	4	4	12

D)

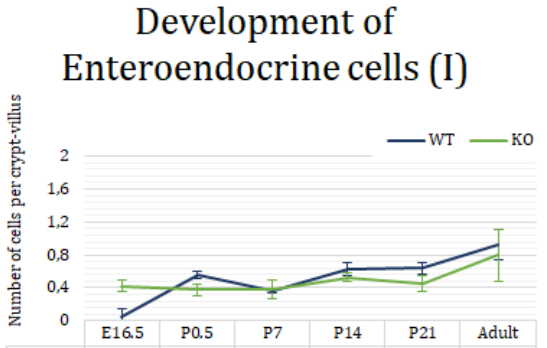

	E16.5	P0.5	P7	P14	P21	Adult
WT	0,057	0,554	0,363	0,627	0,637	0,929
N	4	3	5	5	6	11
KO	0,422	0,374	0,378	0,529	0,450	0,798
N	3	4	3	4	4	11

Figure 4.8: LSD1-ablation does not affect the quantities of enteroendocrine cells
A) IHC of enteroendocrine cells by chromogranin A-staining in duodeni at E16.5-P21 and their corresponding quantifications in
B) Duodenum, **C)** Jejunum and **D)** Ileum
of *Lsd1*$^{f/f}$- (blue) and *Lsd1*$^{\Delta IEC}$ (green) mice at different developmental timepoints.
Scalebar: 100 µm.

Table 4.4: Means, standard deviations of the mean and statistical significance of goblet cell- (GC), tuft cell- (TC) and enteroendocrine cell (EEC) numbers per crypt-villus in duodeni (D), jejuni (J) and ilea (I) of *Lsd1*$^{f/f}$- and *Lsd1*$^{\Delta IEC}$-mice at E16.5-P21

Variable	***Genotype***	***Segment***	***Developmental timepoint and quantifications***					
			E16.5	***P0.5***	***P7***	***P14***	***P21***	***Adult***
GC	WT	D	2.80 ± 0.59	2.80 ± 0.33	2.22 ± 0.29	4.06 ± 0.36	6.17 ± 0.82	13.08 ± 1.62
	KO	D	1.70 ± 0.26	2.00 ± 0.49	2.57 ± 0.77	2.38 ± 0.38	1.95 ± 0.45	5.11 ± 0.89
Significance			N.S.	N.S.	N.S.	*	**	***
GC	WT	J	2.40 ± 0.52	3.25 ± 0.35	2.48 ± 0.31	3.86 ± 0.22	5.30 ± 0.64	10.65 ± 0.92
	KO	J	2.50 ± 0.61	2.03 ± 0.38	1.50 ± 0.20	1.53 ± 0.26	3.50 ± 0.83	4.57 ± 0.77
Significance			N.S.	N.S.	N.S.	***	N.S.	***
GC	WT	I	5.83 ± 0.37	4.88 ± 0.83	3.66 ± 0.61	4.16 ± 0.62	7.65 ± 0.87	16.35 ± 2.34
	KO	I	3.77 ± 1.14	4.25 ± 0.94	2.17 ± 0.15	3.40 ± 0.59	4.85 ± 0.79	13.15 ± 2.72
Significance			N.S.	N.S.	N.S.	N.S.	N.S.	N.S.
TC	WT	D	0	0.09 ± 0.05	0.17 ± 0.06	0.55 ± 0.16	0.99 ± 0.06	1.74 ± 0.24
	KO	D	0	0.23 ± 0.06	0.10 ± 0.05	0.80 ± 0.22	1.24 ± 0.09	2.59 ± 0.20
Significance			-	N.S.	N.S.	N.S.	*	*
TC	WT	J	0	0	0.02 ± 0.01	0.40 ± 0.05	0.63 ± 0.07	1.82 ± 0.18
	KO	J	0	0	0.02 ± 0.02	0.58 ± 0.17	1.05 ± 0.11	3.18 ± 0.27
Significance			-	-	N.S.	N.S.	**	***
TC	WT	I	0	0	0	0.18 ± 0.11	0.31 ± 0.5	1.37 ± 0.26
	KO	I	0	0	0.02 ± 0.02	0.18 ± 0.05	0.51 ± 0.09	2.47 ± 0.28
Significance			-	-	N.S.	N.S.	*	*
EEC	WT	D	0.48 ± 0.12	0.53 ± 0.08	0.51 ± 0.04	0.93 ± 0.09	0.96 ± 0.07	1.53 ± 0.26
	KO	D	0.41 ± 0.08	0.42 ± 0.06	0.42 ± 0.09	0.71 ± 0.03	0.73 ± 0.07	1.11 ± 0.26
Significance			N.S.	N.S.	N.S.	**	N.S.	N.S.
EEC	WT	J	0.48 ± 0.04	0.41 ± 0.05	0.37 ± 0.06	0.82 ± 0.15	0.86 ± 0.06	0.82 ± 0.15
	KO	J	0.37 ± 0.08	0.31 ± 0.02	0.37 ± 0.04	0.74 ± 0.21	0.73 ± 0.11	0.82 ± 0.13
Significance			N.S.	**	N.S.	N.S.	N.S.	N.S.
EEC	WT	I	0.06 ± 0.09	0.55 ± 0.05	0.36 ± 0.03	0.63 ± 0.07	0.64 ± 0.08	0.93 ± 0.19
	KO	I	0.42 ± 0.07	0.37 ± 0.06	0.38 ± 0.11	0.53 ± 0.05	0.45 ± 0.10	0.80 ± 0.32
Significance			N.S.	N.S.	N.S.	N.S.	N.S.	N.S.

Data presented as mean ± standard error of the mean. Statistical comparisons between *wildtype* and *knockout* mice within the same age group indicated by not significant (N.S.) or significant (*, **, ***).

4.6 Investigating underlying mechanisms of LSD1 function in the intestinal epithelium

To uncover the underlying mechanisms of LSD1-mediated regulation of intestinal epithelial differentiation, differences in the dimethylation pattern of H3K4 was assessed by immunohistochemistry (fig. 4.9). Demethylation of H3K4me2 is associated with transcriptional repression and could be a causative factor for alterations in the secretory cell composition in the intestinal epithelium of *Lsd1*$^{\Delta IEC}$ mice. The resultant staining displayed slight variations in the intensities between the replicates, but visual comparisons did not indicate any difference between the small intestines of *Lsd1*$^{f/f}$- and *Lsd1*$^{\Delta IEC}$-mice at any of the developmental timepoints; E16.5, P14 and adult.

4.9)

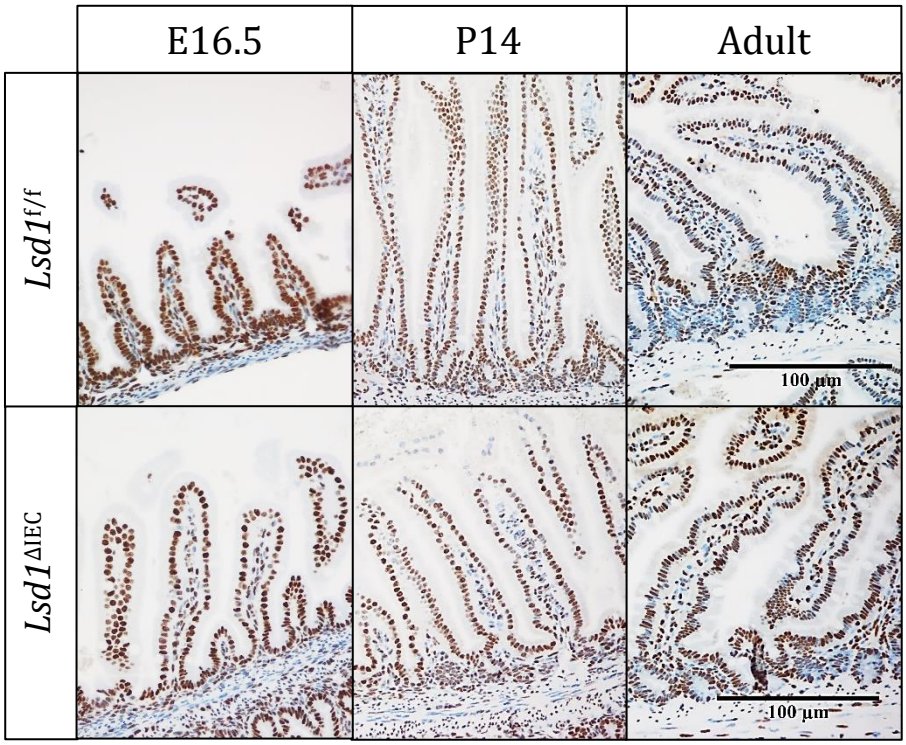

Figure 4.9: No apparent differences in dimethylation pattern of histone H3K4 in Lsd1$^{f/f}$- and Lsd1$^{\Delta IEC}$-mice

Representative images from the H3K4me2-IHC of WT (*Lsd1*$^{f/f}$) and KO (*Lsd1*$^{\Delta IEC}$) mice at E16.5-, P14- and adult mice.
Scalebar: 100 µm.

5.0 Discussion

LSD1 is expressed across a diverse set of organ systems in mammals, and the intestinal tract is not an exception (Wang et al. 2007, Adamo et al. 2011, Muncan et al. 2011, Mould et al. 2015, Haines et al. 2018). Research on the intestinal tract has uncovered organized mechanisms guiding differentiation and development of the organ across species. Regulatory mechanisms of proliferation and differentiation in the intestine and the corresponding epithelium have been discovered and characterized for decades, and has uncovered signaling pathways and specification factors governing the developmental processes (Bry et al. 1994, De Santa Barbara et al. 2003, Noah et al. 2011). Although progress have been made in the field, every piece of the puzzle has still not been identified. Through the targeted deletion of *Lsd1* in the intestinal epithelium, the study aimed to determine the expression pattern and the effects of LSD1 in intestinal epithelial development.

5.1 The LSD1-expression pattern

Expression of LSD1 has been shown to be present in the developing gut tube at E16.5 (Muncan et al. 2011), yet its expression pattern across developmental stages of the intestine has not been identified. During the investigation of the LSD1-expression pattern in intestinal epithelial development of *wildtype* mice, the immunohistochemical staining revealed interesting changes during the postnatal period (fig. 4.1A and fig. 1.5): It looked like LSD1-expression shifted from the villus epithelium in embryonic and neonatal epithelium towards crypts and the intervillous regions later in development, where a gradual increase in staining of crypts occurred between P7-P21 (fig. 4.1B). Of note, one out of three replicates at P14 displayed the same staining pattern as P21 mice, suggesting a transition point around the second to third postnatal weeks. However, the same spatiotemporal expression pattern was not observed for the fluorescent staining, which showed LSD1-expression in the whole epithelium at all developmental timepoints (fig. 4.1D). The specificity and validity of both results were supported by the lack of staining in the intestinal epithelium of *Lsd1*$^{\Delta IEC}$ mice (Fig. 4.1A and 4.1C) and the negative controls used. Still, the divergent results indicate that one or both results are flawed, and the manual handling of each step in both IHC and IF make them prone to errors. Two common mistakes in immunostaining techniques is the prolonged time between euthanization and fixation of tissues and overfixation, which can cause degradation of target proteins or prevent the detection of the targeted epitopes, respectively (O'Hurley et al. 2014, Kim et al. 2016).

However, these errors would have yielded the same LSD1-expression pattern at P7-P21 in replicates shared between the two methods, which was not observed. Another common mistake during staining techniques is the choice of an improper fixative (Katikireddy et al. 2011). It is advised to ensure that fixation is performed in a suitable fixative to avoid artificial or misleading stainings, and the use of FFPE samples is not recommended for immunofluorescent techniques (Katikireddy et al. 2011). Yet, the autofluorescence commonly associated with this was not observed in neither the *Lsd1*$^{f/f}$- or *Lsd1*$^{\Delta IEC}$-intestines (fig. 4.1C-D). As autofluorescence was not observed for any of the LSD1-stainings, improper blocking-, washing- or antibody incubation steps cannot explain the observed differences either (O'Hurley et al. 2014, Kim et al. 2016). Furthermore, it is unlikely that interbatch differences between the LSD1-antibody can account for the difference in staining patterns between the IHC and IF results, as minimal variation is observed for monoclonal antibodies (Katikireddy et al. 2011, O'Hurley et al. 2014). It could be that the detection rate in the two methods are different, but a study comparing the staining results of the same antibody in IHC and IF has shown that there is no significant difference in their detection rates (Qi et al. 2017). Therefore, the difference in staining patterns between the two staining techniques would be more likely to be caused by errors during the execution of the IHC- or IF-protocol. If paraffin was not completely removed from the IHC-tissues or if they dried out during one of the incubation steps, the resultant staining would be reduced or completely absent (O'Hurley et al. 2014, Kim et al. 2016). However, the immunohistochemical protocol has been designed to avoid these problems and every step was monitored to avoid these types of errors. Additionally, the same staining pattern was observed in repeated IHC-experiments. Thus, a more plausible explanation could be the faulty optimization of the immunofluorescent- or the immunohistochemical protocol. The LSD1-IF had to be optimized to fit the LSD1-antibody, as every attempt on LSD1-IF yielded negative results when the IHC-antibody diluent was used to dilute the primary antibody. It was first when the IHC-diluent was substituted with a solution lacking Tween that positive staining was acquired. This could indicate that the immunohistochemical result was compromised. Tween is used to prevent non-specific binding, but it would seem like the high concentration of the detergent washed away antibodies weakly interacting with the targeted epitope. Yet, there is one flaw to this hypothesis: The antibody utilized is monoclonal, meaning that all of the antibodies derive from progeny of a common B-lymphocyte and therefore share the same specificity against the same target epitope (Katikireddy et al. 2011, Murphy et al. 2017). For polyclonal antibodies, the wash-out hypothesis would have made more sense. Polyclonal antibodies would have specificities against different target epitopes (Murphy et al. 2017), where

some of the weaker interacting antibodies could be removed by the detergent. It would still be of interest to test the hypothesis by performing the LSD1-IHC with as many parameters identical to those of the IF – especially regarding the antibody diluent.

Another solution would be to validate one of the stainings through another approach. As the biggest difference in staining was seen in the crypts of P7 and P21 mice, these timepoints would be selected for the analysis. Crypts from P7 and P21 mice could be isolated, disrupted into single cells and sorted for an epithelial marker to exclude non-epithelial cells. Protein could be extracted from a specific number of crypt cells from both timepoints and run through a western blot selecting for LSD1. If the intestinal crypts from P7 mice display lowered intensity than the those from P21 mice, it would verify the immunohistochemical result. A similar verification method could be performed by cell sorting on a given number of crypt cells, where an epithelial population of LSD1-positive and -negative cells could be obtained. All cells of crypts would be LSD1-positive at P21, whereas the number of LSD1-positve and/or -negative cells would determine which of the IHC- or IF-results is true. The same principles could be applied to observe the changes in the expression pattern of villi during the intestinal epithelial development.

5.2 LSD1-ablation does not affect the morphology of the small intestine

Upon birth, murine intestines are immature; The epithelial lining does not consist of all the differentiated cell types present in an adult intestine, crypts have not formed and villi- and the gut have not obtained their full lengths (Muncan et al. 2011, Noah et al. 2011). The immature form persists until the third postnatal week, where the murine intestine is thought to become mature (Muncan et al. 2011). The lengths and number of villi- and crypts continue to increase from their emergence at E14.5 and P5, respectively. Additionally, the proliferative compartment proceed from the intervillous zones to crypts during the same time-period (Muncan et al. 2011). These processes could be affected by the deletion of *Lsd1* in the intestinal epithelium, but our results coincided with these developmental steps and no significant differences were observed. Between P0.5-P7, crypts had emerged in both mouse models, and increased in number and depth from the first to the third postnatal week (fig. 4.2C). At P7, proliferative cells were exclusive to the epithelial lining of the crypts (fig. 4.3C). The proliferation height would thereby indicate crypt depths, and comparison between the measured proliferation height and crypt depths at a given timepoint (P7, P14 or P21) proved to be within the same size range (fig. 4.2C and 4.3D). A growth in villi-lengths were also observed after their emergence in the embryonic intestine, which increased from 140-150 μm at E16.5 to

around 200 μm at P7 (fig. 4.2B). These findings support the notion of continuous growth in morphological features upon their formation. However, after the first postnatal week, villi lengths did not seem to grow, and had dropped in lengths to approximately 180 μm at both timepoints in *Lsd1*$^{f/f}$ and *Lsd1*$^{\Delta IEC}$ mice. These changes could be related to differences in the intestinal development between littermates or litters, but a more plausible cause is the orientation of the villi in the sectioned FFPE sample: Measurements of villi or crypts are never an exact science, and villi lengths are especially prone to variation due to their frequently bent form (Whitehead 1971). The confidence of this method is thereby limited. Despite this fact, the measurements give an approximate value and each developmental timepoint showed no significant difference between WT and KO mice. No morphological changes were observed, which indicates that LSD1 does not affect the intestinal epithelial morphology.

5.3 LSD1 is intrinsic to Paneth cell development

The role of LSD1 in cell differentiation has been an established fact for years, where Adamo et al. (2011) and Haines et al. (2018) has shown the repressive role of LSD1 in differentiation of embryonic stem cells and plasmablasts, respectively. Similarly, our results have provided insight into the effects on intestinal epithelial differentiation upon *Lsd1*-deletion. By the quantification of Paneth cell numbers at five developmental timepoints in *Lsd1*$^{f/f}$- and *Lsd1*$^{\Delta IEC}$-mice, we have shown that the expression of LSD1 is intrinsic to Paneth cell development, as Paneth cells did not develop in LSD1-negative regions. In our case, the incomplete intestinal epithelial knockout led to LSD1-patches, which overlapped with Paneth cell appearance in the intestine of P7-P21 KO mice (fig. 4.4E). The presence of Paneth cells in the KO mice was caused by escaper crypts; Positively stained regions in a knockout model not expected to express the protein. The appearance of escaper crypts is not an uncommon feature of mice harboring a gene deletion (Sato et al. 2011, Van Es et al. 2012, Durand et al. 2012).

Since Paneth cells are interspersed between stem cells at crypt bottoms, the effect of the ablation or reduction of Paneth cells on stem cell quantities were investigated. Previous results by the Oudhoff group showed an increase in ISC numbers in the intestines of adult *Lsd1*$^{\Delta IEC}$ mice (fig. 1.5). The same compensatory mechanism was observed by Garabedian et al. in 1997: An increase in the crypt base columnar cells were observed in the absence of Paneth cells (Garabedian et al. 1997), where these crypt base columnar cells were later identified as intestinal stem cells (Barker et al. 2007). To investigate if the compensatory mechanism included all aspects of development, immunofluorescent staining of the stem cell marker

OLFM4 was performed. In situ hybridization would have been a possible alternative, but the staining was deemed too strong for stem cell quantification based on results acquired by the group prior to this study. The fluorescent staining did not prove to be any better, as individual stem cells could not be distinguished. However, visual interpretation did not indicate any apparent increase in stem cell numbers in the *Lsd1*$^{\Delta IEC}$ mice. This could be explained by three factors: Positive UEA-1 staining of goblet cells was observed for all developmental timepoints, but was either non-existent or extremely weak in Paneth cells at P7-P21. Bry et al. (1994) demonstrated similar expression differences in UEA-1 during murine intestinal development, where Paneth cells did not express UEA-1 before P28 when compared to P14 intestines. The lack of UEA-1 expression in Paneth cells therefore made it difficult to distinguish Paneth cells from stem cells. The diffuse staining of stem cells did not make the matter easier. Although these factors contribute to the uncertainty by visual interpretation, the effects on the stem cell numbers would still be low during the development of the intestinal epithelium: Only 1-2 Paneth cells were quantified out of 5-10 crypts in *Lsd1*$^{f/f}$ intestines at P7, and less than 1 positive cell was present in each crypt on average at P14. Furthermore, *Lsd1*$^{f/f}$ crypts at P21 did not display the adult quantities of Paneth cells. Adult *wildtype* small intestines contain approximately 5 Paneth cells per crypt (Bry et al. 1994, Brennan et al. 1999), whereas the number of Lyz-positive Paneth cells varied from 1-2 cells per crypt at P21 in our *Lsd1*$^{f/f}$ mice (fig. 4.4B-D). Moreover, significant differences between *Lsd1*$^{\Delta IEC}$ and *Lsd1*$^{f/f}$ were not observed before P21, even though the KO mice had fewer Paneth cells than the WTs at P7 and P14. The changes in stem cell quantities would therefore be very subtle in the *Lsd1*$^{\Delta IEC}$-mice compared to *Lsd1*$^{f/f}$ mice in the immature intestinal epithelium.

5.4 Deletion of *Lsd1* in the intestinal epithelium of mice show divergent effects on secretory cell type quantities

Whereas Paneth cells did not develop in the murine intestine of *Lsd1*-knockout mice, the other secretory cells developed normally in early intestinal development. From the second postnatal week to adulthood, goblet cell numbers were significantly decreased in *Lsd1*$^{\Delta IEC}$ mice compared to *Lsd1*$^{f/f}$ mice in the proximal- and mid-SI, although the jejunal difference was deemed non-significant at P21. For tuft cells, a significant increase was observed in *Lsd1*$^{\Delta IEC}$ mice from the third postnatal week in all small intestinal segments. These results suggest a role of LSD1 in their differentiation in late intestinal development, occurring at the suckling-to-weaning transition. The suckling-to-weaning transition is the period at which mice shift from mother's milk to the adult diet, occurring between the second to fourth postnatal weeks (Muncan et al.

2011, Mould et al. 2015). During this transition, the epithelium undergoes major structural and biochemical alterations to be able to digest solid food. Interestingly, the suckling-to-weaning transition coincides with the developmental timepoints where significant alterations in goblet- and tuft cell numbers occur in the small intestines of *Lsd1*$^{\Delta IEC}$ mice compared to *Lsd1*$^{f/f}$ mice. This could indicate that LSD1 is regulated by microbial- or food-stimulated signaling, which ultimately result in the regulation of secretory cell differentiation genes in response to these stimuli.

Although our results show that LSD1 regulate the differentiation of goblet- and tuft cells in late development, LSD1 is not an absolute requirement for their differentiation: The cell types are present, but in abnormal quantities in the small intestines of *Lsd1*$^{\Delta IEC}$ mice. It would therefore be of interest to investigate the mechanism through which LSD1 regulate these processes. As KLF4 and SPDEF are factors involved in goblet cell maturation, a reduction in in one or more of these would account for the decreased quantity of the cell type. Studies have shown that *Klf4*-mutant mice display a reduction in goblet cell numbers, but quantifications based on MUC2-postive goblet cells did not show any difference when compared to *wildtype* mice (Katz et al. 2002, Ghaleb et al. 2011). Thus, a reduction in this zinc-finger transcription factor would not fit the observation made in our results. A more likely suspect would therefore be the other transcription factor mentioned: SPDEF. *Spdef*-mutant mice display slight alterations in goblet cell numbers, and interestingly, a significant reduction is seen proximally but not distally (Gregorieff et al. 2009). The same observation is seen in our *Lsd1*$^{\Delta IEC}$ mice in late development: The ilea of *Lsd1*$^{\Delta IEC}$ mice never display any significant difference compared to *Lsd1*$^{f/f}$ intestines, whereas the duodeni and jejuni do. To validate if LSD1-mediated regulation of *Spdef* account for the reduction in goblet cells in our model, it would be necessary to investigate its presence in the small intestine during intestinal development. RNA-sequencing data of crypts in adult *Lsd1*$^{\Delta IEC}$- and *Lsd1*$^{f/f}$ mice obtained by the Oudhoff group has already shown a significant reduction of its expression in the *Lsd1*$^{\Delta IEC}$ mice (data not shown). Immunohistochemical detection of SPDEF and the comparison of the expression pattern between *Lsd1*$^{\Delta IEC}$- and *Lsd1*$^{f/f}$ mice at P7 and in adult mice could indicate if alterations in SPDEF-abundance is the cause for the observed decrease in goblet cell numbers from P14 in the *Lsd1*$^{\Delta IEC}$ mice. The same approach could be used for tuft cell development. Unfortunately, limited knowledge on tuft cell differentiation (Noah et al. 2011) makes it difficult to pinpoint which one(s) of the tuft-cell specification proteins are regulated by LSD1 and ultimately affect tuft cell numbers in our *Lsd1*$^{\Delta IEC}$-mice.

In contrast to the alterations observed in the other secretory cell types, enteroendocrine cells displayed inconsistent significance across the developmental timepoints. Quantifications in the duodenum of P14 mice and the jejunum of P0.5 mice showed a significant reduction of EECs in KO mice compared to the WTs, whereas all other developmental timepoints in the different intestinal segments showed no major alterations in the enteroendocrine cell numbers (fig. 4.8B-D and table 4.4). Additionally, the goblet cell quantification at P21 in the duodenum did not show significant difference, whereas P14 and adult mice did. The inconsistent significance levels could be designated to the same drawback as described by the morphological analyses: Variation can occur between littermates and litters, and the quantification of a 2-dimensional representation of a more complex 3-dimensional structure will result in approximate values.

5.5 The road to uncover the mechanisms behind Paneth cell ablation in *Lsd1*$^{\Delta IEC}$ mice

Paneth cells were the only secretory cell type to be completely absent from the small intestine upon *Lsd1*-deletion. To study how LSD1 function to mediate this, the epigenetic mark H3K4me2 was targeted by immunohistochemical staining. The repression of genes through H3K4me2-demethylation is the mechanism used by LSD1 to induce B-lymphocyte differentiation (Haines et al. 2018). As H3K4me2 is an active mark for transcription, a reduction would indicate a repressive role of LSD1 in the differentiation of the intestinal epithelium. However, no difference could be seen when comparing the H3K4me2-stainings of *Lsd1*$^{\Delta IEC}$- and *Lsd1*$^{f/f}$ mice. Although it would seem like LSD1 does not act through the demethylation of H3K4me2 to regulate intestinal epithelium, it is important to bear in mind that the staining is of the global dimethylation pattern. It is more likely that LSD1 regulate distinct dimethylation sites and not all H3K4me2, and these differences would be too small to be observed by the immunohistochemical staining. The study of differences in methylation statuses between the crypts of adult *Lsd1*$^{f/f}$ and *Lsd1*$^{\Delta IEC}$ mice has recently been conducted by the Oudhoff lab group by chromatin-immunoprecipitation sequencing. By comparing data from this experiment with the RNA-sequencing data, the group hope to get closer to discovering the genes responsible for the lack of Paneth cells in *Lsd1*$^{\Delta IEC}$ mice. However, there are some prime suspects for the observed phenotype in the intestinal epithelium of our *Lsd1*$^{\Delta IEC}$ mice, especially regarding the absence of Paneth cells. These include the differentiation factors SPDEF, SOX9 and ATOH1. The aforementioned factors are involved in the maturation of other secretory cell lineages, and a decrease in these differentiation factors would affect these cells accordingly. Previous research on ATOH1 have shown that mutant mice fail to develop goblet cells and

enteroendocrine cells in addition to Paneth cells (Yang et al. 2001). We did not see a reduction in enteroendocrine cells in our *Lsd1*$^{\Delta IEC}$ mice, and a reduction in ATOH1-expression cannot explain the complete inhibition of Paneth cell development. In situ hybridization of ATOH1 in adult *Lsd1*$^{f/f}$- and *Lsd1*$^{\Delta IEC}$ intestines by the Oudhoff lab group prior to this study has revealed a reduction, but not complete absence of the factor (data not shown). ATOH1 would therefore be an unlikely causative factor for the Paneth cell ablation. Similarly, SPDEF can be excluded. SPDEF is a factor downstream of ATOH1, and mutant mice display a reduction in Paneth cells instead of the overall lack of the secretory cell type (Gregorieff et al. 2009). The last maturation factor, SOX9, is a better candidate. It has been established that *Sox9*-mutant mice do not form Paneth cells, whereas its role in goblet cell maturation is disputed: Goblet cells numbers are either decreased or not affected by the lack of SOX9 (Bastide et al. 2007, Mori-Akiyama et al. 2007). Yet, RNA-sequencing data obtained on adult intestinal crypts do not show any significant difference in *Lsd1*$^{\Delta IEC}$ mice compared to *Lsd1*$^{f/f}$ mice (data not shown). Thus, the causative factor(s) leading Paneth cell loss in the intestinal epithelium of *Lsd1*$^{\Delta IEC}$ mice remain unknown.

More investigation into the regulatory role of LSD1 in secretory cell maturation is needed. Interestingly, the results generated in this study has provided clues to a possible candidate responsible for the intestinal epithelial phenotype observed in our knockout model. The transcription factor B-lymphocyte-induced maturation protein 1 (BLIMP-1) is a protein involved in the regulation of the intestinal epithelial suckling-to-weaning transition (P14-P21) and the maturation of intestinal epithelial cells (Muncan et al. 2011, Mould et al. 2015). BLIMP-1 is highly expressed in embryonic and neonatal intestines, but is significantly downregulated in the adult intestinal epithelium (Muncan et al. 2011). Thus, staining of BLIMP-1 in *Lsd1*$^{f/f}$ and *Lsd1*$^{\Delta IEC}$ intestines would uncover if the suckling-to-weaning transition coincide with the alterations in the IEC quantities of our *Lsd1*$^{\Delta IEC}$-mice. In addition to its expression during the suckling-to-weaning transition, BLIMP-1 has been shown to play a part in intestinal epithelial development and differentiation (Muncan et al. 2011, Mould et al. 2015). BLIMP-1 act as a repressor of gene transcription through the recruitment of chromatin-modifying complexes (Muncan et al. 2011, Mould et al. 2015). Studies have revealed that the maintained expression of BLIMP-1 in adult intestines or overexpression of the protein preserve the intestinal epithelium in a fetal state. Furthermore, *Blimp-1* mutant mice display an early maturation of Paneth cells (Muncan et al. 2011, Mould et al. 2015), suggesting it as a regulator of Paneth cell development. The RNA-sequencing data obtained by the Oudhoff lab group and the corresponding gene set enrichment analysis suggest LSD1 as a regulator of maturation and

differentiation of the intestinal epithelium. LSD1 is required to maintain the intestinal epithelium in a mature form; an opposite function to the fetal state provided by BLIMP-1. Furthermore, the RNA-sequencing data show a significant upregulation of *Blimp-1* in crypts of adult *Lsd1*$^{\Delta IEC}$ intestines when compared to *Lsd1*$^{f/f}$ intestines. Taken together, these findings lead us to believe that LSD1 is a repressor of BLIMP-1-expression. Thus, in the absence of LSD1 in the intestinal epithelium, the maintained expression of BLIMP-1 during the intestinal epithelial development inhibits Paneth cell differentiation through the repression of genes involved in Paneth cell maturation. Further research is necessary to determine if the hypothesis is true.

6.0 Conclusion

We have investigated the expression pattern of *Lsd1* in the small intestinal epithelium of *Lsd1*$^{f/f}$ mice by immunohistochemistry and immunofluorescence. The chromogenic detection of LSD1 revealed striking changes in the location of the protein during the intestinal epithelial development. Whereas all embryonic and neonatal intestinal epithelial cells expressed LSD1, newly formed crypts contained few positive cells at the first postnatal week. The epithelial lining of the crypts became increasingly positive, whereas cells at villi tips lost expression of *Lsd1* with age. Upon adulthood, staining was present mainly in crypts and intervillous zones, suggesting a dynamic expression pattern during intestinal epithelial development. The immunofluorescent result contradicted these findings, where LSD1-positive cells were present in the whole epithelial cell lining at every developmental timepoint. The divergent outcome in the two methods makes it necessary to further investigate the validity of these results, to uncover the true expression pattern of *Lsd1* during the development of the intestinal epithelium.

The effects of the tissue-specific deletion of the *Lsd1*-gene in the intestinal epithelium has been addressed in this study, where our preliminary results suggest a temporal role of LSD1 in the development of the intestinal epithelium. The morphology of the intestine appears to be unchanged, with subtle or no alterations detected in the number of stem cells or in the measured proliferation height. Significant differences were observed in the cellular composition of secretory cells, with fewer goblet cells, increased quantities of tuft cells and no change to enteroendocrine cells. Paneth cells were shown to not develop in the absence of LSD1. On the other hand, goblet- and tuft cell differentiation was first affected at the second or third postnatal weeks. The change in these secretory cell types coincide with the suckling-to-weaning transition and should be investigated further. By performing staining of BLIMP-1 in *Lsd1*$^{f/f}$ and *Lsd1*$^{\Delta IEC}$ intestinal tissues, it is possible to detect when the suckling-to-weaning transition occurs in our tissues, as *Blimp-1* expression is downregulated during the transition from mother's milk to solid diet.

To uncover the mechanisms behind the observed phenotype in our *Lsd1*$^{\Delta IEC}$ mice, IHC-staining was performed on the LSD1-target H3K4me2. The staining did not display any differences in intensities when comparing the *wildtype*- and *knockout* tissues at different developmental timepoints, which makes it unlikely that LSD1 mediates its effects through the global demethylation of H3K4me2. It is likely that BLIMP-1 is a factor involved in the observed phenotype of our *Lsd1*$^{\Delta IEC}$ mice. Other research groups have shown that *Blimp-1* mutant mice

display premature development of Paneth cells, and the RNA-sequencing data obtained by the Oudhoff lab show a significant increase in BLIMP-1 in the crypts of *Lsd1*$^{\Delta IEC}$ mice compared to *Lsd1*$^{f/F}$ mice. We therefore hypothesize that LSD1 repress the transcription of *Blimp-1* to induce the differentiation of Paneth cells. It would be of interest to investigate its expression in *Lsd1*$^{\Delta IEC}$- and *Lsd1*$^{f/f}$-mice, and further evaluate its role in intestinal epithelial differentiation in our *Lsd1*$^{\Delta IEC}$ mice.

References

Adamo, A., B. Sesé, J. Castaño, I. Paramonov, M. J. Barrero and J. C. Izpisua Belmonte (2011). "LSD1 regulates the balance between self-renewal and differentiation in human embryonic stem cells." Nature Cell Biology **13**(6): 652-659.

Alberts, B., A. Johnson, J. Lewis, D. Morgan, M. Raff, K. Roberts and P. Walter (2014). Molecular Biology of THE CELL. The United States of America, Garland Science, Taylor & Francis Group.

Anderle, P., T. Sengstag, D. M. Mutch, M. Rumbo, V. Praz, R. Mansourian, M. Delorenzi, G. Williamson and M.-A. Roberts (2005). "Changes in the transcriptional profile of transporters in the intestine along the anterior-posterior and crypt-villus axes." BMC Genomics **6**: 69.

Aust, G., C. Kerner, S. Gonsior, D. Sittig, H. Schneider, P. Buske, M. Scholz, N. Dietrich, S. Oldenburg, O. N. Karpus, J. Galle, S. Amasheh and J. Hamanne (2013). "Mice overexpressing CD97 in intestinal epithelial cells provide a unique model for mammalian postnatal intestinal cylindrical growth." Molecular Biology of the Cell **24**(14): 2256-2268.

Barker, N., M. van de Wetering and H. Clevers (2008). "The intestinal stem cell." Genes & Development **22**: 1856-1864.

Barker, N., J. H. van Es, J. Kuipers, P. Kujala, M. van den Born, M. Cozijnsen, A. Haegebarth, J. Korving, H. Begthel, P. J. Peters and H. Clevers (2007). "Identification of stem cells in small intestine and colon by marker gene Lgr5." Nature **449**: 1003-1008.

Basak, O., M. van de Born, J. Korving, J. Beumer, S. van der Elst, J. H. van Es and H. Clevers (2014). "Mapping early fate determination in Lgr5+ crypt stem cells using a novel Ki67-RFP allele." EMBO J. **33**(18): 2057-2068.

Bastide, P., C. Darido, J. Pannequin, R. Kist, S. Robine, C. Marty-Double, F. Bibeau, G. Scherer, D. Joubert, F. Hollande, P. Blache and P. Jay (2007). "Sox9 regulates cell proliferation and is required for Paneth cell differentiation in the intestinal epithelium." Journal of Cell Biology **178**(4): 635-648.

Bell, S. M., L. Zhang, Y. Xu, V. Besnard, S. E. Wert, N. Shroyer and J. A. Whitsett (2013). "Kruppel-like factor 5 Controls Villus Formation and Initiation of Cytodifferentiation in the Embryonic Intestinal Epithelium." Developmental Biology **375**(2): 128-139.

Benoit, Y. D., M. B. Lepage, T. Khalfaoui, É. Tremblay, N. Basora, J. C. Carrier, L. J. Gudas and J.-F. Beaulieu (2012). "Polycomb repressive complex 2 impedes intestinal cell terminal differentiation." Journal of Cell Science **125**(14): 3454-3463.

Bernier-Latmani, J. and T. V. Petrova (2017). "Intestinal lymphatic vasculature: structure, mechanisms and functions." Nature Reviews Gastronenterology & Hepatology **14**(9): 510-526.

Bernstein, B. E., E. L. Humphrey, R. L. Erlich, R. Schneider, P. Bouman, J. S. Liu, T. Kouzarides and S. L. Schreiber (2002). "Methylation of histone H3 Lys 4 in coding regions of active genes." Proceedings of the National Academy of Sciences of the United States of America **99**(13): 8695-8700.

Betts, J. G., P. Desaix, E. Johnson, J. E. Johnson, O. Korol, D. Kruse, B. Poe, J. A. Wise, M. Womble and K. A. Kelly A. Young. (2013). "23.5 The Small and Large Intestines." Anatomy and Physiology Retrieved 27th Apr, 2019, from https://opentextbc.ca/anatomyandphysiology/chapter/23-5-the-small-and-large-intestines/.

Bjerknes, M. and H. Cheng (1981). "The Stem-Cell Zone of the Small Intestinal Epithelium. 1. Evidence From Paneth Cells in the Adult Mouse." Journal of Anatomy **160**(1): 51-63.

Bjerknes, M. and H. Cheng (2010). "Cell Lineage metastability in Gfi1-deficient mouse intestinal epithelium." Developmental Biology **345**(1): 49-63.

Brennan, P. C., J. S. McCullough and K. E. Carr (1999). "Variations in Cell and Structure Populations along the Length of Murine Small Intestine." Cells Tissues Organs **164**: 221-226.

Bry, L., P. Falk, K. Huttner, A. Ouellette, T. Midtvedt and J. I. Gordon (1994). "Paneth Cell Differentiation in the Developing Intestine of Normal and Transgenic Mice." Proceedings of the National Academy of Sciences of the United States of America **91**: 10335-10339.

Chen, X. and P.-C. Yang (2010). "Double staining immunohistochemistry." North American Journal of Medical Sciences **2**(5): 241-245.

Chin, A. M., D. R. Hill, M. Aurora and J. R. Spence (2017). "Morphogenesis and maturation of the embryonic and postnatal intestine." Seminars in Cell & Developmental Biology **66**: 81-93.

Clevers, H. (2013). "The Intestinal Crypt, A Prototype Stem Cell Compartment." Cell **154**(2): 274-284.

Clood, P. A. C., J. Christensen, K. Agger and K. Helin (2008). "Erasing the methyl mark: histone demethylases at the center of cellular differentiation and disease." Genes & Development **22**(9): 1115-1140.

Cook, D. J. and P. J. Warren (2015). Cellular Pathology - An introduction to Techniques and Applications. UK, Scion Publishing.

Coons, A. H., H. J. Creech and R. N. Jones (1941). "Immunological Properties of an Antibody Containing a Fluorescent Group." Experimental Biology and Medicine **47**: 200-202.

Coons, A. H., E. H. Leduc and J. M. Connolly (1955). "STUDIES ON ANTIBODY PRODUCTION I. A METHOD FOR THE HISTOCHEMICAL DEMONSTRATION OF SPECIFIC ANTIBODY AND ITS APPLICATION TO A STUDY OF THE HYPERIMMUNE RABBIT." Journal of Experimental Medicine **102**(1): 49-60.

Cooper, G. M. (2000). Tools of Cell Biology. The Cell: A Molecular Approach. MA, Sinauer Associates.

Cromey, D. and P. Jansma. (2018). "Zeiss ZEN – performing a maximum intensity projection of a Z-stack " Retrieved 5th May, 2019, from http://microscopy.arizona.edu/sites/default/files/sites/default/files/upload/ZEN_max_intensity_projection.pdf.

D'Angelo, A., O. Bluteau, M. A. Garcia-Gonzalez, L. Gresh, A. Doyen, S. Garbay, S. Robine and M. Pontoglio (2010). "Hepatocyte nuclear factor 1alpha and beta control terminal differentiation and cell fate commitment in the gut epithelium." Development **137**(9): 1573-1582.

de Nanassy, J. and D. El Demellawy (2017). "Review of Current Applications of Immunohistochemistry in Pediatric Nonneoplastic Gastrointestinal, Hepatobiliary, and Pancreatic Lesions." Anal Chem Insights **12**: 1177390117690140.

De Santa Barbara, P., G. R. Van Den Brink and D. J. Roberts (2003). "Development and differentiation of the intestinal epithelium." Cellular and Molecular Life Sciences **60**(7): 1322-1332.

Dehmer, J. J., A. P. Garrison, K. E. Speck, C. M. Dekaney, L. Van Landeghem, X. Sun, S. J. Henning and M. A. Helmrath (2011). "Expansion of Intestinal Epithelial Stem Cells during Murine Development." PLoS One **6**(11): e27070.

Demitrack, E. S. and L. C. Samuelson (2016). "Notch regulation of gastrointestinal stem cells." Journal of Physiology **594**(17): 4791-4803.

Ding, J., Z.-M. Zhang, Y. Xia, G.-Q. Liao, Y. Pan, S. Liu, Y. Zhang and Z.-S. Yan (2013). "LSD1-mediated epigenetic modification contributes to proliferation and metastasis of colon cancer." British Journal of Cancer **109**: 994-1003.

Drozdowski, L. A., T. Clandinin and A. B. R. Thomson (2010). "Ontogeny, growth and development of the small intestine: Understanding pediatric gastroenterology." World Journal of Gastroenterology **16**(7): 787-799.

Durand, A., B. Donahue, G. Peignon, F. Letourneur, N. Cagnard, C. Slomianny, C. Perret, N. F. Shroyer and B. Romagnolo (2012). "Functional intestinal stem cells after Paneth cell ablation induced by the loss of transcription factor Math1 (Atoh1)." Proceedings of the National Academy of Sciences of the United States of America **109**(23): 8965-8970

Dworken, H. J., N. C. Hightower, W. Sircus and W. T. Keeton. (22.11.2016). "Human digestive system." Retrieved 24 Sep, 2018, from https://www.britannica.com/science/human-digestive-system.

Elkins, K. M. (2013). DNA Extraction. Forensic DNA Biology, Elsevier.

Elliott, E. N. and K. H. Kaestner (2015). "Epigenetic regulation of the intestinal epithelium." Cellular and Molecular Life Sciences **72**(21): 4139-4156.

Feldman, A. T. and D. Wolfe (2014). "Tissue processing and hematoxylin and eosin staining." Methods in molecular biology **1180**: 31-43.

Fischer, A. H., K. A. Jacobson, J. Rose and R. Zeller (2008). "Hematoxylin and eosin staining of tissue and cell sections." CSH Protocols(6): 655-658.

Forneris, F., C. Binda, A. Dall'Aglio, M. W. Fraajie, E. Battaglioli and A. Mattevi (2006). "A highly specific mechanism of histone H3-K4 recognition by histone demethylase LSD1." Journal of Biological Chemistry **281**(46): 35289-35295.

Foster, C. T., O. M. Dovey, L. Lezina, J. L. Luo, T. W. Gant, N. Barlev, A. Bradley and S. M. Cowley (2010). "Lysine-Specific Demethylase 1 Regulates the Embryonic Transcriptome and CoREST Stability." Molecular and Cellular Biology **30**(20): 4851-4863.

Ganz, J., E. Melancon, C. Wilson, A. Amores, P. Batzel, M. Strader, I. Braasch, P. Diba, J. A. Kuhlman and J. H. Postlethwait (2018). "Epigenetic factors coordinate intestinal development." bioRxiv: 1-21.

Gao, N., P. White and K. H. Kaestner (2009). "Establishment of Intestinal Identity and Epithelial-Mesenchymal Signaling by Cdx2." Developmental Cell **16**(4): 588-599.

Garabedian, E. M., L. J. J. Roberts, M. S. McNevin and J. I. Gordon (1997). "Examining the Role of Paneth Cells in the Small Intestine by Lineage Ablation in Transgenic Mice." Journal of Biological Chemistry **272**(38): 23729-23740.

Gerbe, F., E. Sidot, D. J. Smyth, M. Ohmoto, I. Matsumoto, V. Dardalhon, P. Cesses, L. Garnier, M. Pouzolles, B. Brulin, M. Bruschi, Y. Harcus, V. S. Zimmermann, N. Taylor, R. M. Maizels and P. Jay (2016). "Intestinal epithelial tuft cells initiate type 2 mucosal immunity to helminth parasites." Nature **529**(7585): 226-230.

Gerbe, F., J. H. van Es, L. Makrini, B. Brulin, G. Mellitzer, S. Robine, B. Romagnolo, N. F. Shroyer, J.-F. Bourgaux, C. Pignodel, H. Clevers and P. Jay (2011). "Distinct ATOH1 and Neurog3 requirements define tuft cells as a new secretory cell type in the intestinal epithelium." J Cell Biol **192**(5): 767-780.

Ghaleb, A. M., B. B. McConnell, K. H. Kaestner and V. W. Yang (2011). "Altered Intestinal Epithelial Homeostasis in Mice with Intestine-Specific Deletion of the Krüppel-Like Factor 4 Gene." Developmental Biology **349**(2): 310-320.

Goodwin, P. C. (2014). "A primer on the fundamental principles of light microscopy: Optimizing magnification, resolution, and contrast." Molecular Reproduction and Development **82**(7-8): 502-507.

Greenson, J. K. (2003). "Gastrointestinal Stromal Tumors and Other Mesenchymal Lesions of the Gut." Modern Pathology **16**: 366-375.

Greer, E. L. and Y. Shi (2014). "Histone methylation: a dynamic mark in health, disease and inheritance." Nature Reviews Genetics **13**(5): 343-357.

Gregorieff, A., D. E. Stange, P. Kujala, H. Begthel, M. van den Born, J. Korving, P. J. Peters and H. Clevers (2009). "The ets-domain transcription factor Spdef promotes maturation of goblet and paneth cells in the intestinal epithelium." Gastroenterology **137**(4): 1333-1345.

Grosse, A. S., M. F. Pressprich, L. B. Curley, K. L. Hamilton, B. Margolis, J. D. Hildebrand and D. L. Gumucio (2011). "Cell dynamics in fetal intestinal epithelium: implications for intestinal growth and morphogenesis." Development **138**(20): 4423-4432.

Gulbinowicz, M., B. Berdel, S. Wójcik, J. Dziewiątkowski, S. Oikarinen, M. Mutanen, V.-M. Kosma, H. Mykkänen and J. Moryś (2004). "Morphometric analysis of the small intestine in wild type mice C57BL/6J — a developmental study." Folia Morphologica **64**(4): 423-430.

Haber, A. L., M. Biton, N. Rogel, R. H. Herbst, K. Shekhar, C. Smillie, G. Burgin, T. M. Delorey, M. R. Howitt, Y. Katz, I. Tirosh, S. Beyaz, D. Dionne, M. Zhang, R. Raychowdhury, W. S. Garrett, O. Rozenblatt-Rosen, H. N. Shi, O. Yilmaz, R. J. Xavier and A. Regev (2017). "A single-cell survey of the small intestinal epithelium." Nature **551**: 333-339.

Haegebarth, A., W. Bie, R. Yang, S. E. Crawford, V. Vasioukhin, E. Fuchs and A. L. Tyner (2006). "Protein Tyrosine Kinase 6 Negatively Regulates Growth and Promotes Enterocyte Differentiation in the Small Intestine." Molecular and Cellular Biology **26**(13): 4949-4957.

Haines, R. R., B. G. Barwick, C. D. Scharer, P. Majumder, T. D. Randall and J. M. Boss (2018). "The Histone Demethylase LSD1 Regulates B Cell Proliferation and Plasmablast Differentiation." Journal of Immunology **201**(9): 2799-2811.

Hansson, G. C. (2012). "Role of mucus layers in gut infection and inflammation." Current Opinion in Microbiology **15**(1): 57-62.

Helling, R. B., H. M. Goodman and H. W. Boyer (1974). "Analysis of Endonuclease R-EcoRI Fragments of DNA from Lambdoid Bacteriophages and Other Viruses by Agarose-Gel Electrophoresis." Journal of Virology **14**(5): 1235-1244.

Howitt, M. R., S. Lavoie, M. Michaud, A. M. Blum, S. V. Tran, J. V. Weinstock, C. A. Gallini, K. Redding, R. F. Margolskee, L. C. Osborne, D. Artis and W. S. Garrett (2016). "Tuft cells, taste-chemosensory cells, orchestrate parasite type 2 immunity in the gut." Science **351**(6279): 1329-1333.

Ireland, H., C. Houghton, L. Howard and D. J. Winton (2005). "Cellular inheritance of a Cre-activated reporter gene to determine paneth cell longevity in the murine small intestine." Developmental Dynamics **233**: 1332-1336.

Jenny, M., C. Uhl, C. Roche, I. Duluc, V. Guillermin, F. Guillemot, J. Jensen, M. Kedinger and G. Gradwohl (2002). "Neurogenin3 is differentially required for endocrine cell fate specification in the intestinal and gastric epithelium." EMBO J. **21**(23): 6338-6347.

Kajimura, J., R. Ito, N. R. Manley and L. P. Hale (2016). "Optimization of Single- and Dual-Color Immunofluorescence Protocols for Formalin-Fixed, Paraffin-Embedded Archival Tissues." Journal of Histochemistry and Cytochemistry **64**(2): 112-124.

Kalff, J. C., N. T. Schwarz, K. J. Walgenbach, W. H. Schraut and A. J. Bauer (1998). "Leukocytes of the intestinal muscularis: their phenotype and isolation." Journal of Leukocyte Biology **63**: 683-691.

Katikireddy, K. R. and F. O'Sullivan (2011). "Immunohistochemical and Immunofluorescence Procedures for Protein Analysis." Methods in Molecular Biology **784**: 155-167.

Katz, J. P., N. Perreault, B. G. Goldstein, C. S. Lee, P. A. Labosky, V. W. Yang and K. H. Kaestner (2002). "The zinc-finger transcription factor Klf4 is required for terminal differentiation of goblet cells in the colon." Development **129**(11): 2619-2628.

Kazakevych, J., S. Sayols, B. Messner, C. Krienke and N. Soshnikova (2017). "Dynamic changes in chromatin states during specification and differentiation of adult intestinal stem cells." Nucleic Acids Research **45**(10): 5770-5784.

Kiernan, J. A. (2000). "Formaldehyde, Formalin, Paraformaldehyde And Glutaraldehyde: What They Are And What They Do." Microscope today **8**(1): 8-12.

Kim, S.-W., J. Roh and C.-S. Park (2016). "Immunohistochemistry for Pathologists: Protocols, Pitfalls, and Tips." J Pathol Transl Med **50**(6): 411-418.

Kim, T. H., S. Escudero and R. A. Shivdasani (2012). "Intact function of Lgr5 receptor-expressing intestinal stem cells in the absence of Paneth cells." Proceedings of the National Academy of Sciences of the United States of America **109**(10): 3932-3937.

Kosinski, C., D. E. Stange, C. Xu, A. S. Y. Chan, C. Ho, S. Tsan Yuen, R. C. Mifflin, D. W. Powell, H. Clevers, S. Y. Leung and X. Chen (2010). "Indian Hedgehog Regulates Intestinal Stem Cell Fate through Epithelial–Mesenchymal Interactions During Development." Gastroenterology **139**(3): 893-903.

Krause, W. J. (2000). "Brunner's Glands: A Structural, Histochemical and Pathological Profile " Progress in Histochemistry and Cytochemistry **35**(4): 255-367.

Krishnan, S., S. Horowitz and R. C. Trievel (2011). "Structure and Function of Histone H3 Lysine 9 Methyltransferases and Demethylases." ChemBioChem **12**(2): 254-263.

Laboratory for Optical and Computational Instrumentation and University of Wisconsin (2018). Image J - Image Processing and Analysis in Java, National Institutes of Health.

Landbruks- og matdepartementet. (2015, 5th Apr 2017). "Forskrift om bruk av dyr i forsøk." from https://lovdata.no/dokument/SF/forskrift/2015-06-18-761.

Lavis, L. D. and R. T. Raines (2008). "Bright Ideas for Chemical Biology." ACS Chemical Biology **3**(3): 142-155.

Lee, P. Y., J. Costumbrado, C.-Y. Hsu and Y. H. Kim (2012). "Agarose Gel Electrophoresis for the Separation of DNA Fragments." Journal of Visualized Experiments **62**: 3923.

Lelouard, H., M. Fallet, B. de Bovis, S. Méresse and J. P. Gorvel (2012). "Peyer's patch dendritic cells sample antigens by extending dendrites through M cell-specific transcellular pores." Gastroenterology **142**: 592-601.

Lin, F. and Z. Chen (2014). "Standardization of Diagnostic Immunohistochemistry: Literature Review and Geisinger Experience." Archives of Pathology **138**: 1564-1577.

Lindeboom, R. G., L. van Voorthuijsen, K. C. Oost, M. J. Rodríguez-Colman, M. V. Luna-Velez, C. Furlan, F. Baraille, P. W. Jansen, A. Ribeiro, B. M. Burgering, H. J. Snippert and M. Vermeulen (2018). "Integrative multi-omics analysis of intestinal organoid differentiation." Molecular Systems Biology **14**(6): e8227.

Lorenz, T. C. (2012). "Polymerase Chain Reaction: Basic Protocol Plus Troubleshooting and Optimization Strategies." Journal of Visualized Experiments **63**: 3998.

Luongo de Matos, L., D. C. Trufelli, M. Graciela Luongo de Matos and M. Aparecida da Silva Pinhal (2010). "Immunohistochemistry as an Important Tool in Biomarkers Detection and Clinical Practice." Biomark Insights **5**: 9-20.

Mah, A. T., K. S. Yan and C. J. Kuo (2016). "Wnt pathway regulation of intestinal stem cells." The Journal of Physiology **594**(17): 4827-4847.

Makki, J. S. (2016). "Diagnostic Implication and Clinical Relevance of Ancillary Techniques in Clinical Pathology Practice." Clinical Medicine Insights: Pathology **9**: 5-11.

Mao, S.-Y. and J. M. Mullins (2009). "Conjugation of Fluorochromes to Antibodies." Methods in Molecular Biology **588**: 43-48.

Marshman, E., C. Booth and C. S. Potten (2002). "The intestinal epithelial stem cell." BioEssays **24**(1): 91-98.

Ménard, D., P. Dagenais and R. Calvert (1994). "Morphological Changes and Cellular Proliferation in Mouse Colon During Fetal and Postnatal Development." The Anatomical Record **238**: 349-359.

Meyer, A. M. and J. S. Caton (2016). "Role of the Small Intestine in Developmental Programming: Impact of Maternal Nutrition on the Dam and Offspring." Advances in Nutrition **7**(1): 169-178.

Mohan, K. H., P. Sathish, R. Raghavendra, H. Sripathi and S. Prabhu (2008). "Techniques of immunofluorescence and their significance." Indian journal of dermatology, venereology and leprology **74**: 415-419.

Moran-Ramos, S., A. R. Tovar and Torres (2012). "Diet: friend or foe of enteroendocrine cells--how it interacts with enteroendocrine cells." Advances in Nutrition **3**(1): 8-20.

Mori-Akiyama, Y., M. Van den Born, J. H. Van Es, S. R. Hamilton, H. P. Adams, J. Zhang, H. Clevers and B. de Crombrugghe (2007). "SOX9 Is Required for the Differentiation of Paneth Cells in the Intestinal

Epithelium." Gastroenterology **133**(2): 539-546.

Mould, A. W., A. J. Morgan, A. C. Nelson, E. K. Bikoff and E. J. Robertson (2015). "Blimp1/Prdm1 Functions in Opposition to Irf1 to Maintain Neonatal Tolerance during Postnatal Intestinal Maturation." PLoS Genetics **11**(7): e1005375.

Muncan, V., J. Heijmans, S. D. Krasinski, N. V. Büller, M. E. Wildenberg, S. Meisner, M. Radonjic, K. A. Stapleton, W. H. Lamers, I. Biemond, W. van den Bergh, M A. , D. O'Carroll, J. C. Hardwick, D. W. Hommes and G. R. van den Brink (2011). "Blimp1 regulates the transition of neonatal to adult intestinal epithelium." Nature Communications **2**: 145.

Murphy, K. and C. Weaver (2017). Janeway's Immunobiology. New York, Garland Science, Taylor & Francis Group.

Murray, S. A., J. L. Morgan, C. Kane, Y. Sharma, C. S. Heffner, J. Lake and L. R. Donahue (2010). "Mouse Gestation Length Is Genetically Determined." PLoS One **5**(8): e12418.

Noah, T. K., B. Donahue and N. F. Shroyer (2011). "Intestinal development and differentiation." Experimental Cell Research **317**(19): 2702-2710.

Noah, T. K., A. Kazanjian, J. Whitsett and N. F. Shroyer (2010). "SAM pointed domain ETS factor (SPDEF) regulates terminal differentiation and maturation of intestinal goblet cells." Experimental Cell Research **316**(3): 452-465.

Noor, Z., S. L. Burgess, K. Watanabe and W. A. Petri Jr. (2016). "Interleukin-25 Mediated Induction of Angiogenin-4 Is Interleukin-13 Dependent." PLoS One **11**(4): e0153572.

O'Hurley, G., E. Sjöstedt, A. Rahman, B. Li, C. Kampf, F. Pontén, W. M. Gallagher and C. Lindskog (2014). "Garbage in, garbage out: A critical evaluation of strategies used for validation of immunohistochemical biomarkers." Molecular Oncology **8**(4): 783-798.

Odenwald, M. A. and J. R. Turner (2017). "The intestinal epithelial barrier: A therapeutic target?" Nature Reviews Gastronenterology & Hepatology **14**(1): 9-21.

Peignon, G., A. Durand, W. Cacheux, O. Ayrault, B. Terris, P. Laurent-Puig, N. F. Shroyer, I. Van Seuningen, T. Honjo, C. Perret and B. Romagnolo (2011). "Complex interplay between β-catenin signalling and Notch effectors in intestinal tumorigenesis." Gut **60**(2): 166-176.

Pinto, D., A. Gregorieff, H. Begthel and H. Clevers (2003). "Canonical Wnt signals are essential for homeostasis of the intestinal epithelium." Genes & Development **17**(14): 1709-1713.

Potten, C. S. and M. Loeffler (1987). "A comprehensive model of the crypts of the small intestine of the mouse provides insight into the mechanisms of cell migration and the proliferation hierarchy*." Journal of Theoretical Biology **127**(4): 381-391.

Qhang, W. J., J. Z. Duan, N. Lei, H. Xing, Y. Shao and G. B. Yang (2012). "Cellular bases for interactions between immunocytes and enteroendocrine cells in the intestinal mucosal barrier of rhesus macaques." Cell and Tissue Research **350**(1): 135-141.

Qi, Z., Z. Min, G. Wang, Y. Feng, H. Guo, Y. Li, N. Wang, Y. Li, R. Wang, W. Li and J. Hu (2017). "Comparison of immunofluorescence and immunohistochemical staining with anti-insulin antibodies on formalin-fixed paraffin-embedded human pancreatic tissue microarray sections " International Journal of Clinical and Experimental Pathology **10**(3): 3671-3676.

Robertson, D., K. Savage, J. S. Reis-Filho and C. M. Isacke (2008). "Multiple immunofluorescence labelling of formalin-fixed paraffin-embedded (FFPE) tissue." BMC Cell Biology **9**: 13.

Roostaee, A., Y. D. Benoit, S. Boudjadi and J.-F. Beaulieu (2016). "Epigenetics in Intestinal Epithelial Cell Renewal." Journal of Cell Physiology **231**(11): 2361-2367.

Rowan, B. A., D. K. Seymour, E. Chae, D. S. Lundberg and D. Weigel (2017). "Methods for Genotyping-by-Sequencing." Methods in Molecular Biology **1492**: 221-242.

Sancho, R., C. A. Cremona and A. Behrens (2015). "Stem cell and progenitor fate in the mammalian intestine: Notch and lateral inhibition in homeostasis and disease." EMBO Reports **16**(5): 571-581.

Sato, T. and H. Clevers (2013). "Primary Mouse Small Intestinal Epithelial Cell Cultures." Methods in molecular biology (Clifton, N. J.) **945**: 319-328.

Sato, T., J. H. van Es, H. J. Snippert, D. E. Stange, R. G. Vries, M. van den Born, N. Barker, N. F. Shroyer, M. van de Wetering and H. Clevers (2011). "Paneth cells constitute the niche for Lgr5 stem cells in intestinal crypts." Nature **469**: 415-419.

Sato, T., R. G. Vries, H. J. Snippert, M. van de Wetering, N. Barker, D. E. Stange, J. H. van Es, A. Abo, P. Kujala, P. J. Peters and H. Clevers (2009). "Single Lgr5 stem cells build crypt–villus structures in vitro without a mesenchymal niche." Nature **459**: 262-266.

Schaefer, K. N. and M. Peifer (2019). "Wnt/Beta-Catenin Signaling Regulation and a Role for Biomolecular Condensates." Developmental Cell **48**(4): 429-444.

Schuenke, M., E. Schulte and U. Schumacher (2017). Digestive System. Atlas of Anatomy - Internal Organs. W. A. Cass and H. Zeberg. New York, USA. Stuttgart, Germany. Delhi, India. Rio de Janeiro, Brasil., Thieme Medical Publishers Inc. **2:** 28-38.

Sharbati, R. (1982). "Morphogenesis of the intestinal villi of the mouse embryo: chance and spatial necessity." Journal of Anatomy **135**(Pt 3): 477-499.

Sherwood, R. I., R. Maehr, E. O. Mazzoni and D. A. Melton (2011). "Wnt Signaling Specifies and Patterns Intestinal Endoderm." Mech Dev **128**(7-10): 387-400.

Shi, Y., F. Lan, C. Matson, P. Mulligan, J. R. Whetstine, P. A. Cole, R. A. Casero and Y. Shi (2004). "Histone demethylation mediated by the nuclear amine oxidase homolog LSD1." Cell **119**(7): 941-953.

Shroyer, N. F., D. Wallis, K. J. Venken, H. J. Bellen and H. Y. Zoghbi (2005). "Gfi1 functions downstream of Math1 to control intestinal secretory cell subtype allocation and differentiation." Genes & Development **19**(20): 2412-2417.

Snoeck, V., B. Goddeeris and E. Cox (2005). "The role of enterocytes in the intestinal barrier function and antigen uptake." Microbes and Infection **7**(7-8): 997-1004.

Spence, J. R., R. Lauf and N. F. Shroyer (2011). "Vertebrate Intestinal Endoderm Development." Developmental Dynamics **240**(3): 501-520.

Stubbs, M. and N. Suleyman (2015). CRASH COURSE in Cell Biology and Genetics. Edinburgh, London, New York, Oxford, Philadelphia, St Louis, Sydney, Toronto, Elsevier Mosby.

Takeuchi, T. and T. Gonda (2004). "Distribution of the pores of epithelial basement membrane in the rat small intestine." Journal of Veterinary Medical Science **66**(6): 695-700.

Thavarajah, R., V. K. Mudimbaimannar, J. Elizabeth, U. K. Rao and K. Ranganathan (2012). "Chemical and physical basics of routine formaldehyde fixation." Journal of Oral and Maxillofacial Pathology **16**(3): 400-405.

The Human Protein Atlas. (15th of Nov. 2018). "KDM1A." Version 18.1. Retrieved 30th of May, 2019, from https://www.proteinatlas.org/ENSG00000004487-KDM1A/tissue.

The Jackson Laboratory. "MOUSE STRAIN DATASHEET - 004586

B6.Cg-Tg(Vil1-cre)997Gum/J." 2018, from https://www.jax.org/strain/004586.

Thompson, C. A., K. Wojta, K. Pulakanti, S. Rao, P. Dawson and M. A. Battle (2017). "GATA4 Is Sufficient to Establish Jejunal Versus Ileal Identity in the Small Intestine." Cellular and Molecular Gastroenterology and Hepatology **3**(3): 422-446.

Thorn, K. (2016). "A quick guide to light microscopy in cell biology." Molecular Biology of the Cell **27**(2): 219-222.

Tosic, M., A. Allen, D. Willmann, C. Lepper, J. Kim, D. Duteil and R. Schüle (2018). "Lsd1 regulates skeletal muscle regeneration and directs the fate of satellite cells." Nature Communications **9**: 366.

Tou, L., Q. Liu and R. A. Shivdasani (2004). "Regulation of Mammalian Epithelial Differentiation and Intestine Development by Class I Histone Deacetylases." Molecular and Cellular Biology **24**(8): 3132-3139.

Tsuchiya, K., T. Nakamura, R. Okamoto, T. Kanai and M. Watanabe (2007). "Reciprocal Targeting of Hath1 and β-Catenin by Wnt Glycogen Synthase Kinase 3β in Human Colon Cancer." Gastroenterology **132**(1): 208-220.

Tümmler, B. (2014). "Genotyping Methods." Pseudomonas Methods and Protocols **1149**: 33-47.

Van Es, J. H., A. Haegebarth, P. Kujala, S. Itzkovitz, B.-K. Koo, S. F. Boj, J. Korving, M. van de Born, A. van Oudenaarden, S. Robine and H. Clevers (2012). "A Critical Role for the Wnt Effector Tcf4 in Adult Intestinal Homeostatic Self-Renewal." Molecular and Cellular Biology **32**(10): 1918-1927.

van Es, J. H., P. Jay, A. Gregorieff, M. E. van Gijn, S. Jonkheer, P. Hatzis, A. Thiele, M. van den Born, H. Begthel, T. Brabletz, M. M. Taketo and H. Clevers (2005). "Wnt signalling induces maturation of Paneth cells in intestinal crypts." Nature Cell Biology **7**(4): 381-386.

Verzi, M. P., H. Shin, H. H. He, R. Sulahian, C. A. Meyer, R. K. Montgomery, J. C. Fleet, M. Brown, X. S. Liu and R. A. Shivdasani (2010). "Differentiation-specific histone modifications reveal dynamic chromatin interactions and alternative partners for the intestinal transcription factor CDX2." Developmental Cell **19**(5): 713-726.

Verzi, M. P., H. Shin, L.-L. Ho, X. S. Liu and R. A. Shivdasani (2011). "Essential and Redundant Functions of Caudal Family Proteins in Activating Adult Intestinal Genes." Molecular and Cellular Biology **31**(10): 2026-2039.

Verzi, M. P. and R. A. Shivdasani (2008). "Wnt signaling in gut organogenesis." Organogenesis **4**(2): 87-91.

Volk, N. and B. Lacy (2017). "Anatomy and Physiology of the Small Bowel. ." Gastrointestinal Endoscopy Clinics of North America **27**(1): 1-13.

Wang, J., S. Hevi, J. K. Kurash, H. Lei, F. Gay, J. Bajko, H. Su, W. Sun, H. Chang, G. Xu, F. o. Gaudet, E. Li and T. Chen (2008). "The lysine demethylase LSD1 (KDM1) is required for maintenance of global DNA methylation." Nature Genetics **41**(1): 125-129.

Wang, J., K. Scully, X. Zhu, L. Cai, J. Zhang, G. G. Prefontaine, A. Krones, K. A. Ohgi, P. Zhu, I. Garcia-Bassets, F. Liu, H. Taylor, J. Lozach, F. L. Jayes, K. S. Korach, C. K. Glass, X.-D. Fu and M. G. Rosenfeld (2007). "Opposing LSD1 complexes function in developmental gene activation and repression programmes." Nature **446**(7138): 882-887.

Whitehead, R. (1971). "The interpretation and significance of morphological abnormalities in jejunal biopsies." Journal of Clinical Pathology **5**: 108-124.

Williams, J. M., C. A. Duckworth, M. D. Burkitt, A. J. M. Watson, B. J. Campbell and D. M. Pritchard (2015). "Epithelial Cell Shedding and Barrier Function

A Matter of Life and Death at the Small Intestinal Villus Tip." Veterinary Pathology **52**(3): 445-455.

Wołczuk, K., B. Wilczyńska, M. Jaroszewska and J. Kobak (2011). "Morphometric characteristics of the small and large intestines of Mus musculus during postnatal development." Folia Morphologica **70**(4): 252-259.

Worthington, J. J. (2015). "The intestinal immunoendocrine axis: novel cross-talk between enteroendocrine cells and the immune system during infection and inflammatory disease." Biochemical Society Transactions **43**(4): 727-733.

Xie, R., J.-Y. Chung, K. Ylaya, R. L. Williams, N. Guerrero, N. Nakatsuka, C. Badie and S. M. Hewitt (2011). "Factors Influencing the Degradation of Archival Formalin-Fixed Paraffin-Embedded Tissue Sections." J Histochem Cytochem **59**(4): 356-365.

Yanai, H., N. Atsumi, T. Tanaka, N. Nakamura, Y. Komai, T. Omachi, K. Tanaka, K. Ishigaki, K. Saiga, H. Ohsugi, Y. Tokuyama, Y. Imahashi, S. Ohe, H. Hisha, N. Yoshida, K. Kumano, M. Kon and H. Ueno (2017). "Intestinal stem cells contribute to the maturation of the neonatal small intestine and colon independently of digestive activity." Scientific Reports **7**: 9891.

Yang, Q., N. A. Bermingham, M. J. Finegold and H. Y. Zoghbi (2001). "Requirement of Math1 for Secretory Cell Lineage Commitment in the Mouse Intestine." Science **294**(5549): 2155-2158.

Yaziji, H. and T. Barry (2006). "Diagnostic Immunohistochemistry: what can go wrong?" Adv Anat Pathol **13**(5): 238-246.

Ye, D. Z. and K. H. Kaestner (2009). "Foxa1 and Foxa2 Control the Differentiation of Goblet and Enteroendocrine L- and D-Cells in Mice." Gastroenterology **137**(6): 2052-2062.

Yin, X., H. F. Farin, J. H. van Es, H. Clevers, R. Langer and J. M. Karp (2013). "Niche-independent high-purity cultures of Lgr5+ intestinal stem cells and their progeny." Nature Methods **11**(1): 106-112.

Yoo, B. B. and S. K. Mazmanian (2017). "The Enteric Network: Interactions between the Immune and Nervous Systems of the Gut." Immunity **46**(6): 910-926.

Yu, D.-H., M. Gadkari, Q. Zhou, S. Yu, N. Gao, Y. Guan, D. Schady, T. N. Roshan, M.-H. Chen, E. Laritsky, Z. Ge, H. Wang, R. Chen, C. Westwater, L. Bry, R. A. Waterland, C. Moriarty, C. Hwang, A. G. Swennes, S. R. Moore and L. Shen (2015). "Postnatal epigenetic regulation of intestinal stem cells requires DNA methylation and is guided by the microbiome." Genome Biology **16**: 211.

Zimberlin, C. D., C. Lancini, R. Sno, S. L. Rosekrans, C. M. McLean, H. Vlaming, G. R. van den Brink, M. Bots, J. P. Medema and J.-H. Dannenberg (2015). "HDAC1 and HDAC2 collectively regulate intestinal stem cell homeostasis." THE FASEB Journal **29**(5): 2070-2080.

NTNU
Kunnskap for en bedre verden